

Dissertation

Submitted to the

Combined Faculty of Natural Sciences and Mathematics

Heidelberg University, Germany

For the degree of

Doctor of Natural Sciences (Dr. rer. nat.)

Presented by

Junsheng Li (M. Eng. New Energy Materials)

Born in Wuxue, Hubei, China

Supervisor: Dr. Pavel A. Levkin and Prof. Dr. Michael Grunze

Oral examination: February 28th, 2014

Preparation, characterization and application of functional surfaces based on porous polymethacrylates

This dissertation was carried out at the

Department of Applied Physical Chemistry

Heidelberg University

Referees:

Prof. Dr. Michael Grunze

Prof. Dr. Hans-Robert Volpp

Abstract

Porous polymethacrylates have numerous important applications in different research and industrial fields. These materials have been used as stationary phases for separation and catalysis, as substrates for thin layer chromatography, as materials for solid-phase extraction or filtration, or for making valves in microfluidic devices. The main advantage of porous polymethacrylates is that their physical and chemical properties, such as porosity, pore and polymer globule size, stiffness, hydrophobicity or hydrophilicity, as well as surface functional groups can be conveniently controlled by adjusting the composition of the polymerization mixtures. Porous polymethacrylate can be also functionalized using available surface modification strategies. This unique ability to control properties of porous polymethacrylates makes them suitable for the design and synthesis of novel functional materials. Surprisingly, most of the applications of porous polymethacrylates have been limited to their use inside columns, capillaries or microfluidic channels and their applications as open surfaces remained to a great extent unexplored. The goals of my PhD thesis were to: (1) develop methods for the preparation of (bio)functional porous polymethacrylate surfaces with well-defined surface properties; (2) characterize produced surfaces; (3) explore their unique properties in different biological applications.

Surfaces with gradient properties have been widely used in many cell-surface interaction studies because these gradient surfaces offer the possibility to avoid the difficulties associated with the one-sample-for-one-measurement approach as well as the problems with sample variations. However, up to now, there are only a few methods for the preparation of surfaces with gradient properties. Taking advantage of the tunable porous properties of polymethacrylates, porous poly(butyl methacrylate-*co*-ethylene dimethacrylate) (BMA-EDMA) surfaces with gradient surface morphologies were prepared using a PDMS microfluidic chip designed and produced for this study. The produced BMA-EDMA surface possessed a gradient polymer globule size ranging from $\sim 0.1 \mu\text{m}$ to $\sim 0.5 \mu\text{m}$. The surface with the globule size gradient in this range is useful for cell studies such as investigation of the effect of surface morphology on cell behavior. Porous polymethacrylate surfaces with a gradient in density of functional groups were also prepared via photografting by gradually varying the UV dosage along one direction on the surface during surface modification. The formation of the gradient was confirmed with X-ray photoelectron spectroscopy and water contact angle measurements. To show the potential of using the surface with a gradient density of functional groups, the behavior of human fibrosarcoma HT-1080 cells was studied on the surface.

Recently, bio-inspired slippery liquid infused porous surfaces have attracted much attention due to their unique liquid repellent and self-cleaning properties. In this thesis, stable slippery surfaces were prepared by infusing the porous BMA-EDMA surface with water immiscible hydrophobic poly(hexafluoropropylene oxide) or perfluorotripropylamine. The antibacterial and anti-marine fouling

properties of the slippery BMA-EDMA surfaces were carefully investigated. Our results demonstrated that the slippery BMA-EDMA surfaces had good antibacterial and anti-marine fouling properties. However, the results also revealed that the antibacterial property of the slippery BMA-EDMA surface was bacterial strain dependent. In addition, *Ulva* sporelings (young plants) were able to firmly attach to the slippery surface although the surface is able to resist *Ulva* spore adhesion.

The ability to transform a superhydrophobic surface to a superhydrophilic one is essential for many applications such as creating superhydrophobic-superhydrophilic micropatterns or microarrays. Most of the existing methods for this transformation are time consuming or require harsh conditions. In this thesis, a new facile method to transform the superhydrophobic BMA-EDMA surface to a superhydrophilic one was developed. This method is based on the physisorption of an amphiphilic phospholipid on the hydrophobic surface of porous BMA-EDMA through hydrophobic-hydrophobic interactions. Using this method, superhydrophobic-superhydrophilic micropatterns could be fabricated simply by printing the phospholipid “ink” on the superhydrophobic BMA-EDMA surface with a contact printer.

Zusammenfassung

Poröse Polymethylmethacrylate haben zahlreiche, wichtige Anwendungen in unterschiedlichen Industrie- und Forschungsgebieten. Diese Materialien werden als stationäre Phasen für Separation und Katalyse, als Substrate für Dünnschichtchromatografie, als Materialien für Festphasen-Extraktion oder –Filtration oder für das Herstellen von Ventilen in mikrofluidischen Systemen genutzt. Der Hauptvorteil poröser Polymethylmethacrylate ist, dass ihre physikalischen und chemischen Eigenschaften, wie Porosität, Poren- und Polymerkügelchengröße, Steifigkeit, Hydrophobie, Hydrophile oder auch funktionelle Gruppen, durch das Anpassen der Zusammensetzung der Polymerisierungsmischung relativ einfach kontrolliert werden können. Poröses Polymethylmethacrylat kann auch durch Nutzung von bereits bekannten Oberflächenmodifikationsstrategien funktionalisiert werden. Die einzigartige Möglichkeit die Eigenschaften von porösen Polymethylmethacrylaten zu kontrollieren, prädestiniert diese für die Entwicklung von neuartigen, funktionalen Materialien. Erstaunlicherweise sind die meisten Anwendungen von porösen Polymethylmethacrylaten auf deren Nutzung in Säulen, Kapillarröhren oder mikrofluidischen Kanälen begrenzt deren Anwendungen als offene Oberflächen blieben im Großen und Ganzen unerforscht. Die Ziele meiner Doktorarbeit waren: (1) Methoden zur Darstellung von (bio)funktionalen, porösen Polymethylmethacrylat-Oberflächen mit klar definierten Oberflächeneigenschaften zu entwickeln; (2) hergestellte Oberflächen zu charakterisieren; (3) deren einzigartige Eigenschaften in verschiedenen biologischen Anwendungen zu untersuchen.

Oberflächen mit Gradienten werden in vielen Zelloberflächeninteraktionsstudien genutzt, weil diese sukzessiv variierenden Oberflächen die Möglichkeit bieten „Ein Probe pro Messung“ durchzuführen, und damit Probleme mit der Reproduzierbarkeit der Proben zu vermeiden. Jedoch gibt es bis jetzt nur wenige Methoden zur Herstellung von Oberflächen mit variablen porösen Eigenschaften. In dieser Arbeit werden Poly(butylmethacrylat-co-ethylendimethacrylat) (BMA-EDMA)-Oberflächen mit Gradient-Oberflächenmorphologie unter Verwendung eines mikrofluidischen Chips, zusammengesetzt aus einem Objektträger und einer PDMS-Kammer, hergestellt. Die BMA-EDMA-Oberfläche besaß eine sukzessiv variierende Polymerteilchengröße von $\sim 0,1$ bis $\sim 0,5$ μm . Eine Oberfläche mit einem Größengradienten in diesem Bereich ist für Zellstudien, wie beispielsweise zur Untersuchung des Einflusses der Oberflächenmorphologie auf das Zellverhalten, geeignet. Poröse Polymetacrylatoberflächen mit einer graduell variierten Dichte funktioneller Gruppen wurden durch Photografting erzeugt; wobei die UV-Dosis graduell entlang einer Richtung auf der Oberfläche während der Oberflächenmodifikation verändert wurde. Die Bildung des Gradienten wurde mittels Röntgenphotoelektronenspektroskopie und Wasserkontaktwinkelmessungen bestätigt. Um das Potential für Anwendungen zu demonstrieren wurde das Verhalten von menschlichen Fibrosarkom-HT-1080-Zellen auf der Oberfläche untersucht. Unsere Ergebnisse zeigen, dass die Oberflächenchemie eine entscheidende Rolle für Adhäsion und Wachstum der HT-1080 Zellen spielt.

Vor kurzem zogen mit „Schmiermittel“ beladene poröse Oberflächen (SLIPS) aufgrund ihrer einzigartigen wasserabweisenden und selbstreinigenden Eigenschaften große Aufmerksamkeit auf sich. In dieser Dissertation wurde eine stabile, „rutschige“ Oberfläche durch Durchdringung der porösen BMA-EDMA-Oberfläche mit hydrophoben poly(hexafluoropropylene oxide) oder Perfluorotripropylamin, hergestellt. Die anti-bakteriellen und Meeresorganismen abweisenden Eigenschaften der SLIPS BMA-EDMA-Oberflächen wurden systematisch untersucht. Unsere Ergebnisse zeigen, dass diese Oberflächen gute anti-bakterielle und Meeresorganismen abweisende Eigenschaften besitzen. Jedoch zeigten die Ergebnisse, dass die anti-bakteriellen Eigenschaften der SLIPS BMA-EDMA-Oberfläche vom Bakterienphenotype abhängig sind. Außerdem war es Protonemata/Prothallien möglich sich an der Oberfläche anzulagern, obwohl die Oberfläche resistent gegenüber Sporenadhäsion war.

Umwandlung einer superhydrophoben Oberfläche in eine superhydrophile Oberfläche ist wichtig für viele Anwendungen, wie z.B. für die Erzeugung von superhydrophoben-superhydrophilen Mikromustern oder Mikromatrixen. Die meisten der bestehenden Methoden für diese Umwandlung sind zeitaufwendig oder benötigen harsche Bedingungen. In dieser Doktorarbeit wurde eine neue, einfache Methode entwickelt, um die superhydrophobe BMA-EDMA-Oberfläche in eine superhydrophile Oberfläche zu verwandeln. Diese Methode beruht auf der Physisorption eines amphiphilen Phospholipids auf der hydrophoben Oberfläche der porösen BMA-EDMA Oberfläche durch hydrophobe-hydrophobe Wechselwirkung. Mit dieser Methode konnten superhydrophobe-superhydrophile Mikromuster durch Drucken der Phospholipid "Tinte" auf der superhydrophoben BMA-EDMA-Oberfläche mit einem Kontaktdrucker hergestellt werden.

Contents

1.	Introduction	1
1.1	Porous polymethacrylate monoliths	1
1.2	Preparation and characterization of polymethacrylate monoliths	1
1.2.1	Preparation of polymethacrylate monoliths	1
1.2.2	Porous properties of polymethacrylate monoliths	3
1.2.3	Chemistry of polymethacrylate monoliths	5
1.3	Applications of polymethacrylate monoliths	6
1.3.1	Applications of polymethacrylate monoliths for separation	6
1.3.2	Micropatterning using polymethacrylate substrates	6
1.3.2	Other applications of polymethacrylate monoliths	8
2.	Materials and methods	10
2.1	Chemicals and Materials	10
2.2	Description of experiments and preparation techniques	10
2.2.1	Activation, modification and fluorination of glass slides	10
2.2.2	Preparation of a polymer surface on a glass slide	10
2.2.3	Photografting of a polymer surface	11
2.2.4	Lipid modification of a polymer surface and printing of lipid solutions on a polymer surface	12
2.2.5	Preparation of a porous polymethacrylate SLIPS surface	13
2.2.6	Preparation of a polymer surface with a gradient in pore size	13
2.2.7	Bacterial experiments	13
2.3	Methods and theoretical background	14
2.3.1	Water contact angle measurement	14
2.3.2	Scanning electron microscopy	16
2.3.3	X-ray photoelectron spectroscopy	18
2.3.4	Photoinitiated free radical polymerization	18
2.3.5	Surface modification via photografting	20
2.3.6	Hard X-ray phase contrast tomography	21
3.	Results and discussion	23

3.1 Formation of porous polymethacrylate polymer surfaces with gradient morphology	23
3.1.1 Background	23
3.1.2 Preparation of porous polymer surfaces with different morphologies	23
3.1.3 Preparation of porous polymer surface with a gradient in pore size using microfluidic chips	25
3.1.4 Hydrodynamic characterization of the microfluidic chip.....	30
3.1.5 Summary	33
3.2 Porous polymethacrylate surface with gradient density of functional group for the investigation of the effect of surface morphology and surface chemistry on HT-1080 fibrosarcoma cells.....	34
3.2.1 Background	34
3.2.2 Preparation of the porous polymethacrylate surfaces with gradient density of functional groups	35
3.2.3 Characterization.....	36
3.2.5 The impact of surface morphology and surface chemistry on HT-1080 cell adhesion	42
3.2.6 Summary	43
3.3. Slippery liquid infused porous surface for antibacterial and marine antifouling applications	44
3.3.1 Slippery liquid infused porous surfaces (SLIPS): background.....	44
3.3.2 Antibacterial properties of the slippery liquid infused porous surface.....	45
3.3.2.1 Morphology and stability of the slippery porous polymethacrylate surface	46
3.3.2.2 Biofilm formation of <i>P. aeruginosa</i> strain PA49 on the BE103	52
3.3.2.3 Biofilm formation of different strains of <i>P. aeruginosa</i> on the BE103 in high nutrient medium.....	53
3.3.2.4 Toxicity tests	54
3.3.2.5 Effect of components in the bacterial culture medium on the biofilm formation of <i>P. aeruginosa</i> on the surface.....	55
3.3.3 Marine antifouling properties of the slippery porous polymethacrylate surface.....	56
3.3.3.1. Stability of the slippery BMA-EDMA surface in artificial seawater	57
3.3.4 Summary	58
3.4. Printable superhydrophobic-superhydrophilic micropatterns based on supported lipid layers.	59

3.4.1 Background	59
3.4.2 Modification of porous polymethacrylate surfaces with phospholipids	59
3.4.3 Fabrication of the superhydrophobic-superhydrophilic micropatterns.....	65
3.4.4 Summary	67
4. Conclusion and outlook.....	69
5. Appendix	72
5.1 Hydrodynamic characterization of the microfluidic chip.....	72
5.2 The impact of surface morphology and surface chemistry on HT-1080 cell behavior	74
5.3 Toxicity test of PFPE liquid	78
5.4 Acknowledgement.....	79
5.5 List of publications	81
5.6 List of abbreviations.....	83
5.7 Bibliography	85

1. Introduction

1.1 Porous polymethacrylate monoliths

Porous materials are usually classified by their pore sizes. Porous materials with pore sizes in the range of 2 nm and below are termed microporous materials.¹⁻² Porous materials with pore sizes in the range of 2 nm to 50 nm and between 50 nm and 300 nm are described as mesoporous materials and macroporous materials, respectively.¹⁻² Porous materials are important in many applications because the pores in porous materials can be engineered to host different guests such as functional molecules and cells. Porous polymers, combining the advantages of porous materials and polymeric materials,³ have many applications in different fields such as gas storage⁴⁻⁵ and separation,⁶⁻⁷ catalyst supports,⁸ cell scaffolds,⁹ templates for the synthesis of nanostructures¹⁰ and carriers for drug delivery.¹¹

Porous polymethacrylate monoliths have attracted much research interest due to their great potential in separation applications. The preparation, characterization and functionalization of porous polymethacrylate monoliths have been intensively investigated.¹²⁻¹⁵ It was shown that porous polymethacrylate monoliths could be prepared in different molds using free radical polymerization of monomers in the presence of porogens and that their porous properties could be well controlled.¹⁶ Other properties of the polymethacrylate monoliths, such as rigidity, could also be finely tuned.¹⁷ In addition, the pores of the porous polymethacrylates could be readily functionalized on demand.¹⁸ The easily controllable physical and chemical properties of porous polymethacrylate monoliths make them particularly useful in surface related studies. However, to date, the applications of porous polymethacrylates are mainly limited to separation applications.

1.2 Preparation and characterization of polymethacrylate monoliths

1.2.1 Preparation of polymethacrylate monoliths

Reports about the preparation of the polymethacrylate monoliths can be traced back to as early as the 1970s.¹⁹⁻²⁰ Coupek et al.¹⁹ synthesized poly(2-hydroxyethyl methacrylate-*co*-ethylene dimethacrylate) (HEMA-EDMA) monolith by a suspension copolymerization initiated by azobisisobutyronitrile (AIBN). It was proposed that the prepared macroporous HEMA-EDMA with globular morphology could be used in chromatography and as catalyst supports. In a following study which was aimed at the fabrication of reactive polymethacrylate monoliths, Svec et al.²⁰ prepared poly(glycidyl methacrylate-*co*-ethylene dimethacrylate) (GMA-EDMA) monoliths using a similar method. To prepare the GMA-EDMA monoliths, they first mixed the monomers (glycidyl methacrylate (GMA) and ethylene dimethacrylate (EDMA)) with the thermal initiator AIBN in the inert phase consisting of lauryl alcohol and cyclohexanol. The polymerization mixture was then dispersed in a solution of polyvinylpyrrolidone in water. After removal of air from the suspension, the polymerization was initiated by heating. The prepared GMA-EDMA polymers were porous and showed globular

morphology (Fig. 1.1). Owing to the presence of epoxy groups in the GMA-EDMA polymer, the macroporous GMA-EDMA could be easily functionalized.²⁰

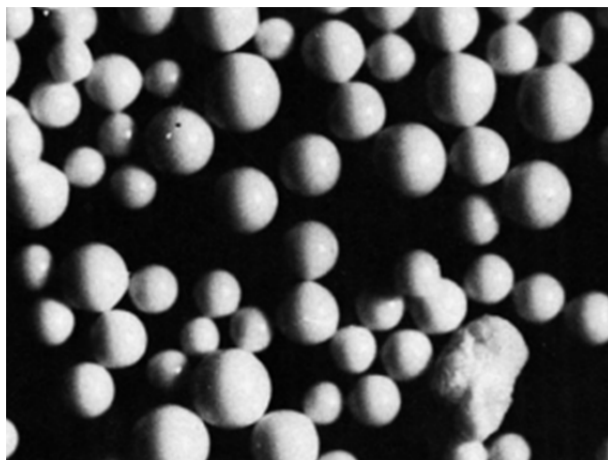


Figure 1.1: SEM image of the GMA-EDMA surface. The globule size ranges from 250 to 400 μm . Reproduced from reference.²⁰

Later, the GMA-EDMA monoliths were prepared in different molds and used in various types of separation applications. Tennikova et al.²¹ prepared the monolith by thermally-induced polymerization inside a mold composed of two heating plate. Preparation of a GMA-EDMA monolith in a rod format was also reported. Svec et al.²² used a stainless steel column as a mold to polymerize a mixture containing methyl acrylate monomers (GMA and EDMA, 60:40 vol%), porogens (cyclohexanol and dodecanol, 80:20 vol%) and initiator (AIBN, 1 wt% with respect to monomers). Polymerization was conducted at 70 °C for 6 hours inside the column. After polymerization, the porogenic solvents and other soluble moieties in the polymer monolith were washed out by pumping methanol at a flow rate 1 mL/min for 2 hours.

Thermally initiated polymerization of monomers to produce polymethacrylate monoliths usually have to be carried out for 6-24 hours at elevated temperatures. To ease the preparation of polymethacrylate monoliths, Viklund et al.²³ used photoinitiated polymerization. They performed the polymerization in quartz glass tubes (length: 38 mm; inner diameter: 2.4 mm; outer diameter: 4.1 mm.) modified with vinyltrichlorosilane. The polymerization mixture containing photoinitiator (benzoin methyl ether), monomers (GMA and trimethylolpropane trimethacrylate (TRIM)) and porogens (isooctane and toluene) was sonicated and purged with helium prior to injection into the quartz mold. After injection of the polymerization mixture, the mold was sealed with PTFE plugs. The polymerization was initiated by irradiating the mold with 365 nm UV light for 1 hour (intensity: 10 mW/cm²). Although the penetration depth of UV light is limited, it was proven that homogeneous GMA-TRIM monolith could be obtained. The effect of the composition of the polymerization mixture on the porous properties of the GMA-TRIM monolith was also investigated. It was demonstrated that the porous properties of the GMA-TRIM monolith could be easily controlled by changing the composition of the

polymerization mixture when photoinitiated polymerization was used. Recently, Levkin et al.²⁴ also showed preparation of porous polymethacrylate layers in a mold made of two glass plates and thin Teflon spacers by using photoinitiated polymerization.

1.2.2 Porous properties of polymethacrylate monoliths

The porous properties of porous polymethacrylate monoliths are largely determined by the composition of the polymerization mixture. The ratio of monomer to crosslinker determines the chemical composition and rigidity of the polymer. The porogens in the polymerization mixture are used to dissolve the monomer/crosslinker and to control the porous properties of the prepared porous polymer monoliths.^{12,25} The ratio of the porogens to monomer and crosslinker determines the porosity and affects the rigidity. During the polymerization, phase separation occurs and the polymer phase separates from the porogens due to its limited solubility in the porogens.²⁶ When the porogen content is high, the porosity of the obtained porous monolith is high.²⁷⁻²⁹ The homogeneity of the pore size in porous monolith also decreases with an increase of the porogens content.²⁷⁻²⁹ Generally, porous monoliths with larger pores are obtained if the porogens are poor solvents for the monomer/crosslinker, whereas porous polymer monoliths with smaller pores are obtained if the porogens are good solvents for the monomer/crosslinker.²⁶ For example, GMA-EDMA monolith is usually prepared using binary porogens comprising cyclohexanol and 1-dodecanol. A higher content of 1-dodecanol leads to porous monoliths with larger pores because 1-dodecanol is a poor solvent for the monomer/crosslinker (See Fig. 1.2). In contrast, a higher content of cyclohexanol, which is a good solvent for the monomers, leads to porous monoliths with smaller pores.

The porous properties of polymethacrylates are also dependent on some other factors, such as the temperature at which polymerization is performed and the type/concentration of the initiator in the polymerization mixture.¹⁶ Svec et al.¹⁶ studied the effect of polymerization temperature on the porous properties of the GMA-EDMA polymer monolith using mercury intrusion porosimetry and a Brunauer-Emmett-Teller (BET) sorptometer. They found that the pore size of the GMA-EDMA monolith generally decreased with an increase of the polymerization temperature (Fig. 1.3). At higher polymerization temperatures, more free-radicals are produced and thus more nuclei and globules are formed in the early stage of the polymerization, leading to the formation of a GMA-EDMA monolith with smaller globule and pore sizes.

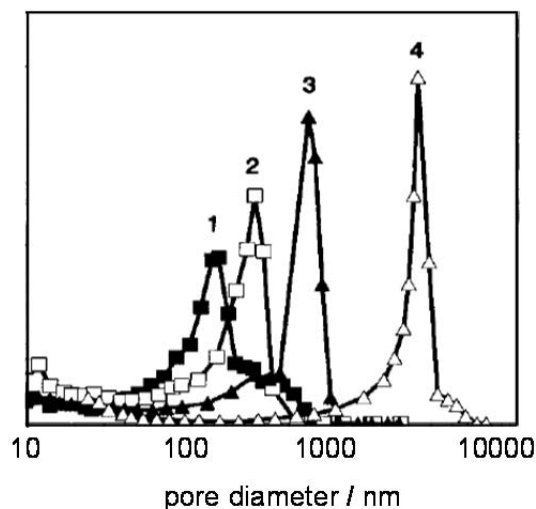


Figure 1.2: Effect of 1-dodecanol content in the polymerization mixture on the pore size distribution of the GMA-EDMA monolith prepared by thermally initiated polymerization. Cyclohexanol and 1-dodecanol contents in the polymerization mixture: (1) 60 vol% + 0 vol %; (2) 57 vol% + 3 vol %; (3) 54 vol % + 6 vol %; (4) 45 vol % + 15 vol %. Reproduced with permission.²⁶ Copyright American Chemical Society.

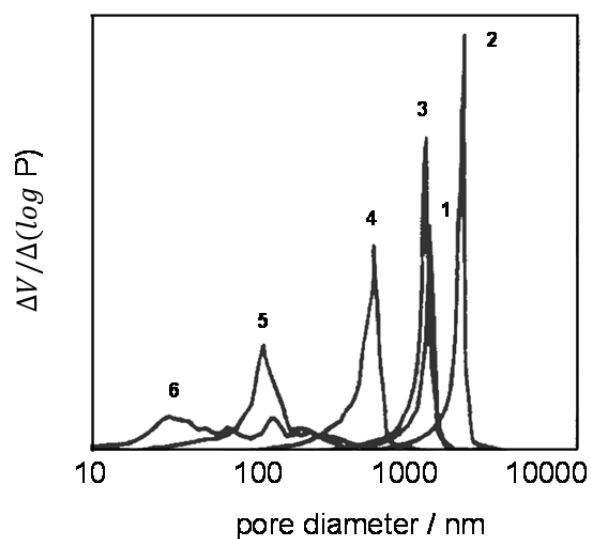


Figure 1.3: Pore size distribution curves of the GMA-EDMA monolith prepared by thermally initiated polymerization at different temperatures: (1) 55°C, (2) 60°C, (3) 65°C, (4) 70°C, (5) 80°C and (6) 90°C. Reproduced with permission.¹⁶ Copyright American Chemical Society.

As shown above, the porous properties of polymethacrylate monoliths prepared by thermally initiated polymerization can be finely tuned by changing the composition of the polymerization mixture or by changing the temperature in molds with small sizes (e.g. in tubes with diameter of ~ 10-25 mm).²⁹ However, accurate control of the porous properties of polymethacrylate monoliths prepared in larger

molds by thermally initiated polymerization was difficult.²⁹ This is because the heat generated during the polymerization could not dissipate effectively and therefore the temperature varied significantly in the large molds, resulting in the inhomogeneous porous structures of the monolith. Peters et al.³⁰ first proved the preparation of polymethacrylate monoliths with homogeneous pore structures in a large mold (diameter 50 mm) using the “gradual addition” method. Instead of injecting the polymerization mixture into the mold all at once before the polymerization, they slowly added the polymerization mixture to the mold during the polymerization. The polymerization mixture was fed into the mold at a rate of 20 mL/h for 12 hours at 55 °C. The temperature varied only slightly during polymerization in the mold in this case. The pore distribution of the GMA-EDMA monolith prepared by the “gradual addition” approach was studied and it was found that the homogeneity of the GMA-EDMA monolith could be greatly improved when the “gradual addition” approach was used.

1.2.3 Chemistry of polymethacrylate monoliths

Chemistry of polymethacrylate monoliths can be controlled in two different ways. The first approach involves polymerization of monomers bearing side chains with certain functionality. A variety of monomers and crosslinkers with different functional groups can be used for the preparation of polymethacrylate monoliths in molds. Some of the functionalized monomers and crosslinkers which have been proved for the preparation of polymethacrylate monoliths were reviewed elsewhere.²⁹ However, it should be noted that the conditions for the polymerization of these monomers could differ from each other. Functional groups can also be introduced by modification of the reactive polymethacrylate monoliths. One of the most commonly used reactive polymethacrylate monolith is the GMA-EDMA monolith. Due to the presence of the epoxy groups in the GMA-EDMA monolith, the surface of the monolith could be easily functionalized with either diol groups or amino groups by treating the monolith with either sulfuric acid or diethylamine, respectively.²¹ The GMA-EDMA monolith could also be functionalized with large molecules such as proteins.³¹

Another strategy for the modification of polymethacrylate monoliths is to functionalize the surface after the monolith is prepared.³²⁻³⁵ Photografting is a powerful surface modification tool which can be applied to many different polymers.³²⁻³⁵ Inert polymer surfaces could be grafted with reactive vinyl monomers via UV-triggered photografting in the presence of a hydrogen abstracting photoinitiator.³⁴ Rohr et al.³⁶ used the photografting technique to modify the poly(butyl methacrylate-*co*-ethylene dimethacrylate) (BMA-EDMA) monolith with 2-acrylamido-2-methyl-1-propanesulfonic acid. They showed that the photografting method was facile and highly efficient. In another study,³⁷ Rohr et al. proved the high efficiency of photografting of a number of vinyl monomers onto different polymer surfaces. One of the main advantages of the photografting technique is that it allows for spatially confined surface modification. Different patterns of functional groups can be easily established on different polymer surfaces simply by photografting the surface through a photomask.³⁷⁻⁴⁰

Porous polymethacrylate monoliths with bimodal chemistry are needed in some applications, for

example when separating complex mixtures. Svec et al. proposed the concept of a pore size specific modification and proved it using a macro porous GMA-EDMA monolith.¹⁸ They used poly(styrenesulfonic acid) to modify the epoxy groups in the GMA-EDMA monolith. The poly(styrenesulfonic acid) is too large to enter the smaller pores in the monolith. Therefore, the epoxy groups remained in the smaller pores after the modification and were later modified using octadecylamine, the size of which is small enough to enter the small pores in the monolith.

1.3 Applications of polymethacrylate monoliths

1.3.1 Applications of polymethacrylate monoliths for separation

The tunable globular microstructure and the rigid nature of polymethacrylates allow for their permeability to liquids and gases. The chemistry of polymethacrylates can be also controlled conveniently by using monomers with the desired functional groups or post modification of the as-prepared monolith. Therefore, the affinity of chemicals to the polymethacrylate monoliths in separation processes can be tuned. GMA-EDMA monolith membrane based chromatography was used for the separation of proteins.²¹ Compared to the column based chromatography, a much lower pressure was needed during the separation process and a significantly higher loading could be achieved for the GMA-EDMA monolith membrane based chromatography. Although the monolith membrane based chromatography showed good performance, their applications were limited because the membrane had low capacities and could be used only in certain separation applications. Later, Svec et al.²² developed the GMA-EDMA monolith filled rod columns for high-performance liquid chromatography (HPLC) applications. Since then, great efforts have been devoted to develop novel polymethacrylate monolith based stationary phases. For example, Moravcova et al.²⁸ studied the BMA-EDMA monolith as the stationary phase for HPLC applications. They found that the BMA-EDMA monolith with certain porous properties showed good lipophilic character and permeability and could be used for efficient and fast separations in HPLC. Applications of the polymethacrylate monoliths in HPLC systems have been reviewed in details elsewhere.^{13, 15, 41-42}

1.3.2 Micropatterning using polymethacrylate substrates

An emerging application of the polymethacrylates is surface patterning. Zahner et al.⁴⁰ prepared a porous hydrophobic BMA-EDMA surface on a glass substrate through photoinitiated polymerization (Fig. 1.4A). The superficial nonporous layer was removed by tapping to increase the roughness of the surface. The resulting BMA-EDMA surface was superhydrophobic because of the combination of surface hydrophobicity and roughness. The superhydrophobic BMA-EDMA surface was photografted with AMPS monomer through a photomask for 15 minutes (see Fig. 1.4B). After photografting, the irradiated region of the surface became superhydrophilic because of the grafting of hydrophilic AMPS, while the unirradiated background remained superhydrophobic (see Fig. 1.4C). Superhydrophobic-superhydrophilic micropatterns with different geometries could be prepared on the BMA-EDMA surface by using a photomask with the desired patterns (Fig. 1.4D). When the aqueous solutions were

injected into the hydrophilic channels, the solutions would be confined in the hydrophilic channels because of the extremely high wettability difference between the superhydrophilic channel and the superhydrophobic background. These BMA-EDMA based micropatterns have potential applications in the field of microfluidic and diagnostic devices.

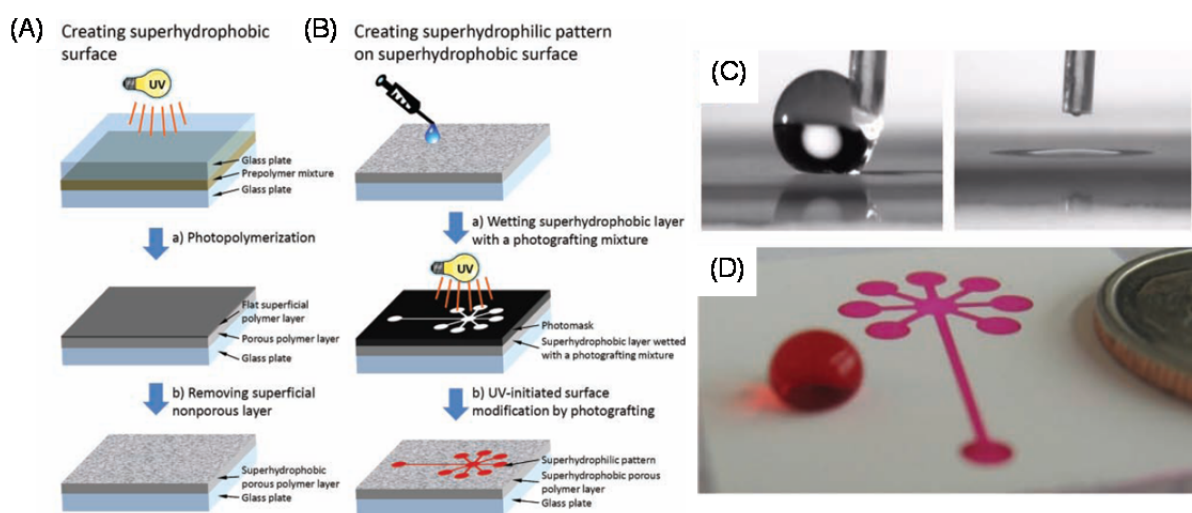


Figure 1.4: (A) Schematic representation of the preparation of the superhydrophobic BMA-EDMA surface. (B) Schematic representation of the preparation of the superhydrophobic-superhydrophilic micropatterns. (C) Water droplet on the superhydrophobic BMA-EDMA surface (left) and AMPS photografted BMA-EDMA surface (right). (D) Superhydrophobic-superhydrophilic micropattern filled with dye solutions. Reproduced with permission.⁴⁰ Copyright John Wiley & Sons.

Geyer et al.³⁸ also reported the preparation of superhydrophobic-superhydrophilic micropatterns based on the photoinitiated surface grafting of polymethacrylate surface. The prepared micropatterns were used to culture HEK-293 cells and it was found that the cells preferred to settle and grow on the hydrophilic region of the pattern because of the existence of “air barriers” on the superhydrophobic region caused by the Cassie-Baxter regime.⁴³ Due to the preferential settlement of the cells on the superhydrophilic part of the pattern, high density cell arrays could be obtained on the superhydrophobic-superhydrophilic micropattern (Fig. 1.5A). The same pattern was later used by Ueda et al.⁴⁴ for the patterning of micro droplets and hydrogels. 3D cell culture in the patterned hydrogel was also demonstrated (Fig. 1.5B). These results suggest that the polymethacrylate based superhydrophobic-superhydrophilic micropattern could be used as a platform for the screening of cells, proteins, drug candidates and some other biologically active compounds. In addition, a similar superhydrophobic-superhydrophilic micropattern based on the porous polymethacrylate was also reported and used for cell-cell communication studies (Fig. 1.5C).⁴⁵

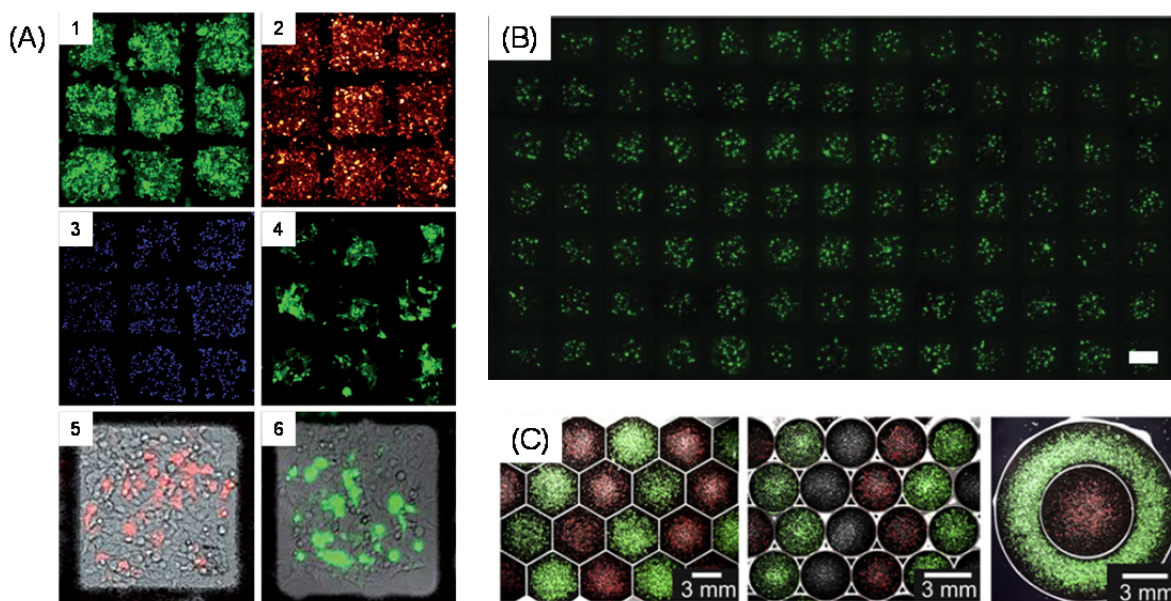


Figure 1.5: (A) Fluorescent microscope images of four different cell lines after 48 hours growing on the superhydrophobic-superhydrophilic patterned HEMA-EDMA surface. (1) MTly-eGFP cells. (2) MTly-mCherry cells. (3) HEK cells, DAPI stained. (4) Hepa cells, eGFP expressing. (5) HEK cells transfected with mCherry plasmid. (6) HEK cells transfected with eGFP plasmid. Reproduced with permission.³⁸ Copyright John Wiley & Sons. (B) Fluorescent HeLa-GFP cells cultured in individual microdroplets for 18 hours. Reproduced with permission.⁴⁴ Copyright Royal Society of Chemistry. (C) Merged bright-field and fluorescence micrographs of different cells patterned in different geometries and in close proximity. Reproduced with permission.⁴⁵ Copyright Elsevier.

1.3.2 Other applications of polymethacrylate monoliths

Porous polymethacrylate were also used for the preparation of superhydrophobic coatings.²⁴ Levkin et al.²⁴ fabricated a porous BMA-EDMA monolith on a glass substrate. By controlling the morphology of the BMA-EDMA monolith, a superhydrophobic surface with a static water contact angle as high as 172° could be prepared.²⁴ The prepared superhydrophobic BMA-EDMA monolith could be further grinded into powder and transferred onto other surfaces as superhydrophobic coatings by using an adhesive tape.

Other applications of the polymethacrylate monoliths, such as support for catalyst, have also been demonstrated.^{17, 46} A porous polymethacrylate monolith is composed of polymer globules and pores with different sizes (meso pores, macro pores and micro pores). Due to the presence of the hierarchical porous structure, the mass transfer and the catalytic activity in catalyst loaded polymethacrylate monoliths could be well balanced. Bandari et al.⁴⁷ prepared the GMA based polymethacrylate by electron beam triggered free radical polymerization and performed pore-size-specific modification¹⁷⁻¹⁸ of the epoxy groups in the pores of the monolith. The epoxy groups in the large pores were hydrolyzed with poly(styrene sulfonic acid). The epoxy groups in the small pores (pore size < 7 nm) were

modified with norborn-5-en-2-ylmethylamine and subsequently anchored with norborn-2-ene (NBE) groups. The NBE groups were then modified with the Grubbs initiator $[\text{RuCl}_2(\text{PCy}_3)_2(\text{CHPh})]$. Later, the pores were grafted with different monomers, such as *N, N*-di-2-pyridyl-norborn-5-ene-2-carboximide. Palladium and platinum nanoparticles were immobilized in the pores of the polymethacrylate monolith through the coordination between the nanoparticles and the di-2-pyridylamide. It was shown that porous polymethacrylate supported catalyst had good catalytic activity and a long lifetime.⁴⁷

2. Materials and methods

2.1 Chemicals and Materials

Sodium hydroxide (98%), Acetic acid (100%), hydrochloride (37%, in water) and Brain Heart Infusion (BHI) broth were ordered from Merck KGaA (Darmstadt, Germany). 3-(trimethoxysilyl)propyl methacrylate (98%), trichloro(1H,1H,2H,2H-perfluorooctyl)silane (97%), butyl methacrylate (BMA, 99%), ethylene dimethacrylate (EDMA, 98%), 2-hydroxyethyl methacrylate (HEMA, 97%), cyclohexanol (99%), 1-decanol (99%), 2,2-dimethoxy-2-phenylacetophenone (DMPAP, 99%), 2-acrylamido-2-methyl-1-propanesulfonic acid (AMPS, 99%), [2-(methacryloyloxy) ethyl]dimethyl-(3-sulfopropyl)ammonium hydroxide (MDSA, 97%), [2-(methacryloyloxy) ethyl]trimethylammonium chloride (META, 80% in water), benzophenone (99%), *tert*-butanol (99.5%), Fluorinert FC-70, 1,2-Dioleoyl-*sn*-glycero-3-phosphoethanolamine (DOPE, 98%) and 2-oleoyl-1-palmitoyl-*sn*-glycero-3-phospho-*rac*-(1-glycerol) ammonium salt (POPG, 97%) were ordered from Sigma-Aldrich (Munich, Germany). 5-cyano-2,3-ditolyl tetrazolium chloride (CTC) was ordered from Polysciences Europe GmbH (Eppelheim, Germany). 4',6-diamidino-2-phenylindol dihydrochloride (DAPI) was ordered from AppliChem GmbH (Darmstadt, Germany). Krytox GPL 100 and Krytox GPL 103 were purchased from H Costenoble GmbH & Co. KG (Eschbom, Germany). Water of MilliQ grade (≥ 99.9 vol%, Millipore, Germany) was in all the experiments.

Nexterion glass B was purchased from Schott AG (Mainz, Germany). Teflon and polyimide sheets were ordered from Durafilm Co. (Holliston, US.).

2.2 Description of experiments and preparation techniques

2.2.1 Activation, modification and fluorination of glass slides

To create anchoring sites for the polymethacrylate surface, Nexterion glasses were first activated by immersion sequentially in 1 M NaOH solution for 1 h and in 1 M HCl solution for 30 min, followed by washing with deionized water and drying with compressed air. To modify the glass slide, 3-(trimethoxysilyl)propyl methacrylate solution in ethanol (20 vol%, adjusted to pH 5 with acetic acid) was dropped on one activated glass slide, which was then covered by another activated glass slide to assist the spreading of the droplets over the whole slide. Care should be taken to avoid trapping of air bubbles between the glass slides. The solution was reapplied after 30 min. After 1 h, the slides were harvested after washing in acetone and drying with compressed air. To fluorinate the glass slide, the activated glass slide was incubated in a vacuumed desiccator (~ 50 mbar) with ~ 50 μ L of trichloro(1H,1H,2H,2H-perfluorooctyl)silane overnight. After incubation, the glass slides were washed with acetone and dried with compressed air.

2.2.2 Preparation of a polymer surface on a glass slide

Poly(butyl methacrylate-*co*-ethylene dimethacrylate) (BMA-EDMA) polymer surfaces with different

surface morphologies (abbreviated as BE1, BE2, BE3, BE4, BE5 and BE6, respectively) were prepared using photoinitiated polymerization. Poly(2-hydroxyethyl methacrylate-*co*-ethylene dimethacrylate) surfaces with different surface morphologies (abbreviated as HM and HN) were also prepared. The compositions of polymerization mixtures for making the surfaces are listed in Table 2.1.

In order to make the polymer surfaces, the polymerization mixture was injected into a mold made of two glass plates, which were separated by two thin strips of polyimide or Teflon (American Durafilm Co.) with a thickness of 50 μm . For making BE1, BE2, BE3, BE4, HM and HN surfaces, two modified glass slides were used. For making BE5 and BE6 surface, one modified glass slide (top plate) and one fluorinated glass slide (bottom plate) were used. The glass slides were then fixed with multiple clamps and placed under the 260 nm UV-lamp (OAI model 30 deep-UV collimated light source (San Jose, CA) fitted with a 500 W HgXe lamp) for 15 min of irradiation. The intensity of the UV irradiation was set at 12 mW/cm². After irradiation, the glass slides were carefully opened with a scalpel. The polymer surface on the upper glass plate was ready for use after washing extensively with methanol, immersing into methanol overnight, and then drying with a nitrogen gun.

Table 2.1: Compositions of the polymerization mixtures for making BMA-EDMA surfaces and HEMA-EDMA surfaces with different morphologies.

Name of the polymerization mixture / produced surface	Composition of the polymerization mixture					
	BMA	HEMA	EDMA	cyclohexanol	1-decanol	DMPAP
Mixture 1 / BE1	20 wt%	0	30 wt%	0	50 wt%	0.5 wt%
Mixture 2 / BE2	20 wt%	0	30 wt%	10 wt%	40 wt%	0.5 wt%
Mixture 3 / BE3	20 wt%	0	30 wt%	20 wt%	30 wt%	0.5 wt%
Mixture 4 / BE4	20 wt%	0	30 wt%	30 wt%	20 wt%	0.5 wt%
Mixture 5 / BE5	20 wt%	0	30 wt%	50 wt%	0	0.5 wt%
Mixture 6 / BE6	40 wt%	0	60 wt%	0	0	1 wt%
Mixture 7 / HM	0	20 wt%	30 wt%	0	50 wt%	0.5 wt%
Mixture 8 / HN	0	20 wt%	30 wt%	30 wt%	20 wt%	0.5 wt%

2.2.3 Photografting of a polymer surface

BE1, BE5, HM and HN surfaces were used as substrates and modified with three different acrylate monomers by photografting. The polymer surfaces were wetted with grafting mixtures and then covered with a fluorinated glass slide. The covered surfaces were then irradiated with 260 nm UV light.

To make surfaces with gradient densities of functional groups, the covered surfaces were placed under a moving UV opaque mask during UV irradiation (See Fig. 3.8B). The overall irradiation time was 5 minutes and the velocity of the moving mask was 1.2 cm/min. The grafted surface was cleaned and stored in methanol after carefully removing the fluorinated glass plate from the surface.

The compositions of the photografting mixtures are listed below:

Photografting mixture 1: 2-acrylamido-2-methyl-1-propanesulfonic acid (AMPS) (16 wt%), 1:3 (v/v) mixture of water : *tert*-butanol (83.75 wt%), ethylene dimethacrylate (1 wt%), benzophenone (0.25 wt%).

Photografting mixture 2: [2-(methacryloyloxy) ethyl]dimethyl-(3-sulfopropyl)ammonium hydroxide (MDSA) (16 wt%), 1:3 (v/v) mixture of water : *tert*-butanol (83.75 wt%), ethylene dimethacrylate (1 wt%), benzophenone (0.25 wt%).

Photografting mixture 3: [2-(methacryloyloxy) ethyl]trimethylammonium chloride (META) (16 wt%), 1:3 (v/v) mixture of water : *tert*-butanol (83.75 wt%), ethylene dimethacrylate (1 wt%), benzophenone (0.25 wt%)

The BE1, BE5, HM and HN surfaces with gradient densities of functional groups prepared using photografting mixture 1 are abbreviated as BE1-AMPS, BE5-AMPS, HM-AMPS and HN-AMPS, respectively. The BE1, BE5, HM and HN surfaces with gradient densities of functional groups prepared using photografting mixture 2 are abbreviated as BE1-MDSA, BE5-MDSA, HM-MDSA and HN-MDSA, respectively. The BE1, BE5, HM and HN surfaces with gradient densities of functional groups prepared using photografting mixture 3 are abbreviated as BE1-META, BE5-META, HM-META and HN-META, respectively.

2.2.4 Lipid modification of a polymer surface and printing of lipid solutions on a polymer surface

Porous BMA-EDMA surfaces with different morphologies (BE1, BE3, BE5 and BE6) were modified with phospholipids. Two phospholipids: 1,2-Dioleoyl-*sn*-glycero-3-phosphoethanolamine (DOPE) and 2-oleoyl-1-palmitoyl-*sn*-glycero-3-phospho-*rac*-(1-glycerol) ammonium salt (POPG), were used for the modification. To modify the surfaces, a few drops of a lipid solution (10 mg/ml in ethanol) were applied on the surface, making sure the surface was completely covered with the lipid solution. After approximately 20 minutes, or until the surface was completely dry, the surface was carefully washed with water and dried gently with a nitrogen gun.

The lipid solutions were printed onto the porous BMA-EDMA surfaces using an OmniGrid100 microarrayer (Genomic Solutions, Ann Arbor, USA) and Arrayit SMP4 pins, which have a pin diameter of 1/16" and uptake and delivery volumes of 0.25 μ L and 1.0 nL, respectively. The pin was dipped into the source well three times for 1000 ms (millisecond) each, then printed onto a blot pad five times with a spacing of 1000 μ m and contact time of 2 ms to get rid of excess solution on the pin

tip before printing onto the superhydrophobic porous BMA-EDMA surface. The contact time for printing onto the hydrophobic BMA-EDMA surface was 0 ms.

2.2.5 Preparation of a sporous polymethacrylate SLIPS surface

An excess amount of the perfluorinated liquids (Krytox GPL 100, Krytox GPL 103 or Fluorinert FC-70) was applied onto porous BMA-EDMA surfaces (BE1 and BE5). The liquids were maintained on the surfaces overnight to fully saturate the pores in the polymer. Afterwards, samples were tilted vertically for 4 h to get rid of excess fluorocarbon lubricant. The prepared surfaces were kept in de-ionized water before using.

2.2.6 Preparation of a polymer surface with a gradient in pore size

A microfluidic chip was used to make the polymer surface with gradient pore size. The microfluidic chip consisted of (1) a micro-structured poly(dimethylsiloxane) (PDMS) part containing a micromixer with two inlets and subsequent reaction chamber for creating the gradient and (2) a modified glass slide sealing the microchannels (Fig. 3.2). The structured part of the microfluidic chip is made from PDMS and subsequently covered with a glass slide using a curing agent coating applied with a stainless steel roller. The assembled chip was cured at 65 °C for 45 min in an oven. Tubes were inserted into the punched holes on the PDMS part. Polyamide tubes (inner diameter 1.5 mm) were used for the inlets and polysulfone tubes (inner diameter 1.5 mm) were used for the outlets. All microstructures on the PDMS part have a height of 680 μm . Zigzag channels of the micromixer have a width of 400 μm . The reaction chamber is 15 mm wide and 19 mm long from the zigzag channels to the outlet. External dimensions of the PDMS part are standardized to the size of a glass slide (26 x 76 mm²). These microfluidic chips were produced and provided by Ludmilla Popp and Kristina Kreppenhofner (IMT, KIT).

The microfluidic chip was connected directly to 20 ml syringes (B. Braun Melsungen AG) filled with polymerization mixtures (Fig. 3.2). Mixture 1 ($\rho = 0.8537 \text{ g/cm}^3$) and Mixture 5 ($\rho = 0.9160 \text{ g/cm}^3$) were injected into the microfluidic chip for the preparation of gradient surface. A syringe pump (Harvard Apparatus PHD Ultra) was used to inject the polymerization mixtures into the microfluidic chip. Both syringes were added on one rider to ensure equal flow rates. The microfluidic chip was mounted below a UV lamp used for polymerization. The microfluidic chips were mounted with the PDMS part on the top. Stabilization of the gradient was ensured by visual observation. UV exposure (260 nm, 12 mW/cm²) started immediately after the pump was stopped. The exposure time was 15 min. After polymerization, the PDMS part was manually removed from the glass slide. The surface of the polymer film was dried with a nitrogen stream. The polymer film was kept in methanol overnight to remove porogens before use.

2.2.7 Bacterial experiments

Clinical wastewater samples were taken from the sewers close to the surgery department and from the

clinic's wastewater collection pipes in a German city. Conventional API 20NE (BioMérieux, Nürtingen, Germany) was used for taxonomic identification. *P. aeruginosa* were grown in the medium (BM2 mineral medium) consisting of 62 mM potassium phosphate buffer (pH 7.0), 7 mM (NH₄)₂SO₄, 2 mM MgSO₄, 10 μM FeSO₄, and 0.4 % (w/v) glucose or 1:4 diluted high nutrient BHI broth (Merck, Darmstadt, Germany). Overnight cultures were used to start the biofilm reactor experiments to analyze the bacterial adhesion on slippery BMA-EDMA surfaces and the impact of PFPE liquid (Krytox GPL 103) on the bacterial growth (toxicity test).

The slippery BMA-EDMA surfaces were incubated with bacterial suspension in an in-house constructed Plug Flow Reactor (PFR) (chamber dimensions length 29.0 cm, inner diameter 4.6 cm) in IFG, KIT. Uncoated glass slides were used as controls for all experiments. The slides were thoroughly washed with ethanol and deionized water and no further modification or treatments were done to the glass slides prior to the bacterial experiments. The biofilm reactor was inoculated with diluted bacterial suspensions ($\sim 10^8$ CFU*mL⁻¹). After a 1 hour static inoculation period, a continuous flow rate of 0.94 mL min⁻¹ was applied and kept for 7 or 14 days at room temperature (22 ± 2 °C). Staining of viable bacteria was performed and the staining was based on intracellular enzymatic reduction of CTC to red fluorescent formazan crystals. For the staining of the total cell count, the DNA specific DAPI staining was applied.⁴⁶ For maximum detection of respiring bacteria, the CTC solution (3.8 mM) was freshly prepared. After culture, the surfaces were removed from the reactor and gently washed with sterile cell wash buffer (5 mM Magnesium acetate, 10 mM Tris, pH 8.0), followed by incubation in the CTC staining solution upon gentle shaking in darkness at room temperature (22 ± 2 °C) for 3 hours. Subsequently, DAPI staining was performed by incubation the surface in DAPI solution (11.4 μM) for 10 minutes. The tested surfaces were washed again with sterile cell wash buffer. The biofilm formation on the surface was analyzed by epifluorescence microscopy with 200-fold magnification using an Axioplan 2 imaging system (Carl Zeiss, Oberkochen, Germany) with the filters sets for CTC (BP 546/12, FT 580, LP 590) and DAPI (G 365, FT 395, BP 445/50). Digital images of each sample were obtained with a Zeiss AxioCAM MRm camera and the AxioVision 4.6 software. The surface coverage of the respiring bacteria (CTC stained, red) of five independent images was determined for each sample with the BioFlux 200 software (Version 2.3.0.2; Fluxion Biosciences/IUL Instruments GmbH, Königswinter, Germany). The bacterial experiments were performed with the help of Dr. Thomas Swartz and Tanja Kleintschek (IFG, KIT).

2.3 Methods and theoretical background

2.3.1 Water contact angle measurement

Water contact angle (WCA) measurements are used to determine the wettability of the surface. A surface with a static water contact angle greater than 90° is defined as a hydrophobic surfaces and a surface with a static water contact angle of less than 90° is called a hydrophilic surface (Fig. 2.1). The water contact angle of a smooth surface can be described using Young's equation (Equation (2.1)),

where γ_{SA} is the surface tension between the surface and air, γ_{SL} is the surface tension between the surface and water and γ_{LA} is the surface tension between water and air.⁴⁸

$$\cos\theta_Y = \frac{\gamma_{SA} - \gamma_{SL}}{\gamma_{LA}} \quad (2.1)$$

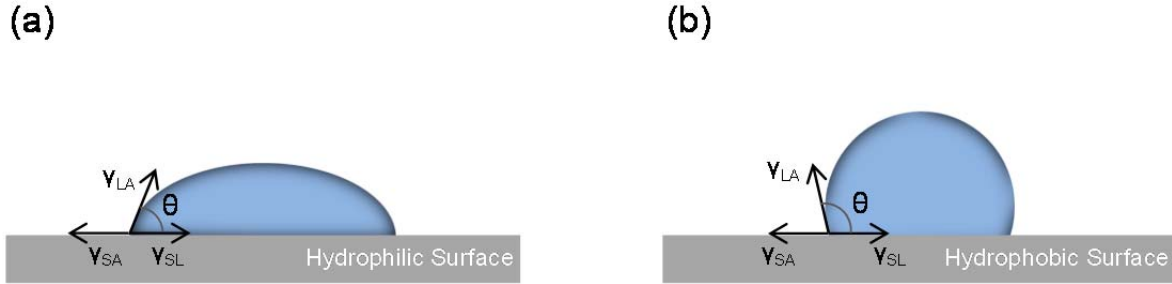


Figure 2.1: Water droplets on smooth (a) hydrophilic and (b) hydrophobic surfaces.

Water contact angles on the rough surfaces were described using either the Wenzel model or Cassie-Baxter model. According to the Wenzel model,⁴⁹ space between the protrusions are filled completely by water when a water droplet is applied on the surface (Fig. 2.2a). The water contact angle on a rough surface is calculated with equation 2.2, in which r is the surface roughness defined as the ratio of the actual surface area to the projected area. In the Cassie-Baxter state, air is trapped inside the porous or rough surface leading to a composite air-solid interface between the water droplet and the surface (Fig. 2.2b). According to the Cassie-Baxter model, the water contact angle on a rough surface is described using equation (2.3), where f_s is the fraction of the solid on the surface, in the Cassie-Baxter model. It is generally believed that the two hydrophobic states (Wenzel state and Cassie-Baxter state) coexist on a rough superhydrophobic surface.⁵⁰⁻⁵¹ The coexistence of the two hydrophobic states on a superhydrophobic surface was directly proven using both cryogenic Scanning Electron Microscope⁵²⁻⁵³ and confocal microscope.⁵⁴

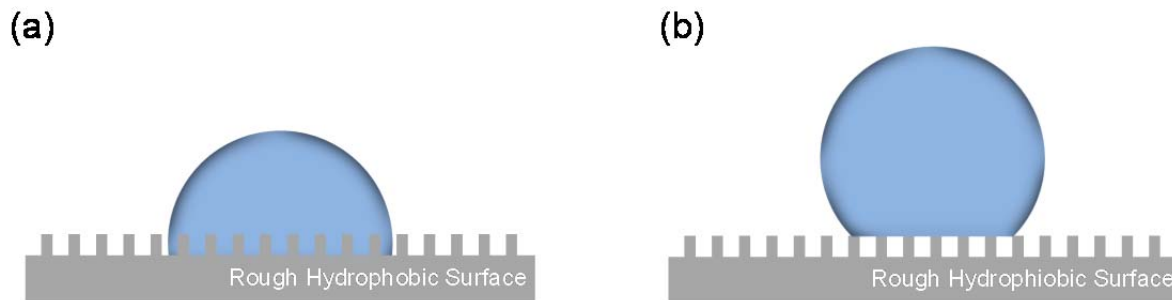


Figure 2.2: (a) Wetted contact line between the water droplet and rough surface (Wenzel state);⁴⁹ (b) Non-wetted state between the water droplet and the rough surface (Cassie-Baxter state).⁴³

$$\cos\theta_W = r * \cos\theta_Y \quad (2.2)$$

$$\cos\theta_{CB} = f_s * (1 + \cos\theta_Y) - 1 \quad (2.3)$$

The sessile drop method and captive bubble method are the most popular methods for water contact angle measurements. Sessile drop method is the most widely used WCA measurement method which uses sessile water droplet for the characterization of WCA. In a captive bubble WCA measurement, an air bubble is formed at the tip of a micro-syringe and pressed to the surface. Advancing WCA and receding WCA can be measured by inflation and deflation of the air bubble, respectively.⁵⁵ Both the sessile drop method and captive bubble method allows for precise and reproducible measurement of static and dynamic WCA.⁵⁶ Although the sessile drop method was considered to be equivalent to the captive bubble method, different WCA (both static and dynamic) values were identified experimentally with these two methods.⁵⁷⁻⁵⁸ To understand such difference, Marmur et al. performed theoretical calculation using a model surface which was chemically heterogeneous and smooth. It was concluded that the measured advancing and receding WCA on the surface with low WCA depended greatly on the volume of the air bubble used in the captive bubble method.⁵⁹ Therefore, it was suggested that the sessile drop method is used for the low WCA surface.⁶⁰ While for a heterogeneous smooth surface with high WCA, the captive bubble is recommended.⁶⁰ Comparison of the sessile drop method and captive bubble method on a homogeneous and rough surface was reported recently.⁶¹ It was found that the asymmetry of the surface features significantly influenced the fluctuation of the WCA results for both methods and the measuring method for the low fluctuation WCA measurement was also provided in different cases.⁶¹

In this thesis, water contact angles were measured using the sessile drop method with a home-built water contact angle measurement device. Static water contact angle and dynamic water contact angles (advancing water contact angle and receding water contact angle) on the surfaces were measured. For the static water contact angle measurement, 3 μ L of deionized water was used. For the advancing and receding water contact angle measurements, the increasing or decreasing rate of the water volume was controlled with a syringe pump (Microliter Flow Modular Pump Component, HarvardAppartus, Inc. US.) and set at 12 μ L/min. Pictures of the water droplets on the surface were taken with a UK 1115 digital camera (EHD imaging, Germany). Image J software with the Dropsnake plug-in was used to analyze the images. The reported water contact angle values are the average of at least three WCA values from individual experiment. Standard deviations of the water contact angle values were also reported.

2.3.2 Scanning electron microscopy

The scanning electron microscope is an electron microscope that images the sample using a high energy focused beam of electrons. During the imaging process, the electron beam scans the surface in a raster way. The electrons are scattered and the current leaving the sample is collected, amplified and

used for characterization of the sample properties.⁶² Backscattered electrons, secondary electrons, auger electrons and characteristic X-rays are generated from the sample upon interaction with the incident electron beam. X-rays were used primarily for chemical analysis of the sample while the secondary electrons and the backscattered electrons were used mainly for imaging of the sample.⁶³ The setup of a typical SEM is shown in Fig. 2.3.

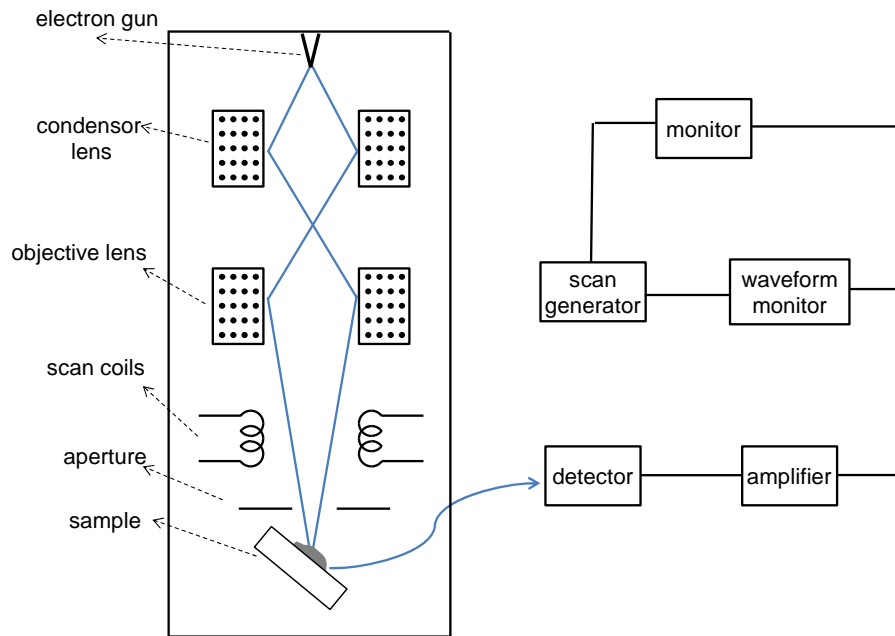


Figure 2.3: Schematic diagram showing the main components of a scanning electron microscope (redrawn from reference⁶³).

The theoretical resolution of the electron microscope can be estimated with equation (2.4),⁶³ where α is the semi-angle through which the electron beam is reflected, μ is the refractive index of the medium between the object and the objective length and λ is the wave length of the electron beam. $\mu * \alpha$ is usually called the numerical aperture (NA).

$$r = \frac{0.61\lambda}{\mu * \alpha} \quad (2.4)$$

$$h = \frac{0.61\lambda}{\alpha^2} \quad (2.5)$$

Assuming an electron beam of 100 kV is used and $\alpha=0.1$ radians, the theoretical resolution of the electron microscope is 0.02 nm.⁶³ Although the theoretical resolution of the electron microscope could not be achieved due to the lens aberrations, SEM still offers much higher resolution compared to a light microscope. The very small angular aperture of the electron microscope permits a large depth of field in focus at once, according to equation (2.5). As a result, the rough samples may be seen in focus across the whole sample with the electron microscope at low magnification.⁶⁴

In this thesis, the SEM measurements were performed on a LEO 1530 Gemini scanning electron

microscope (Zeiss, Germany). The accelerating voltage was 2 kV or 5 kV for the measurement. The samples were sputtered with a ~ 30 nm thick gold layer using a Cressington108 auto sputter coater (Cressington Scientific Instruments Ltd. UK) before the SEM measurements. The SEM images of the porous polymer surfaces were analyzed using Image J software to quantify the pore size and globule size of the surfaces. The reported pore size and globule size is the average size of at least 20 pores and globules chosen from a representative SEM image of the surface.

2.3.3 X-ray photoelectron spectroscopy

X-ray photoelectron microscopy (XPS), also known as Electron Spectroscopy for chemical analysis, is a highly sensitive technique for surface analysis. The basic components of XPS component is the X-ray source, extraction optics, energy filter and detection system. The X-ray tubes (monochromatic sources or standard sources) or synchrotron sources are used as the X-ray sources for XPS. During XPS measurement, a sample is irradiated with the X-ray. Upon X-ray irradiation, photoelectrons are emitted from the sample. Energy conservation of the photoemission process can be described using Equation (2.6), where $E_{h\nu}$ is the energy of the X-ray, E_k is the kinetic energy of the emitted photoelectron, E_ϕ is the work function of the analyzer and E_b is the binding energy. E_k can be measured with an energy analyzer and E_ϕ is constant and known for a certain system. Therefore, the binding energy (E_b), which is element specific, can be determined using Equation (2.6).

$$E_{h\nu} = E_k + E_\phi + E_b \quad (2.6)$$

Although X-rays can penetrate micrometers below the surface, only photoelectrons produced at the surface (within 10 nm or less below the surface) contribute to the XPS signals due to the limited electron mean path. Therefore, XPS is highly surface specific. The sensitivity of the XPS measurement is mainly dependent on the spectra background level and the photoelectron cross section, which is element specific.⁶⁵ In general, a high sensitivity (concentration down to 0.1 atomic%) can be achieved in XPS measurement.⁶⁵

The XPS spectra in section 3.3 were taken on the VG SCienta R4000 UHV-IR/XPS spectrometer (Bruker, Karlsruhe, Germany) with the help of Dr. Hikmet Sezen at IFG, KIT. The XPS spectra in section 3.2 and 3.4 were collected on the Leybold-Heraeus MAX200 XPS spectrometer (Leybold-Heraeus GmbH, Germany) with the help of Hao Lu at APC, University of Heidelberg.

2.3.4 Photoinitiated free radical polymerization

Polymerization initiated by free radical species produced from initiators is called free radical polymerization. Thermal initiators, redox initiators and photoinitiators are commonly used to initiate the free radical polymerization. During the free radical polymerization, reactive centers are generated from the excited initiator and polymerization proceeds by the propagation of the reactive center by successive additions of monomer molecules. The growth of the polymer is terminated by elimination

of the reactive center. The elimination of the reactive center occurs by combination of two reactive center or combination of a reactive center and an initiator radical. Free radical polymerization of vinyl monomers are shown as an example in Fig. 2.4.

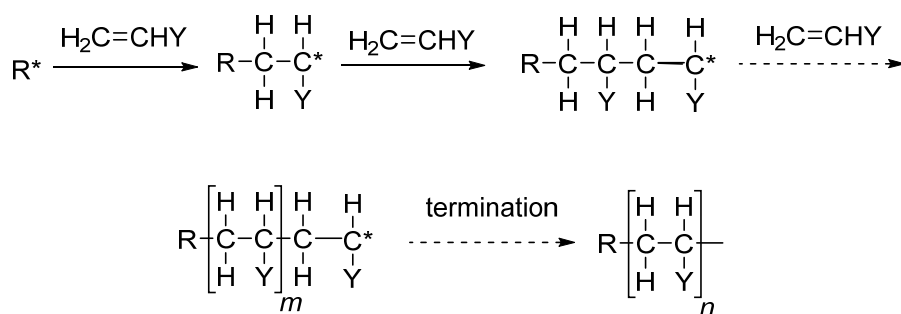


Figure 2.4: Scheme showing the initiation, propagation and termination of free radical polymerization of vinyl monomers.

Photoinitiated free radical polymerization offers several advantages compared to other free radical polymerization methods such as thermally initiated polymerization. First of all, photoinitiated free radical polymerization can be started or stopped on demand by turning on or off the irradiation source. Secondly, spatial control of the polymerization can be achieved using photoinitiated free radical polymerization. Furthermore, photoinitiated free radical polymerization is particularly useful in some biological applications because the polymerization can be carried out at room temperature.⁶⁶ Due to these advantages, photoinitiated free radical polymerization has been widely used in many applications. The production of free radicals in the photoinitiated free radical polymerization is based on one of the two pathways: (1) the photoinitiator (type I) is excited by energy absorption and decomposes into free radicals because of the excitation; (2) the photoinitiator (type II) is excited and the excited species interacts with a co-initiator (hydrogen donors) to form the free radicals (Fig. 2.5).⁶⁷ The schematic representation of the free radical formation during photoinitiated polymerization is shown in Fig. 2.5 A and Fig. 2.5B. Benzoin and its derivatives, which undergo the α cleavage to form two radical species, are the most common type I photoinitiators. Other type I photoinitiator include α -dialkoxyacetophenone, α -hydroxyalkylphenone, acylphosphine oxides and etc. Benzophenone and its derivatives, thioxanthone, benzyl, quinones and organic dyes (in combination with the hydrogen donors such as alcohols, ethers, amines and thiols) are frequently used as type II photoinitiators.⁶⁸ Some of the commercially available photoinitiators are listed in Fig. 2.5C. In this thesis, 2,2-dimethoxy-2-phenylacetophenone (type I) was used as the photoinitiator.

The major drawback of photoinitiated free radical polymerization is that polymerization may take place only on the surface due to the penetration depth of the light into material is limited.⁶⁶ To ensure homogeneous polymerization in the bulk material, high energy light sources are usually used for the photoinitiated polymerization. In this thesis, high intensity UV light (260 nm, 12 mW/cm²) was used

to perform the polymerization and photografting. The detailed procedure for the preparation of the polymer surface is described in section 2.1.2.

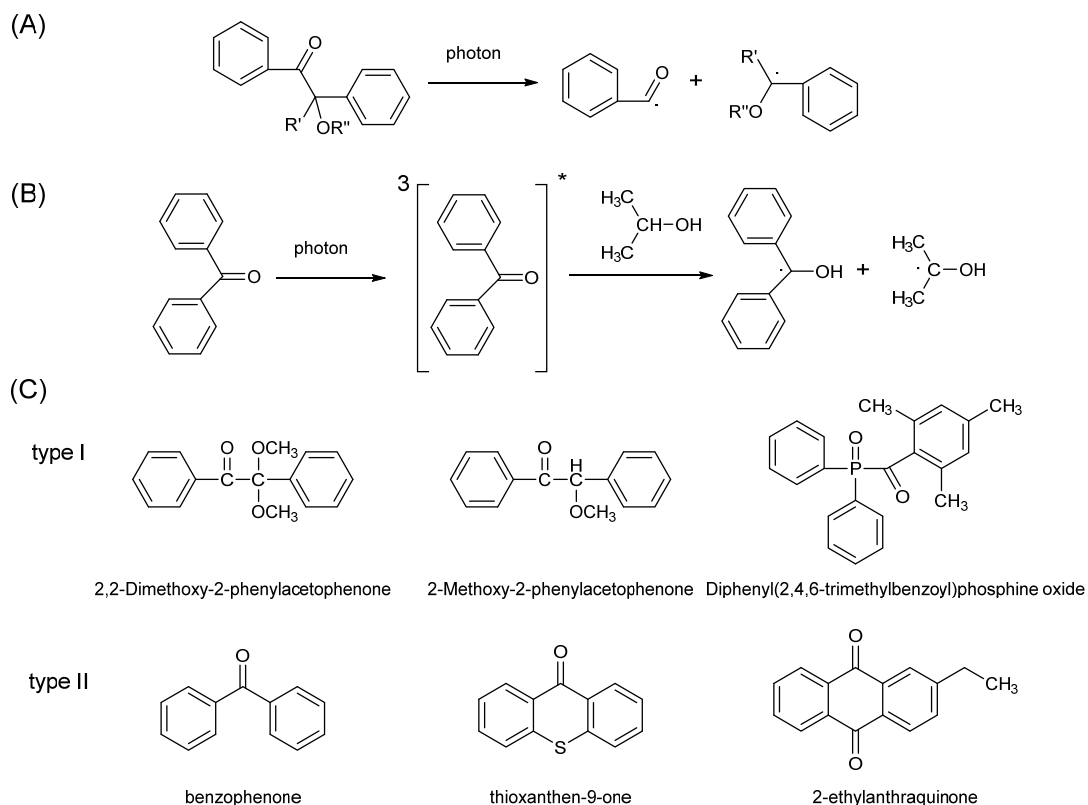


Figure 2.5: Scheme showing the production of the free radicals from (A) type I and (B) type II photoinitiators and (C) examples of commercially available photoinitiators.

2.3.5 Surface modification via photografting

Photografting, also termed as photoinitiated graft-polymerization, is an efficient and versatile method for photoinitiated modification of polymer surfaces.^{35, 69-70} Modification of polymer surface, such as natural rubber,⁶⁹ nylon and polypropylene film using photografting was demonstrated.³²⁻³³ Ranby et al.³⁴ proposed that the photoinitiator could be excited to a singlet state (S_1) and subsequently transform to the triplet state (T_1) by intersystem crossing in the presence of UV light. The triplet species can abstract hydrogen from the polymer surface and lead to the formation of radicals on the surface. The grafting polymerization from the surface occurs because of the presence of radicals on the surface (Fig. 2.6). Branched and crosslinked polymer chains are formed on the surface after photografting. The efficiency of the photografting is dependent on many factors, such as the chemistry of the polymer substrate, chemistry of the reactive vinyl monomers, type and concentration of the photoinitiator.³³ Therefore, the photografting system should be carefully designed to achieve a higher efficiency. The method for photografting of polymethacrylate monoliths has been well established.^{24, 37-40, 71-74} In this

thesis, benzophenone was used as the initiator and a mixture of *tert*-butanol and water as the solvents for the monomers and initiator. The detailed procedure for the photografting of the polymethacrylate surface is shown in section 2.1.3.

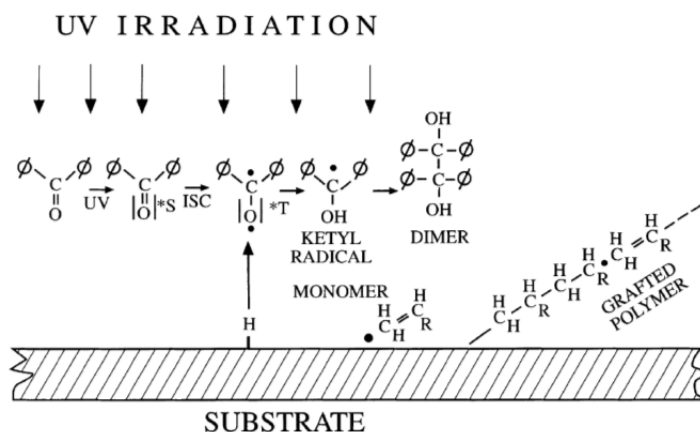


Figure 2.6: Schematic representation of photografting a vinyl monomer onto a polymer substrate in the presence of photoinitiator. Reproduced with permission.³⁴ Copyright Elsevier.

2.3.6 Hard X-ray phase contrast tomography

With the development of highly brilliant and coherent X-ray sources, X-ray imaging techniques have been widely used as a powerful tool for imaging the internal microstructures of materials non-destructively.⁷⁵⁻⁷⁸ In general, X-ray imaging is based on either the generated absorption contrast or phase contrast when the X-ray passes through the material.⁷⁹⁻⁸⁰ The absorption contrast arises mainly from the attenuation differences of the materials while the phase contrast mainly results from the phase shift of the X-ray wavefront induced by material density variations. However, there is little absorption of X-rays and therefore poor image contrast for light materials such as polymers. In comparison, the phase contrast techniques provide much higher imaging contrast because they are much more sensitive to the density variations compared to the attenuation based technique. Therefore, phase contrast X-ray imaging was widely used for imaging of low X-ray adsorptive materials.^{79, 81} Several of the phase contrast methods for X-ray imaging, such as propagation-based imaging (PBI),⁸²⁻⁸³ analyzer-based imaging (ABI)⁷⁹ and grating interferometry (GI),⁸⁴ have been developed so far. In this thesis, the PBI method was used to image the SLIPS BMA-EDMA surfaces. The setup of the imaging system is shown in Fig. 2.7.

The imaging experiments were carried out on the nano-imaging endstation ID22 at the European Synchrotron Radiation Facility (ESRF, SI2552) with Yin Cheng (IPS, KIT) and Heikki Suhonen (ESRF). The X-ray beam was monochromatized and focused using X-ray reflective optics to a spot size of 50*50 nm². The pink beam with energy of 29.6 KeV was used for imaging. The sample was placed behind the focal spot and imaged onto a scintillator screen and a CCD camera at a fixed distance downstream of the focal spot. Phase contrast images were obtained and inputted into a

tomographic reconstruction algorithm based on filtered back projection. Slippery BMA-EDMA surface was prepared on 1 mm thick PMMA substrates. To prevent the evaporation of the PFPE liquid layer caused by the heat generated during the measurement, the BMA-EDMA SLIPS surface was fixed vertically in water in a closed PMMA vial (inner diameter 5 mm, Eppendorf, Germany) during the test. The image reconstruction in this thesis was done by Yin Cheng (IPS, KIT) and Heikki Suhonen (ESRF).

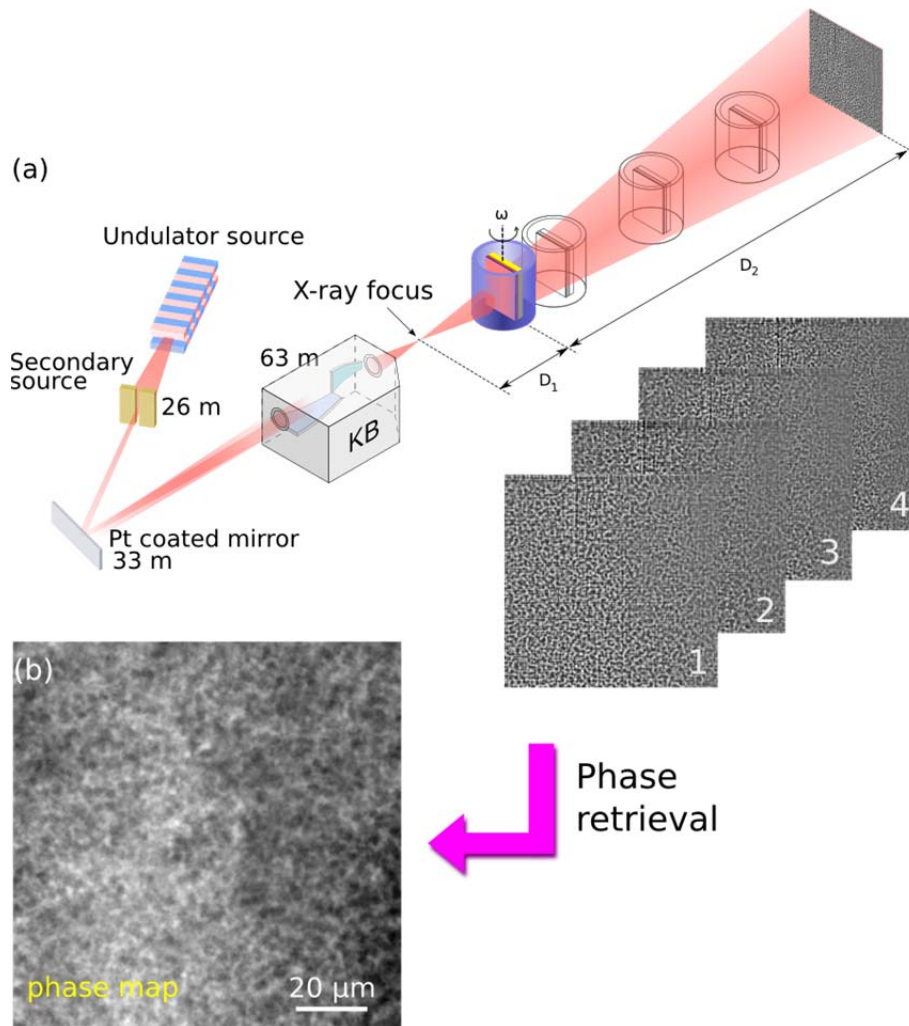


Figure 2.7: Schematic representation of the (a) imaging setup and (b) data reconstruction.

3. Results and discussion

3.1 Formation of porous polymethacrylate polymer surfaces with gradient morphology

3.1.1 Background

Surface porosity has been shown to have a significant influence on cell behavior.⁸⁵⁻⁸⁶ Surfaces with continuous varying pore size along one direction offer the possibility to avoid difficulties associated with the one-sample-for-one-measurement approach and sample variations in cell screening studies. Furthermore, they can increase the throughput and reduce the sample consumptions of the screening studies. However, up to now, there are only few methods reported for the preparation of a surface with a gradient in pore size. Collins et al.⁸⁷ described a method for the preparation of gradient porous silicon films using electrochemical etching in hydrofluoric acid. The pore size of the prepared silicon surface ranged from < 10 nm to > 500 nm. Later, this method was used to prepare silicon surfaces with a gradient of pore sizes for studying the effect of surface morphology on the adhesion/differentiation of neuroblastoma cells⁸⁸ and mesenchymal stem cells⁸⁹ on the surface. Woodfield et al.⁹⁰ presented a 3D fiber deposition technique to produce polymer scaffolds mimicking the organization of an articular cartilage with pore sizes increasing from 200 to 1650 μm . Oh et al.⁹¹ used centrifugal forces to fabricate cylindrical scaffolds with gradient pore sizes ranging from 88 to 405 μm .

In this section, a microfluidic chip enabling the fabrication of porous polymethacrylate surfaces possessing gradients of pore sizes in the range between tens of nanometers to sub-micrometer is described. The method is based on the ability to precisely control the morphology of a porous polymethacrylate by varying the composition of porogenic solvents in the polymerization mixture. Using a microfluidic cascade micromixer, a thin film of polymerization mixture possessing a gradient of porogenic component is created. Subsequent UV-initiated polymerization of the film results in a porous polymer surface with a gradient in pore size.

3.1.2 Preparation of porous polymer surfaces with different morphologies

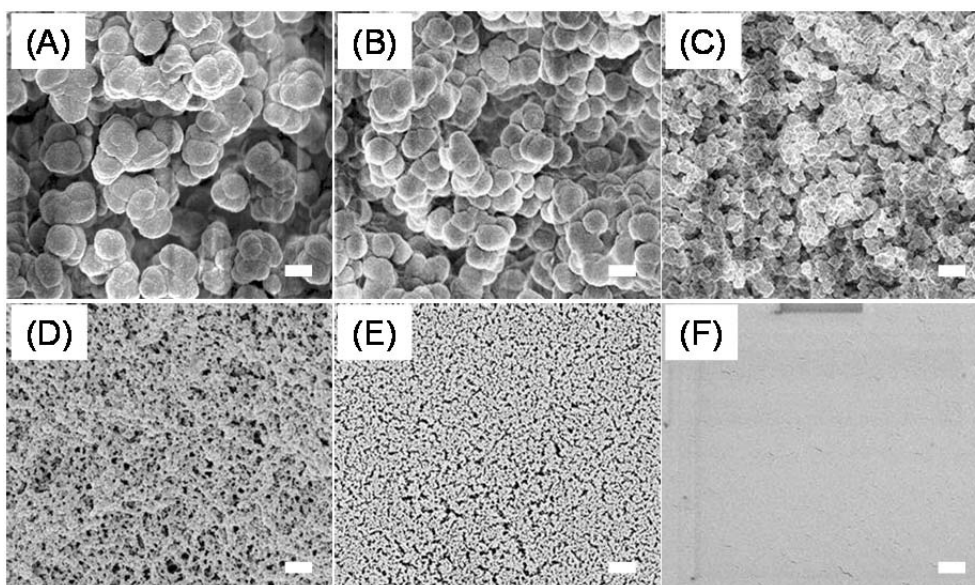


Figure 3.1: SEM images of the (A) BE1, (B) BE2, (C) BE3, (D) BE4, (E) BE5, (F) BE6 surface (scale bar 1 μm).

BMA-EDMA surfaces were prepared on glass substrates by using polymerization mixtures with different porogen compositions (see Tab. 2.1). The total porogen content was kept at 50 wt% in all the polymerization mixtures. The morphologies of these BMA-EDMA surfaces were investigated with SEM (Fig. 3.1). It was found that the BMA-EDMA surfaces prepared from the polymerization mixture containing porogens showed porous and globular morphology and the surface morphology was highly dependent on the composition of the porogens in the polymerization mixture. When 1-decanol was used as the sole porogen in the polymerization mixture, a porous surface (BE1) with a globule size of $\sim 1 \mu\text{m}$ was obtained. When cyclohexanol was used as the only porogen in the polymerization mixture, a porous surface (BE5) with globule size and pore size in the range of tens of nm was obtained. With the decrease of 1-decanol content and increase of cyclohexanol content in the polymerization mixture, the pore size of prepared surface decreases gradually. Morphologies of the surfaces were quantified by measuring the pore size and globule size with the SEM images (see Tab. 3.1). These results suggested that a BMA-EDMA polymer surface with gradient morphology could be prepared if the composition gradient of the porogens content could be generated.

The water contact angles on the BMA-EDMA surfaces were also measured (see Tab. 3.1). It was found that the BM1, BM2, BM3 and BM4 surfaces were highly hydrophobic. The high hydrophobicity of these surfaces resulted from the combination of the surface roughness and hydrophobic nature of the polymer globules. In contrast, the BE5 surfaces are much less hydrophobic because of the low roughness on the surface. As shown in the table, the pore size and the globule size of the BMA-EDMA gradually decrease with the increase of cyclohexanol content in the polymerization mixture.

Table 3.1: Globule size, pore size and water contact angles of the BE1, BE2, BE3, BE4, BE5 and BE6 surfaces. (“NP” means the surface is non-porous.)

	BE1	BE2	BE3	BE4	BE5	BE6
Globule size / μm	1.14 ± 0.17	0.99 ± 0.15	0.21 ± 0.06	0.15 ± 0.04	0.12 ± 0.04	NP
Pore size / μm	0.59 ± 0.24	0.53 ± 0.16	0.10 ± 0.05	0.07 ± 0.03	0.07 ± 0.02	NP
Static WCA / $^\circ$	138.6 ± 1.0	137.1 ± 2.8	142.5 ± 1.2	141 ± 3.2	110.4 ± 3.5	69.9 ± 2.4
Advancing WCA / $^\circ$	160.8 ± 1.5	159.8 ± 1.4	158.7 ± 3.4	162.2 ± 1.8	133.9 ± 1.4	81.7 ± 2.4
Receding WCA / $^\circ$	102.3 ± 8.0	103.0 ± 7.2	108.2 ± 5.8	110.8 ± 11.2	78.2 ± 3.4	57.7 ± 1.6

3.1.3 Preparation of porous polymer surface with a gradient in pore size using microfluidic chips

To generate a composition gradient of the porogens, a microfluidic chip composed of a glass slide and PDMS chamber (Fig. 3.2(A)) was used in this study. The PDMS chamber was prepared by using a steel master shown in Fig. 3.2(B). One possible concern for the application of PDMS materials is the poor compatibility between PDMS and organic solvents.⁹² The compatibility between PDMS and different solvents was predicted by comparing the solubility parameter of PDMS ($\sim 7.3 \text{ cal}^{1/2} \cdot \text{cm}^{-3/2}$) with that of the solvents. Generally, solvents that have solubility parameter (ranging from $7.3 \text{ cal}^{1/2} \cdot \text{cm}^{-3/2}$ to $9.5 \text{ cal}^{1/2} \cdot \text{cm}^{-3/2}$) similar to that of PDMS were thought to be less compatible with PDMS.⁹³ Here, a polymerization mixture composed of butyl methacrylate, ethylene dimethacrylate and 1-decanol (or cyclohexanol) was used. Alcohols generally have a good compatibility with PDMS⁹³ and the reported solubility parameter for butyl methacrylate is $9.61 \text{ cal}^{1/2} \cdot \text{cm}^{-3/2}$.⁹⁴ Therefore, it was expected that the polymerization mixtures used here would have a good compatibility with PDMS.

In order to produce a porous polymer surface possessing a gradient of pore sizes, two different polymerization mixtures (Mixture 5 and Mixture 1) were pumped into the chip from the two inlets (Fig. 3.2(C) a). Mixture 5 containing cyclohexanol as a porogen forms a porous polymer surface with pore diameters in the range of tens of nanometers after polymerization. The use of 1-decanol (mixture 1) as the sole porogenic solvent gives a porous polymer surface with the average globule size in the range of 1-2 μm . The two mixtures were pumped into the chip at the flow rate of 0.25 ml/min or 7.5 ml/min for 30 s to fill the whole chamber. All flow rate values reported in the section refer to the flow rate applied at one inlet of the micro-mixer. UV-initiated polymerization started immediately after stopping the syringe pump. A polymer film was formed in the microfluidic chamber after 15 minutes of polymerization. The chip was then opened and a porous polymer surface was obtained on the glass substrate (Fig. 3.2(C) b). The prepared surfaces had external dimensions of $12 \times 15 \text{ mm}^2$

and a thickness of $\sim 450 \mu\text{m}$. The deviation of the polymer thickness from the height of the microfluidic chamber ($680 \mu\text{m}$) was probably caused by the shrinkage of the porous polymethacrylate, which has been observed in other applications of the porous polymethacrylate in chromatography.⁹⁵ Another possible reason for the reduced thickness of the polymethacrylate film could be swelling of PDMS induced by the polymerization mixture. Absorption of some organic solvents by PDMS was reported before.^{92, 96}

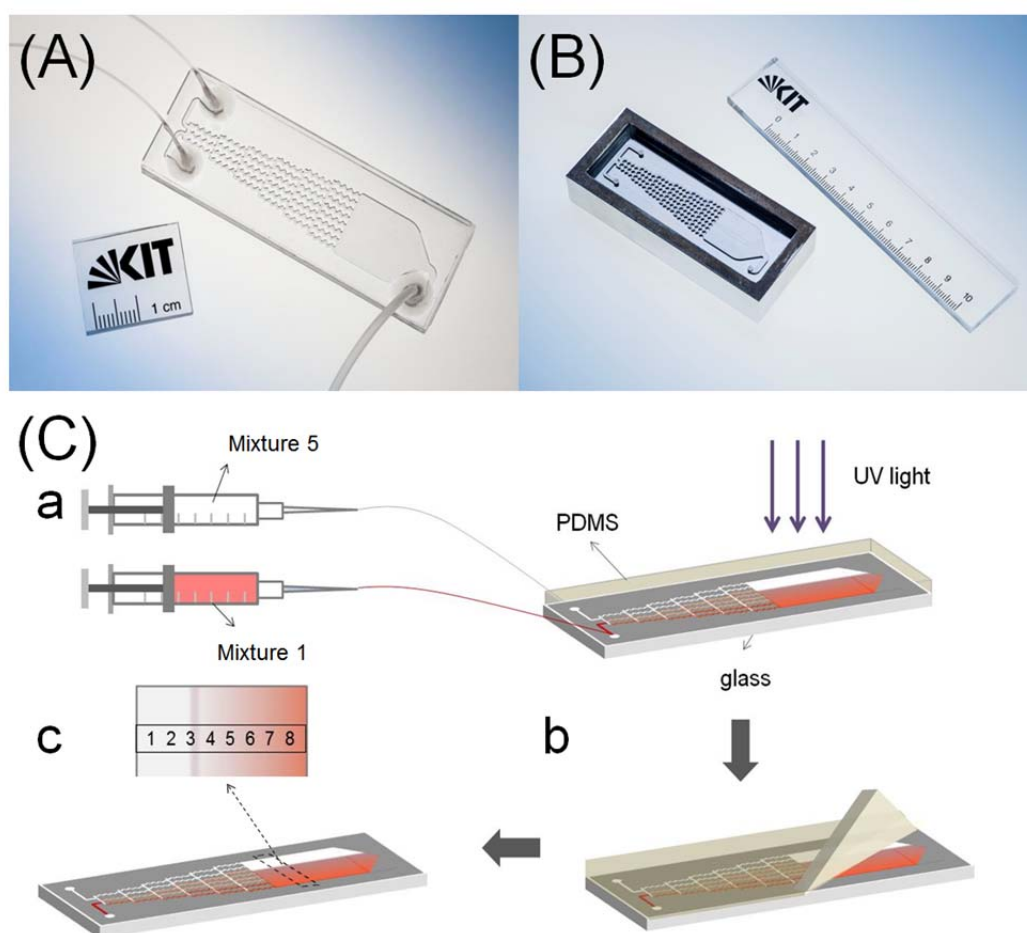


Figure 3.2: (A) A PDMS microfluidic chip for generating gradient polymer films. (B) Micro-milled aluminum master structure with cascade micro-mixer (left side) and subsequent reaction chamber (right side). The frame allows for a reproducible thickness of the replicated PDMS parts. (C) Fabrication of a polymer gradient film using the microfluidic chip. a: Polymerization mixtures were injected into the microfluidic chip by syringe pump building a gradient. The mixture in the reaction chamber was then exposed to UV light for polymerization. b: Removal of the PDMS part of the microfluidic chip. c: Resulting gradient polymer film on the glass slide.

The morphology of the porous surface was analyzed by SEM at two different positions of the polymer film: at the surface (see Fig. 3.3 and Fig. 3.4) and at the cross section roughly $50 \mu\text{m}$ below the surface (see Fig. 3.6). Images were taken at eight equidistant points along the gradient direction 10 mm down the reaction chamber (see Figure 3.2(C)c). One set of surface SEM images (flow rate 0.25 ml/min) is

shown in Fig. 3.3. The SEM images show a highly porous polymer structure with a gradient of roughness from micro- to nanoscale.

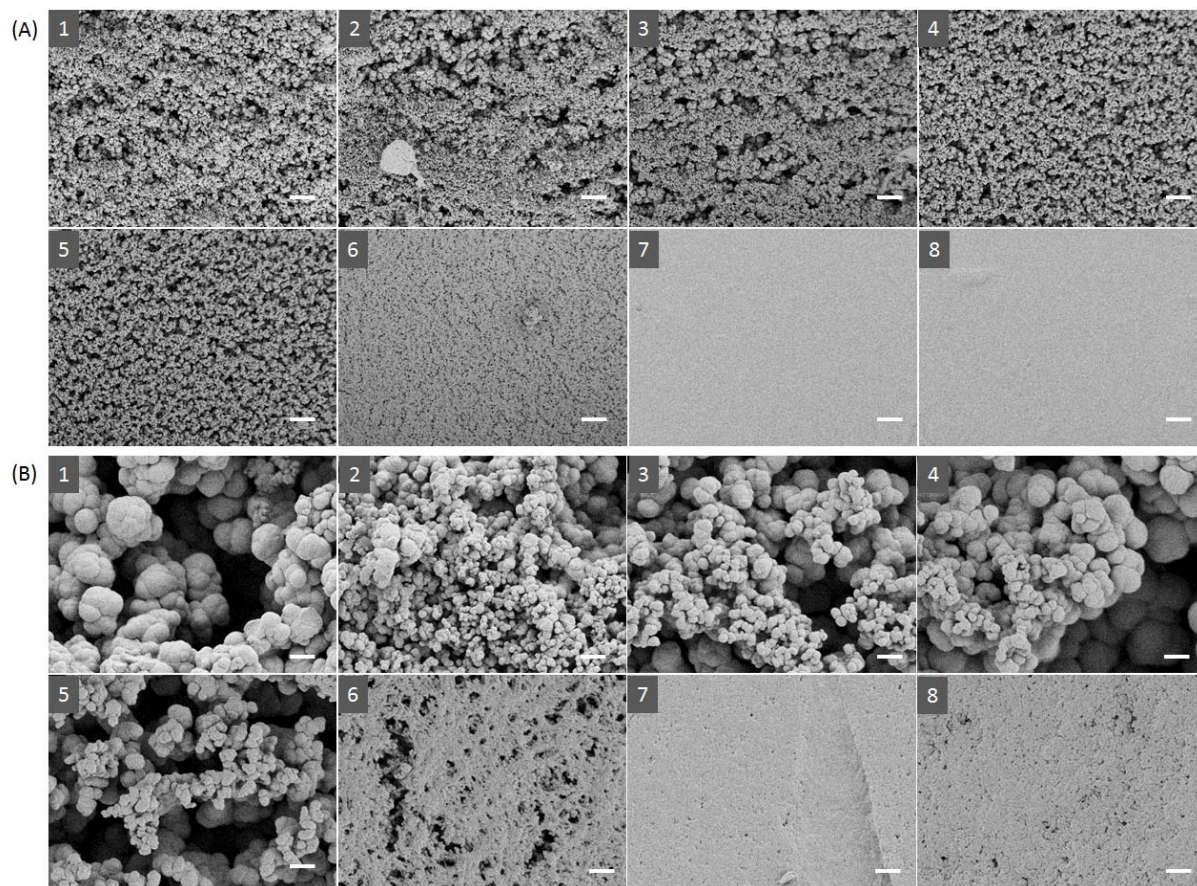


Figure 3.3: Scanning electron microscopy (SEM) images of the poly(butyl methacrylate-*co*-ethylene dimethacrylate) surface with a gradient of porous morphology. The polymer surface was generated inside a microfluidic chip with a flow rate of 0.25 mL/min. (A) low magnification (scale bar 20 μm) and (B) high magnification (scale bar 2 μm) SEM images. The SEM images are taken on the surface of the polymer.

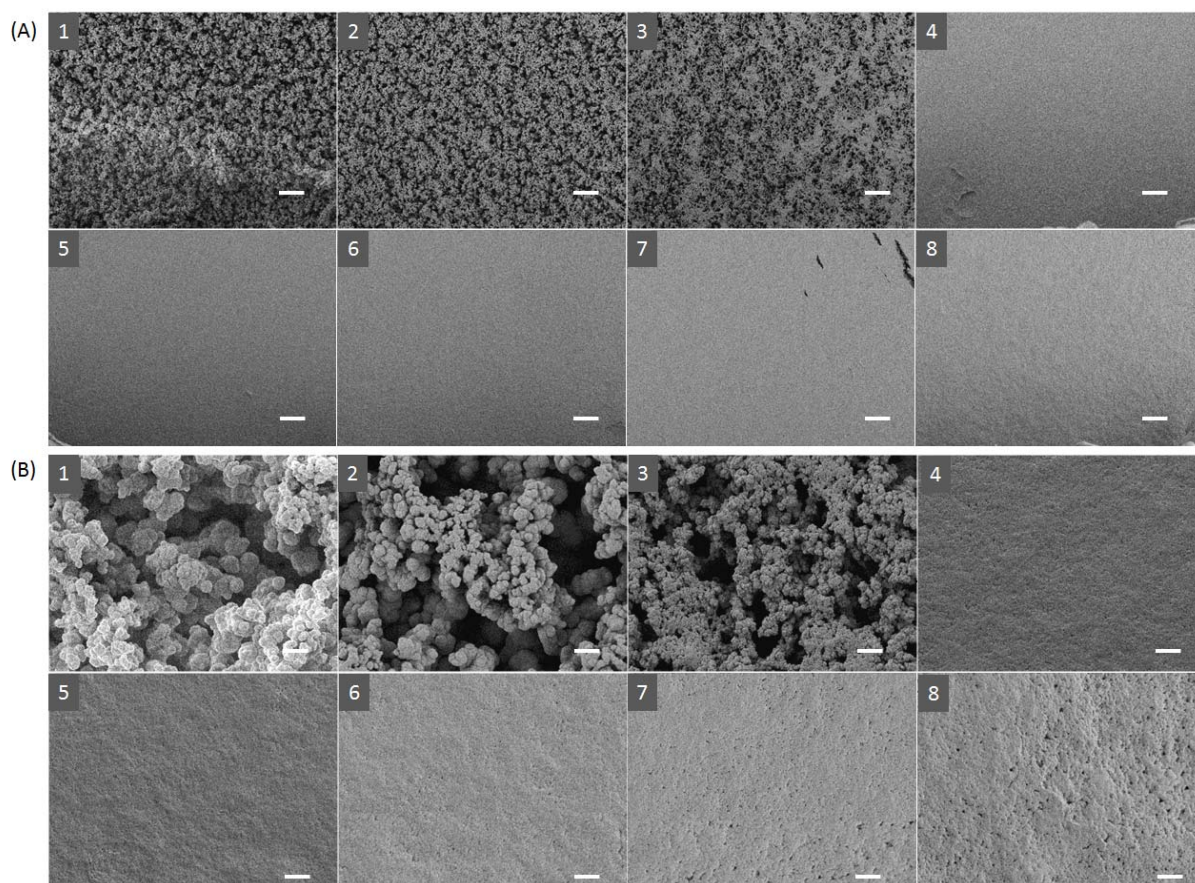


Figure 3.4: SEM images of a poly(butyl methacrylate-*co*-ethylene dimethacrylate) surface with a gradient of porous morphology. The polymer surface was generated inside a microfluidic chip with a flow rate of 7.5 ml/min at (A) low magnification (scale bar 20 μm) and (B) high magnification (scale bar 2 μm) SEM images. The SEM images are taken on the surface of the polymer.

Both the pore sizes and polymer globule sizes were quantified using the SEM micrographs (see Tab. 3.2 and Fig. 3.5). Polymer globule sizes and pore sizes were measured from representative SEM micrographs manually with Image J software. Three polymer surfaces were analyzed for each flow rate (0.25 ml/min and 7.5 ml/min). The average values of globule and pore sizes are summarized in Table 3.2 and plotted in Fig. 3.5 and Fig. 3.6C. For the polymer surface produced using low flow rate (0.25 mL/min), the mean globule sizes at the cross section (50 μm below the surface) range from $1.60 \pm 0.37 \mu\text{m}$ to $0.16 \pm 0.04 \mu\text{m}$ in a clear gradient way. For the polymer surface produced using a high flow rate (7.5 mL/min), the mean globule size at the cross section (50 μm below the surface) decreases from $1.61 \pm 0.34 \mu\text{m}$ to $\sim 0.16 \pm 0.04 \mu\text{m}$ in a steep gradient, which is consistent with the reduced diffusion time in this case. The SEM micrographs obtained at the surface of the porous polymer film revealed a similar gradient of the porous structure along the width direction of the polymer films, which was also dependent on the flow rate. Higher flow rate would lead to the formation of sharp step-like pore/globule size gradient while the low flow rate will lead to the formation of a shallower pore/globule size gradient in the polymer film. For some positions on the gradient surfaces (e.g.

positions 2 and 3 for surfaces produced at 0.25 ml/min flow rate (see Fig. 3.3) and position 3 for the surface made at 7.5 ml/min flow rate (see Fig. 3.4)), the formation of a hierarchical surface morphology with the incorporation of smaller polymer globules at the polymer surface was observed. This phenomenon may be explained by a stronger absorption of 1-decanol (“micro porogen”) by the PDMS layer leading to a localized increase of the concentration of cyclohexanol (“nano porogen”) at the interface between PDMS and the layer of the polymerization mixture. It was also observed that the polymer surface had a smaller globule/pore size on the surface than in the bulk. This is in agreement with the previous observation that the morphology of the polymer at the superficial layer was dependent on the interface being in contact with the polymerization mixture.^{38,40} The superficial layer of the porous polymer film can be removed by using an adhesive tape.²⁴

Table 3.2: Globule size and pore size distribution of the poly(butyl methacrylate-*co*-ethylene dimethacrylate) surfaces prepared using flow rate of 0.25 ml/min and 7.5 ml/min.

	Flow rate	Size	Position 1	Position 2	Position 3	Position 4	Position 5	Position 6	Position 7	Position 8
surface	0.25 ml/min	globule size/ μm	0.46 \pm 0.03	0.43 \pm 0.03	0.37 \pm 0.07	0.35 \pm 0.17	0.30 \pm 0.12	0.23 \pm 0.10	0.19 \pm 0.08	0.19 \pm 0.03
		pore size/ μm	0.27 \pm 0.02	0.26 \pm 0.03	0.25 \pm 0.06	0.24 \pm 0.05	0.21 \pm 0.11	0.18 \pm 0.08	0.14 \pm 0.01	0.12 \pm 0.04
	7.5 ml/min	globule size/ μm	0.43 \pm 0.05	0.41 \pm 0.16	0.35 \pm 0.10	0.16 \pm 0.03	0.15 \pm 0.02	0.14 \pm 0.02	0.14 \pm 0.02	0.15 \pm 0.04
		pore size/ μm	0.24 \pm 0.01	0.24 \pm 0.04	0.24 \pm 0.05	0.16 \pm 0.05	0.10 \pm 0.02	0.10 \pm 0.01	0.08 \pm 0.01	0.11 \pm 0.02
~ 50 μm below the surface	0.25 ml/min	globule size/ μm	1.60 \pm 0.37	1.46 \pm 0.32	1.51 \pm 0.41	1.40 \pm 0.33	1.03 \pm 0.59	0.55 \pm 0.58	0.17 \pm 0.05	0.16 \pm 0.04
		pore size/ μm	1.22 \pm 0.55	1.17 \pm 0.52	1.13 \pm 0.31	1.09 \pm 0.50	0.74 \pm 0.42	0.39 \pm 0.38	0.12 \pm 0.04	0.11 \pm 0.04
	7.5 ml/min	globule size/ μm	1.61 \pm 0.34	1.61 \pm 0.25	1.14 \pm 0.75	0.14 \pm 0.04	0.16 \pm 0.04	0.15 \pm 0.04	0.16 \pm 0.04	0.16 \pm 0.04
		pore size/ μm	1.12 \pm 0.31	1.06 \pm 0.25	0.74 \pm 0.46	0.14 \pm 0.04	0.13 \pm 0.05	0.12 \pm 0.04	0.13 \pm 0.04	0.13 \pm 0.06

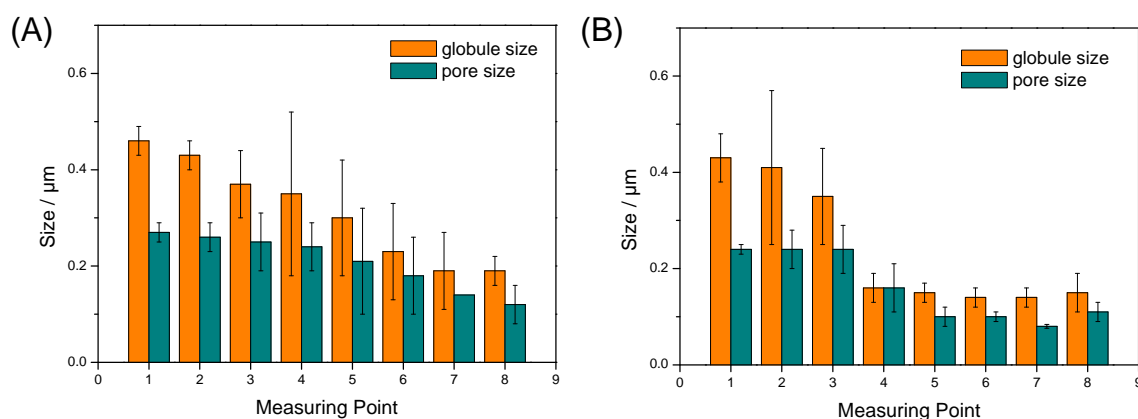


Figure 3.5: Summary of the pore and globule sizes measured from SEM images (taken at the surface) for poly(butyl methacrylate-*co*-ethylene dimethacrylate) surfaces produced using flow rates of: (A) 0.25 ml/min and (B) 7.5 ml/min.

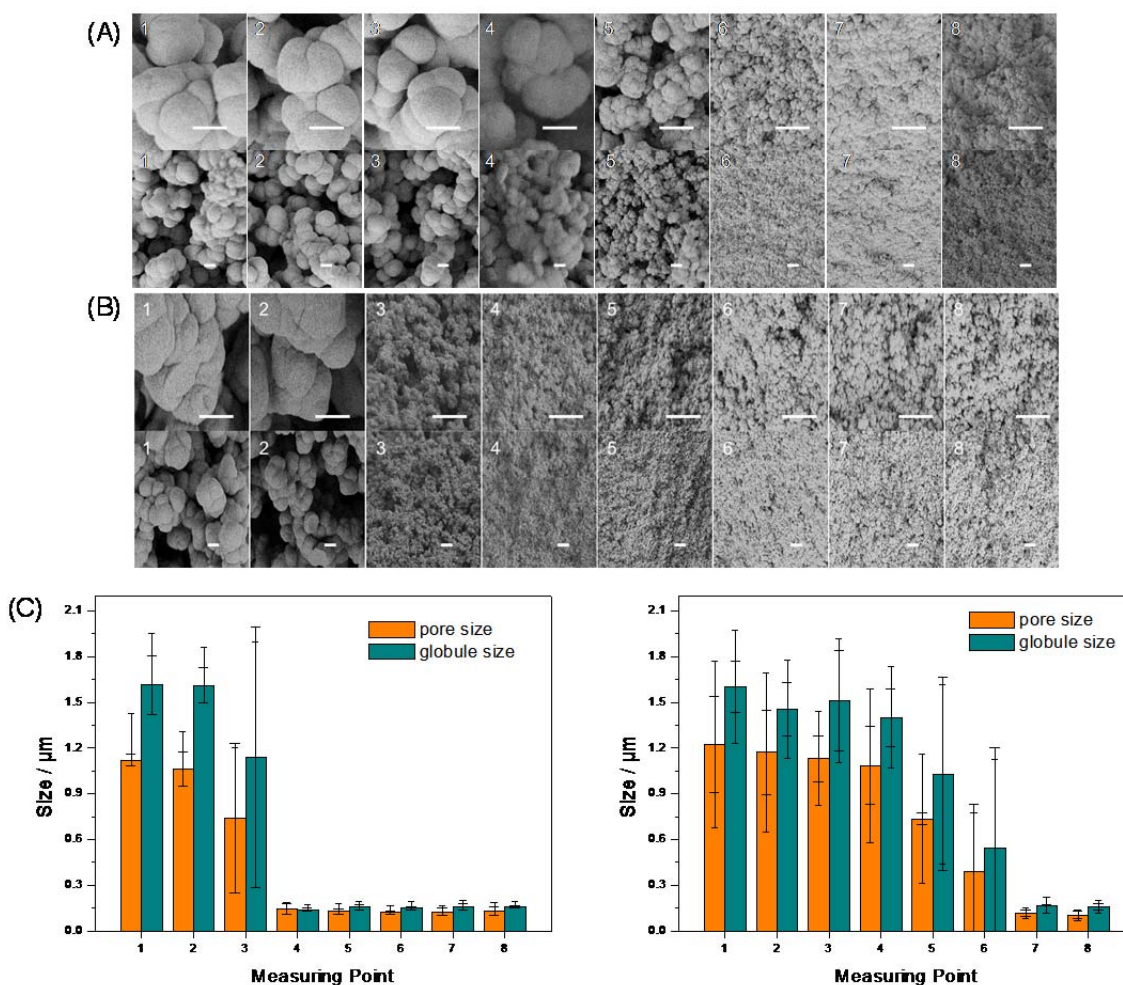


Figure 3.6: Scanning electron microscopy (SEM) images of poly(butyl methacrylate-*co*-ethylene dimethacrylate) surfaces generated with a flow rate of (A) 0.25 ml/min and (B) 7.5 mL/min. The SEM images were taken at the cross section 50 μm below the surface; scale bar 1 μm . First row shows magnified details of the second row. (C) Summary of pore and globule size distribution on the surfaces produced with high flow rate (7.5 mL/min, left) and low flow rate (0.25 mL/min). The pore sizes and globule sizes were quantified using the SEM images.

3.1.4 Hydrodynamic characterization of the microfluidic chip

To understand the formation of the gradient, a hydrodynamic characterization of the micro-mixer using model fluids and the polymerization mixtures was performed. The theoretical calculation of the concentration profile of a cascade micromixer was described elsewhere.⁹⁷⁻⁹⁸ Assuming homogeneous mixing in each zigzag channel, the concentration at the end would show a linear gradient profile. In the named literature, homogeneous mixing was achieved by diffusion. In the present micromixer mixing can occur due to two phenomena:

- 1) Diffusion: effective at low flow rates, when the rate of advection of the flow in the main direction is comparable with the rate of diffusion.

2) Forced convection: effective at higher flow rates, when transversal secondary flows arise as a consequence of the meandering shape of the zigzag channels.⁹⁹⁻¹⁰⁰

Turbulent mixing is prevented by the channel dimensions.

The μ LIF technique⁴⁸ was used to visualize the concentration gradients in the reaction chamber under different experimental conditions. The fluorescent microscope images in this section were taken by Massimiliano Rossi from Universität der Bundeswehr München. The detailed experimental procedure was described elsewhere before.¹⁰¹ Briefly, a fluorescent marker was dissolved in one of the two fluids and images of the mixing fluids were taken using an epifluorescence microscope. The image intensity is proportional to the concentration of the marker in the fluid volume. For the present set up, the images were taken using a Leica M165 FC fluorescence-microscope connected to an Imager sCMOS camera (LaVision GmbH). The flow was established by a syringe pump (Harvard PHD 2000), using the same flow rate at the two mixer inlets. Rhodamine B was used as a fluorescent marker and dissolved in one of the two fluids. Injection of only one model fluid into the micromixer was first characterized.¹⁰² This experiment was performed by Massimiliano Rossi. Isopropanol was injected in both inlets, having the fluid marked with Rhodamine B in the lower inlet. The resulting diffusion gradients for the respective flow rates of 0.001 mL/min, 1 mL/min and 20 mL/min are shown in Fig. 5.1. The red lines in the figure mark the boundaries of the reaction chamber. Two different mixing phenomena can be clearly observed: linear concentration gradient is present at 0.001 ml/min due to diffusive mixing, and at 20 ml/min due to convective mixing. At 1 ml/min the flow is too fast for diffusive mixing and too slow for the secondary flows, resulting in practically no mixing at the end. To analyze the performance of the micro-mixer injected with two different fluids, a second experiment using isopropanol (from the upper inlet, marked with Rhodamine B) and water (from the lower inlet) was performed.¹⁰² This experiment was performed by Massimiliano Rossi. Results are shown in Fig. 5.2. In this case, an apparent uniform mixing is observed for 0.001 mL/min and a linear concentration gradient for 1 mL/min. What is actually happening depends on the fact that the fluids have different densities (density ratio ~ 1.3). In the horizontal orientation of the chip, the lower density isopropanol tends to slip over the water during the propagation through the microfluidic channels. At 0.001 mL/min water and isopropanol are stacked one on top of the other resulting in an apparent uniform concentration (compare scheme of the cross section). At 1 mL/min there is less time for the less dense fluid to slip over the other, resulting in a 2D wedge-like arrangement of the two fluids (compare scheme of the cross section) that looks like a linear gradient from the top view of the μ LIF visualization. This hypothesis was supported by repeating the experiment with a vertically oriented microfluidic chip (see Fig. 5.3). In this case, gradients formed at 0.001 and 1 ml/min flow rates more resembled the situation with two fluids of the same density (Fig. 5.1). The dependence of a gradient shape on the orientation of a microfluidic chip can be explained if the fluid density has an effect on the gradient formation, thereby confirming the hypothesis of the wedge-like gradient formation in Fig. 5.2.

An additional confirmation of the density driven wedge-like gradient formation was obtained by analyzing a cross-section of the gradient polymer film by SEM (see Fig. 3.8).

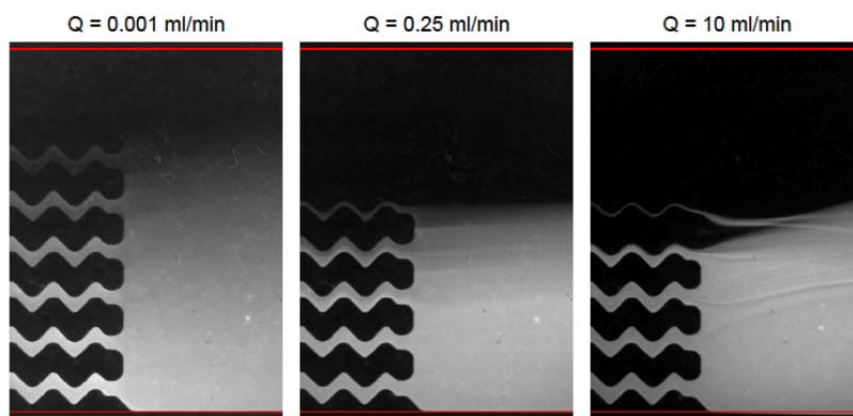


Figure 3.7: Images from μ LIF measurements (left) using mixture 5 (upper inlet) and mixture 1 marked with Rhodamine B (lower inlet) for the injection in the micromixer (flow direction left to right) and observed by fluorescence microscopy.¹⁰² At 0.001 ml/min and 0.25 ml/min, mixture 1 slips over mixture 5 in a wedge-like arrangement. At 10 ml/min, convective mixing starts to take place.

Finally, the experiment with the polymerization mixture 5 from the upper inlet and the polymerization mixture 1 was repeated, dyed with Rhodamine B, from the lower inlet.¹⁰² This experiment was performed by Massimiliano Rossi. In this case, the density ratio is smaller (~ 1.1) and the two fluids are significantly more viscous than water and isopropanol.¹⁰² The apparent concentration gradient, corresponding to the wedge-like arrangement as discussed above, was observed already at 0.001 ml/min and up to 0.25 ml/min, as shown in Fig. 3.7. Some convection effects can be observed at 10 ml/min although the fluids remain substantially unmixed. It was not possible to go to higher flow rates with the current syringe pump equipment. The burst pressure of the microfluidic chips is 0.36 MPa. It was measured using water and a pressure transducer (WIKA Alexander Wiegand SE & Co. KG). This value fits well in the range for so called irreversible bonds described elsewhere.¹⁰³

The μ LIF measurements showed that the polymer film created using 0.25 ml/min possesses a pore size wedge-like gradient as a consequence of the density difference between the two fluids. The two dimensional wedge-like gradient was confirmed by analyzing the polymer surface's cross-section by SEM, shown in Fig. 3.8.

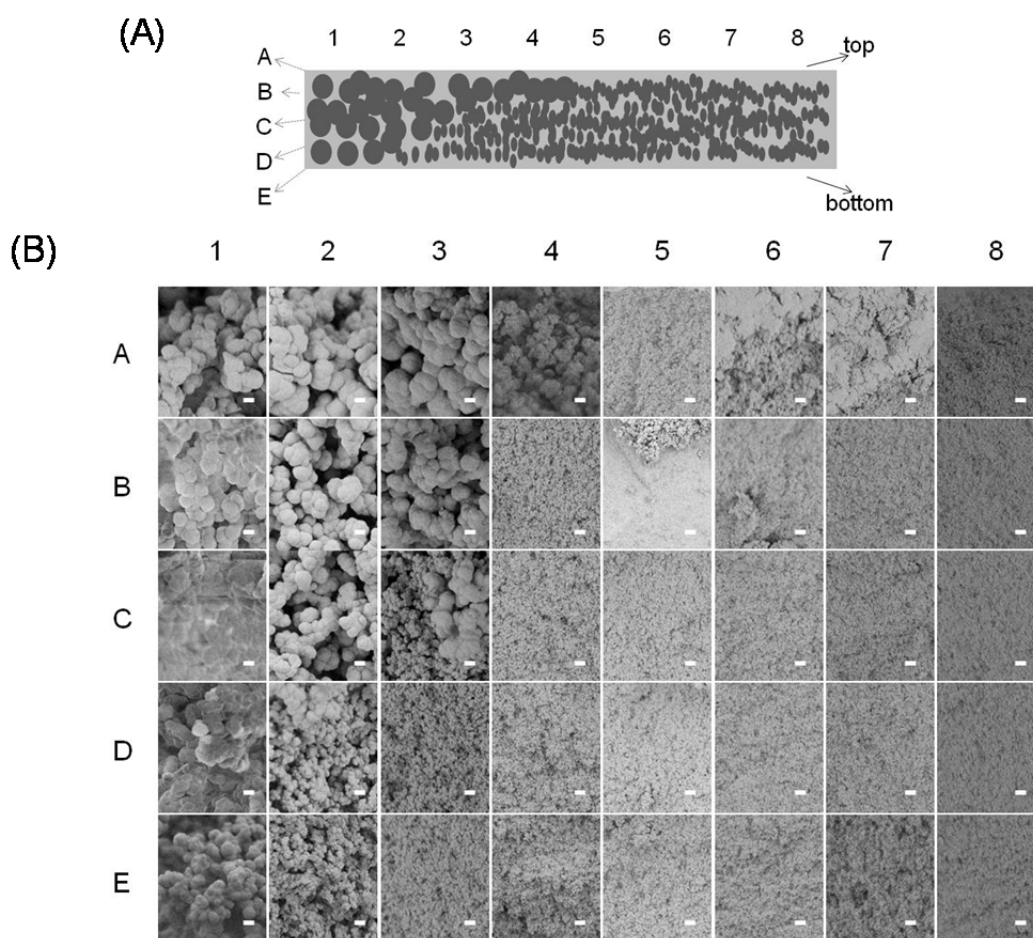


Figure 3.8: (A) Scheme and (B) SEM images of the overall cross section of a poly(butyl methacrylate-*co*-ethylene dimethacrylate) surface showing the density driven wedge-like pore size gradient (scale bar 1 μm).

3.1.5 Summary

Controlled, facile fabrication of thin polymer surfaces possessing a gradient of pore size was demonstrated using a microfluidic chip. The microfluidic chip contained a cascade micromixer to generate a gradient of two polymerization mixtures and a subsequent reaction chamber for the photoinitiated polymerization. The concentration gradient obtained in the reaction chambers could be controlled by the flow rate, type of the used fluids and the orientation of the microfluidic chip. The formation of density driven two dimensional wedge-like gradients was confirmed by both μLIF and SEM of polymer film cross-sections. For the polymerization mixtures the micromixer enabled convective effects and a gradient using the mentioned wedge-like distribution. Using a flow rate of 0.25 ml/min, polymer film with a gradient of porous morphology with pore sizes ranging from $\sim 0.1 \mu\text{m}$ to $\sim 0.3 \mu\text{m}$ was generated. These results demonstrate a convenient way for the generation of polymer surfaces with defined gradients of morphology. It is expected that the polymer surfaces with gradient morphology could find many applications in screening studies of cell-surface interactions.

3.2 Porous polymethacrylate surface with gradient density of functional group for the investigation of the effect of surface morphology and surface chemistry on HT-1080 fibrosarcoma cells

3.2.1 Background

The ability to control cell behavior on surfaces is essential in different research fields, such as tissue engineering and development of biomedical device or biosensors. Much effort has been devoted to investigate the influence of surface properties on the cell behavior. Synthetic surfaces with defined physical and chemical properties have been prepared to study their influence on cell viability, proliferation, differentiation, motility and adhesion.^{86, 104-108,109} For example, surface chemistry was proved to play an important role for the maintenance of the stem cells pluripotency. As reported by Mei et al.,¹⁰⁴ control of polyacrylate surface chemistry could improve the maintenance of pluripotency of the human embryonic stem cells (hES) and of the induced pluripotent stem cells (hiPS) on the surface. Recently, polymer surfaces with zwitterionic functional groups have been intensively studied and used for various applications due to their biomimetic structure.¹¹⁰⁻¹¹⁴ Surface coatings with antifouling,¹¹⁵⁻¹¹⁸ nonthrombogenic^{114, 119} and antimicrobial¹¹⁹ properties were developed based on zwitterionic polymers. Villa-Diaz et al.¹⁰⁶ reported that poly[2-(methacryloyloxy) ethyldimethyl-(3-sulfopropyl)ammonium hydroxide] could promote the attachment and long-term proliferation of undifferentiated hES. Albeit the molecular mechanism of this phenomenon is not completely understood, it is likely that the surface chemistry defines adhesive abilities of the cells, modulates molecular composition of the cell membrane and consequently downstream intracellular signaling cascades. Apart from surface chemistry, it was shown that surface roughness and porosity^{89, 120-125} are also important regulators of cell behavior. Surface porosity, for example in the case of basement membrane, enables cell turnover and also functions as a filter and conduit for nutrition.¹²⁴ However, up to now, there are only few studies on the combinatorial effect of surface porosity and surface chemical properties on cell behavior on the surface.^{108, 126}

Although it has been known that tumor cells are influenced by their microenvironment, a direct impact of surface physical and chemical properties on tumor cell behavior remained unclear. Fibrosarcomas are rare tumors of mesenchymal origin, arising either in the connective tissues or in the bones. Fibrosarcomas are able to spread into the surrounding soft tissues as fat, muscles, nerves, joint tissues and to build bone metastasis.¹²⁷ Fibrosarcoma exhibits a high degree of plasticity and adaptation to different growth conditions, as confirmed by Wolf in Friedl for the human fibrosarcoma cell line HT-1080.¹²⁸ In this section, different porous polymethacrylate surfaces with gradient in density of surface functional groups are prepared and used to investigate the impact of surface morphology and surface chemistry on the tumor cells behavior on these surfaces. Human fibrosarcoma cell line HT-1080 is used as a tumor model.

3.2.2 Preparation of the porous polymethacrylate surfaces with gradient density of functional groups

To investigate the effect of surface morphology on the cell behavior, BMA-EDMA surfaces (BE1 and BE5) and HEMA-EDMA (HM and HN) surfaces with different morphologies were prepared on the glass slides. After thoroughly cleaning the as-prepared surfaces with ethanol, the surfaces were subsequently modified with acrylate monomers by photografting. Three acrylate monomers: the positively charged [2-(methacryloyloxy) ethyl] trimethylammonium chloride (META), negatively charged 2-acrylamido-2-methyl-1-propanesulfonic acid (AMPS) and zwitterionic [2-(methacryloyloxy) ethyl]dimethyl-(3-sulfopropyl)ammonium hydroxide (MDSA), were used for photografting (Fig. 3.9 A). These acrylate monomers were chosen for the modification of the polymethacrylate surfaces because corresponding polymers were previously shown to be biologically active.^{110, 129-130} For instance, META modified surface could support neuron cell culture.¹¹⁰ In order to improve the efficiency of our study, surfaces with gradient densities of functional groups were prepared as described below and used for cell studies.

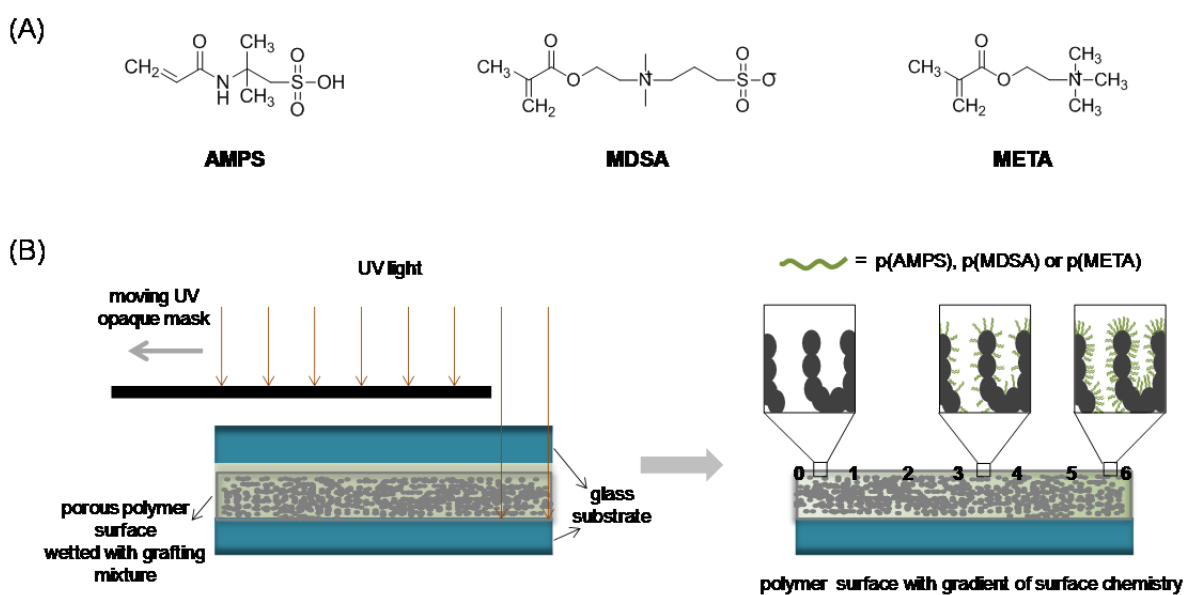


Figure 3.9: (A) Acrylate monomers used for the surface modification. (B) Schematic representation of the method for preparing the polymer surface with gradient density of functional groups via photoinitiated grafting.

It was known that the extent of photografting depends on the UV dosage¹³¹ and the methods for preparing surfaces with density gradients of functional groups based on photografting have been reported.¹³²⁻¹³³ In this project, a moveable UV opaque mask was used to control the UV dosage on the surface during the photografting. The surface was covered completely with the mask before photografting. When the photografting started, the mask started to move with a constant velocity of 1.2 cm/min and thus gradually exposing the surface with UV light. The grafting time on the resulted gradient surface increased from 0 min (position 1 in Fig 3.9B) to 5 min (position 6) and the length of

the gradient surface was 6 cm.

3.2.3 Characterization

All the surfaces were analyzed with SEM (Fig. 3.10 and Fig. 3.11) to investigate the morphology change of the surfaces after photografting. The pore and globule sizes were quantified (Tab. 3.3) using these SEM images. It was observed from the SEM images that the BE1 polymer became less rough after photografting. Average globule size of BE1-MDSA increased from 0.84 μm to 1.28 μm while the pore size decreased from 0.57 μm to 0.50 μm after 5 min of photografting. The increased polymer globule size is the result of polymerization of MDSA monomers on the surface. Similarly, the globule sizes of the BE5 surface, HM and HN surfaces increase while the pore sizes decrease after photografting (Tab. 3.3).

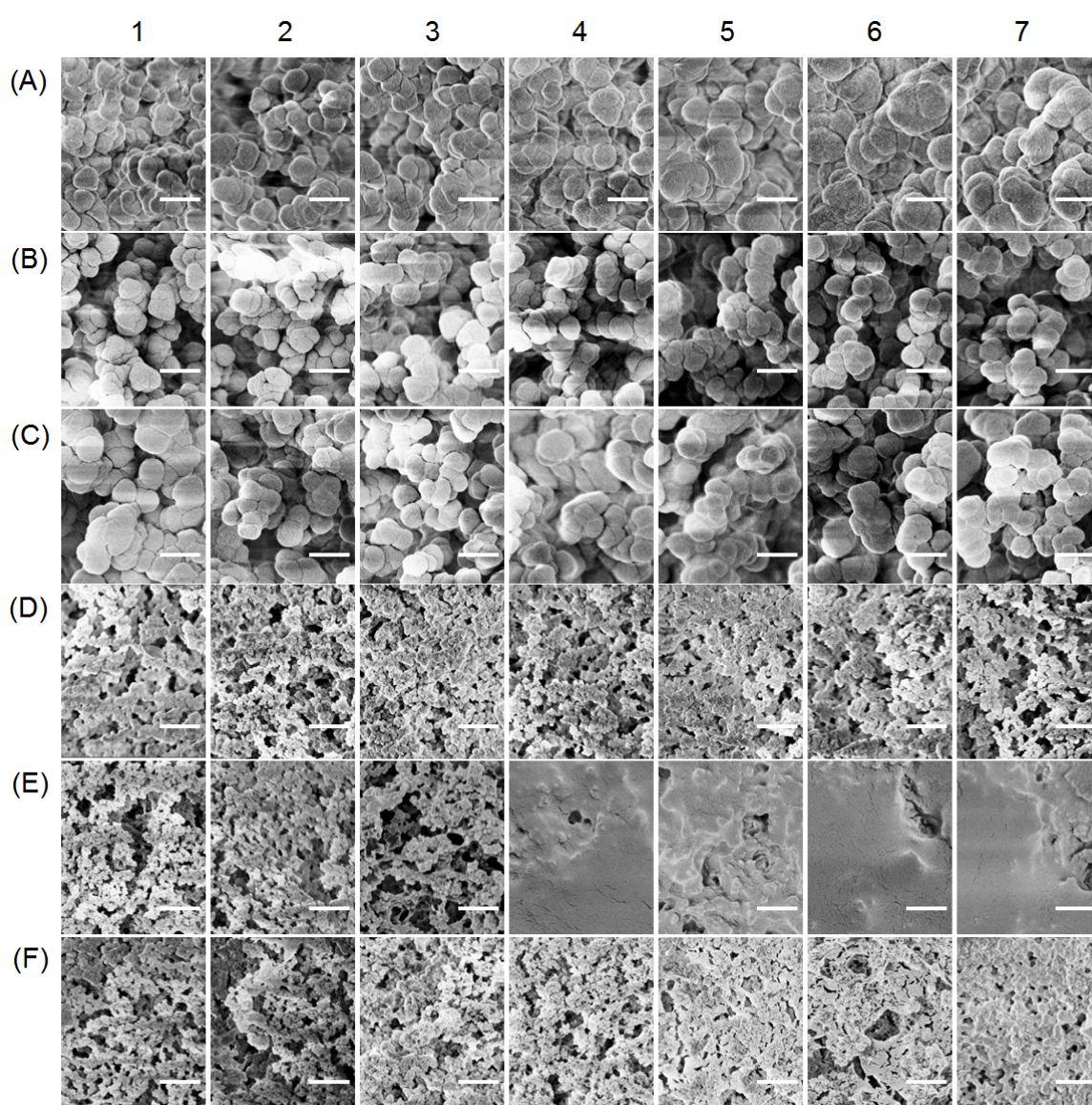


Figure 3.9: SEM images taken at different positions on (A) BE1-AMPS, (B) BE1-MDSA, (C) BE1-META, (D) BE5-AMPS, (E) BE5-MDSA and (F) BE5-META surfaces (scale bar 1 μm).

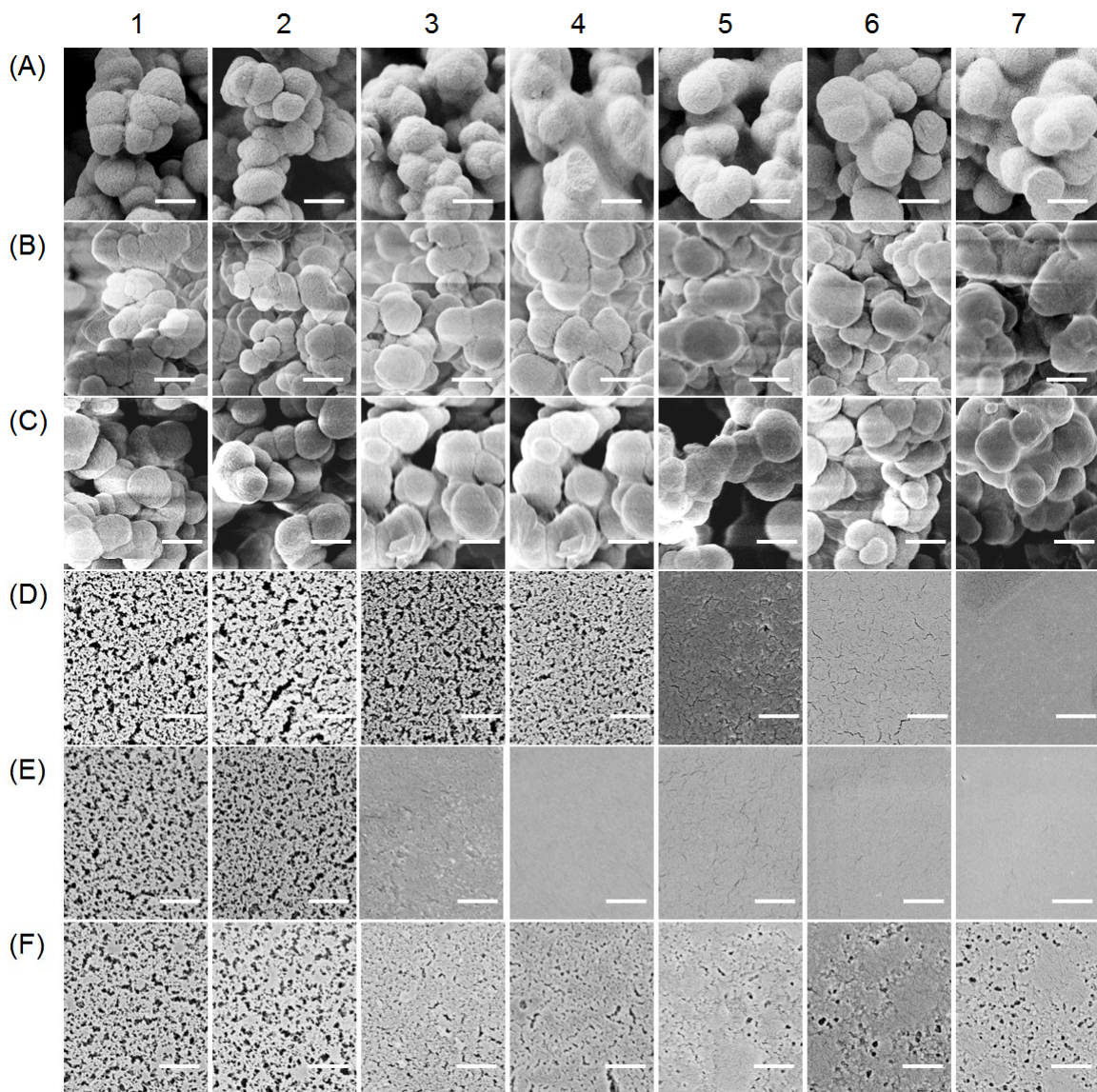


Figure 3.10: SEM images taken at different positions on (A) HM-AMPS, (B) HM-MDSA, (C) HM-META, (D) HN-AMPS, (E) HN-MDSA and (F) HN-META surfaces (scale bar 1 μm).

Table 3.3: Globule sizes and pore sizes measured at different positions on the BMA-EDMA and HEMA-EDMA surfaces photografted with different monomers using the “moving mask” method (“NP” means the surface is nonporous.).

Surface	Size	Position 0	Position 1	Position 2	Position 3	Position 4	Position 5	Position 6
BE1-AMPS	globule size/ μm	0.67 \pm 0.16	0.74 \pm 0.16	0.86 \pm 0.16	0.91 \pm 0.14	0.91 \pm 0.17	1.04 \pm 0.20	0.95 \pm 0.16
	pore size/ μm	0.55 \pm 0.13	0.56 \pm 0.19	0.59 \pm 0.13	0.53 \pm 0.32	0.42 \pm 0.15	0.62 \pm 0.20	0.47 \pm 0.13
BE1-MDSA	globule size/ μm	0.84 \pm 0.15	0.90 \pm 0.14	0.99 \pm 0.25	1.13 \pm 0.20	1.02 \pm 0.23	1.11 \pm 0.22	1.28 \pm 0.20
	pore size/ μm	0.57 \pm 0.15	0.79 \pm 0.30	0.74 \pm 0.24	0.66 \pm 0.28	0.57 \pm 0.16	0.53 \pm 0.34	0.50 \pm 0.19
BE1-META	globule size/ μm	0.98 \pm 0.24	1.11 \pm 0.23	1.16 \pm 0.25	1.04 \pm 0.26	1.28 \pm 0.26	1.26 \pm 0.28	1.49 \pm 0.36
	pore size/ μm	0.67 \pm 0.33	0.71 \pm 0.33	0.65 \pm 0.33	0.65 \pm 0.23	0.74 \pm 0.38	0.64 \pm 0.20	0.73 \pm 0.29
BE5-AMPS	globule size/ μm	0.08 \pm 0.02	0.08 \pm 0.02	0.07 \pm 0.01	0.08 \pm 0.02	NP	NP	NP
	pore size/ μm	0.11 \pm 0.03	0.10 \pm 0.02	0.10 \pm 0.04	0.08 \pm 0.20	NP	NP	NP
BE5-MDSA	globule size/ μm	0.07 \pm 0.01	0.07 \pm 0.02	NP	NP	NP	NP	NP
	pore size/ μm	0.10 \pm 0.03	0.10 \pm 0.03	NP	NP	NP	NP	NP
BE5-META	globule size/ μm	0.07 \pm 0.01	0.07 \pm 0.01	0.08 \pm 0.02	0.10 \pm 0.02	NP	NP	NP
	pore size/ μm	0.09 \pm 0.02	0.10 \pm 0.03	0.06 \pm 0.01	0.07 \pm 0.02	NP	NP	NP
HM-AMPS	globule size/ μm	0.79 \pm 0.14	0.79 \pm 0.16	0.75 \pm 0.10	0.84 \pm 0.12	0.82 \pm 0.14	0.93 \pm 0.18	1.07 \pm 0.23
	pore size/ μm	0.42 \pm 0.16	0.37 \pm 0.10	0.37 \pm 0.10	0.40 \pm 0.16	0.36 \pm 0.10	0.36 \pm 0.08	0.30 \pm 0.09
HM-MDSA	globule size/ μm	0.73 \pm 0.11	0.68 \pm 0.14	0.78 \pm 0.13	0.82 \pm 0.14	0.91 \pm 0.15	1.02 \pm 0.17	1.06 \pm 0.18
	pore size/ μm	0.40 \pm 0.10	0.43 \pm 0.18	0.34 \pm 0.12	0.33 \pm 0.12	0.34 \pm 0.13	0.33 \pm 0.09	0.32 \pm 0.10
HM-META	globule size/ μm	0.85 \pm 0.18	0.81 \pm 0.14	0.86 \pm 0.12	0.82 \pm 0.15	0.97 \pm 0.28	0.96 \pm 0.15	0.99 \pm 0.24
	pore size/ μm	0.34 \pm 0.13	0.34 \pm 0.09	0.29 \pm 0.08	0.30 \pm 0.09	0.32 \pm 0.10	0.32 \pm 0.09	0.34 \pm 0.10
HN-AMPS	globule size/ μm	0.12 \pm 0.03	0.11 \pm 0.02	0.11 \pm 0.02	0.11 \pm 0.02	0.10 \pm 0.02	0.11 \pm 0.03	0.12 \pm 0.03
	pore size/ μm	0.14 \pm 0.04	0.11 \pm 0.03	0.11 \pm 0.03	0.10 \pm 0.03	0.09 \pm 0.04	0.10 \pm 0.03	0.09 \pm 0.03
HN-MDSA	globule size/ μm	0.10 \pm 0.02	0.11 \pm 0.03	0.10 \pm 0.20	NP	NP	NP	NP
	pore size/ μm	0.09 \pm 0.03	0.09 \pm 0.03	0.09 \pm 0.03	NP	NP	NP	NP
HN-META	globule size/ μm	0.16 \pm 0.04	0.16 \pm 0.03	0.21 \pm 0.03	0.19 \pm 0.04	0.17 \pm 0.04	0.20 \pm 0.04	0.23 \pm 0.07
	pore size/ μm	0.17 \pm 0.05	0.12 \pm 0.03	0.17 \pm 0.14	0.13 \pm 0.03	0.14 \pm 0.04	0.13 \pm 0.03	0.14 \pm 0.03

To prove the formation of gradient density of functional group on the surface produced using this method, XPS measurements were performed. BE5-MDSA surfaces were tested as an example. The XPS measurements were performed at 5 different measuring points (position 0, position 1, position 2, position 4 and position 5 as shown in Fig. 3.9B) along the gradient direction on the BE5-MDSA. The XPS spectra of N 1s peak and S 2p peaks are shown in Fig. 3.12. Characteristic peaks from MDSA (N 1s and S 2p) could be clearly identified in the spectra collected from position 1, position 2, position 4 and position 5, while these peaks are absent in the spectra collected from position 0. A chemical shift of the S 2p doublet peaks toward higher binding energy (~ 168.5 eV) region was observed, suggesting the presence of sulfur in high oxidation states (in agreement with the SO_4^- group in MDSA).¹³⁴ To fit the S 2p peak, the background due to the scattered photoelectrons was first subtracted using the Shirley method. Then, the S 2p peak was fitted with Voigt peak profiles in accordance with reference data (spin-orbit splitting 1.18 eV, peak ratio 2 : 1).¹³⁵ The low FWHM (Full Width at Half Maximum) of the fitted peaks indicated that only a single sulfur species was on the surface. The presence of the S 2p and N 1s peaks demonstrated that the BE5 surface was successfully modified with MDSA by photografting. Moreover, the intensities of the N 1s or S 2p emission increases gradually from the

spectra taken at position 0 to the spectra taken at position 4, which indicates the formation of the gradient in grafting density. To further confirm this, a quantitative analysis was performed. The quantitative evaluation of the spectra was performed by determining the areas of C 1s, O 1s, S 2p and N 1s peaks and dividing them by appropriate photoionization cross sections¹³⁶. The results are listed in Tab. 3.4. As can be seen from the table, the S 2p / C 1s ratio on the surface increased from position 0 to position 4, confirming the formation of the gradient on BE5-MDSA. A slightly lower S 2p / C 1s ratio was observed on position 5 than on position 4. This could be caused by the drying out of the grafting mixture at the end of the surface (e.g. position 5) during photografting, which would decrease the efficiency of photografting. The calculated O 1s / C 1s ratio on the surface was close to the stoichiometric ratio of oxygen to carbon in BMA (1:4). This could be because of the enrichment of BMA component on the sunface of polymer globules due to the phase separation during polymerization.

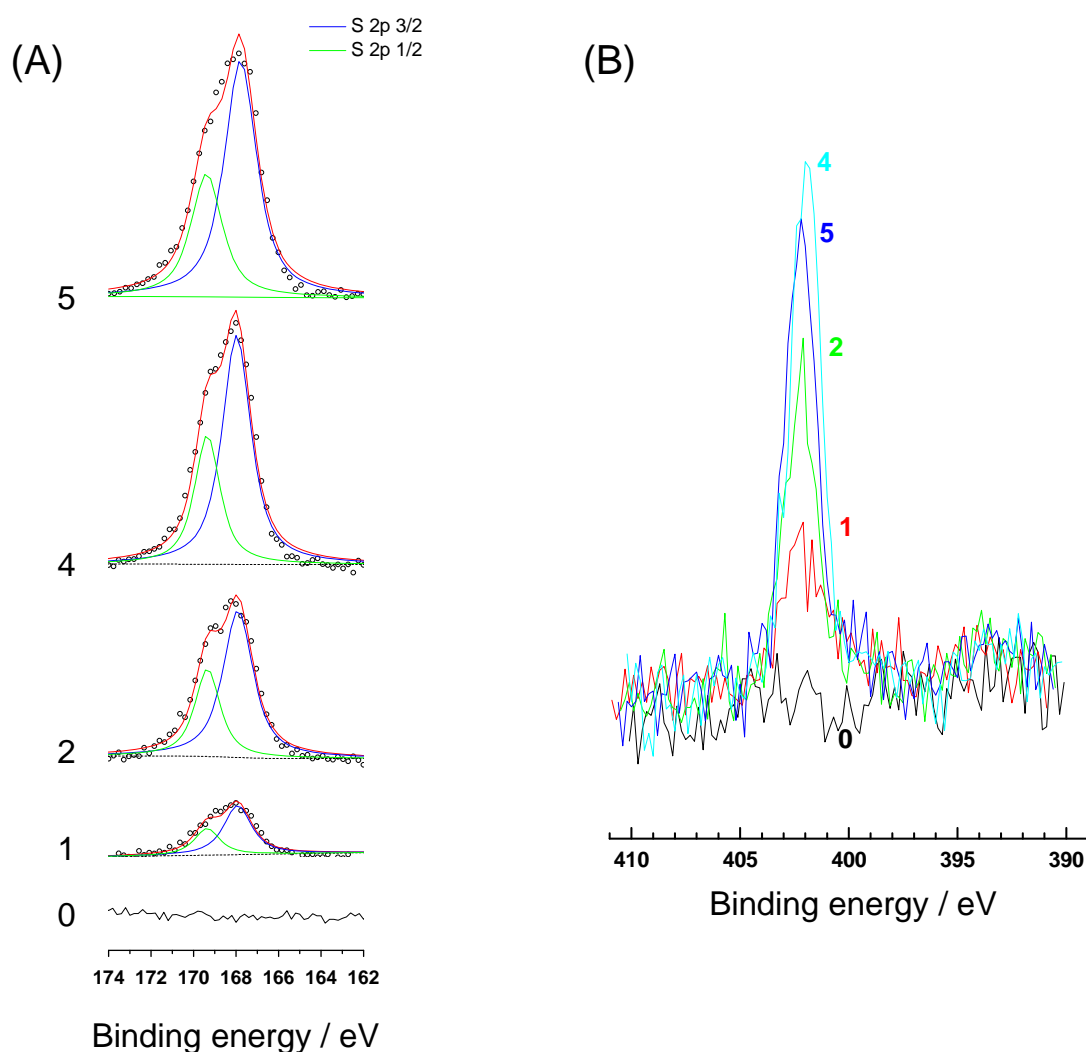


Figure 3.12: X-ray photoelectron spectroscopy (XPS) spectra taken at different measuring points (positions 0, 1, 2, 4 and 5, as shown in Fig. 3.9) of the BE5-MDSA surface. (A) S 2p peak; (B) N 1s peak.

Table 3.4: Surface composition on different measuring points of the BE5-MDSA surface.

Measuring point	O 1s : C 1s	S 2p : C 1s	N 1s : C 1s
0	0.210	0	0
1	0.243	0.007	0.011
2	0.234	0.021	0.021
4	0.279	0.036	0.031
5	0.280	0.031	0.024

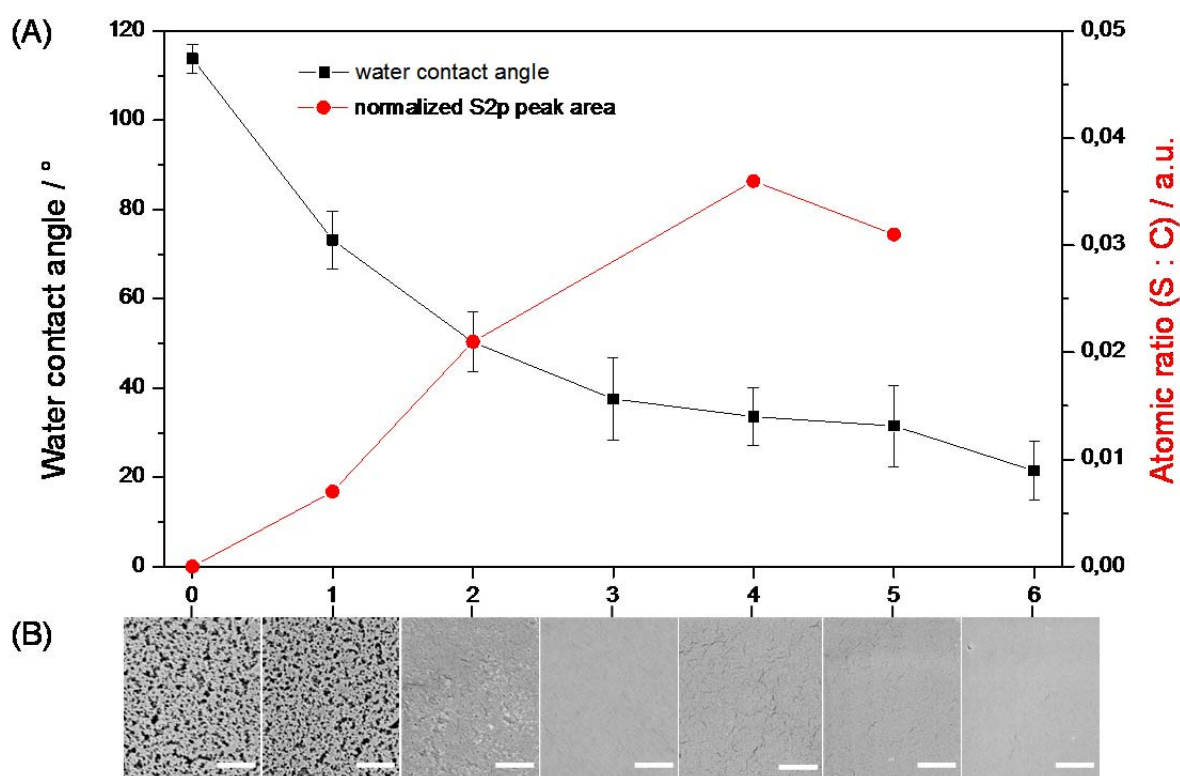


Figure 3.13: (A) Static water contact angle and the normalized S 2p peak area measured at different positions along the gradient direction on the BE5-MDSA surface. Water contact angles were measured on at least three samples and the measurements were repeated 3 times on each sample. The values reported here are the averages of the results from individual measurements. The error bars represent the standard deviations. (B) SEM images of the BE5-MDSA surface along the gradient direction (scale bar 1 μm).

Water contact angles of the BE1-AMPS, BE1-MDSA, BE1-META, BE5-AMPS and BE5-META surfaces were also measured. The measured water contact angles are listed in Table 3.5 and Fig. 5.13. For the BE5-MDSA surface, the static water contact angle of the surface is $113.8 \pm 3.3^\circ$ on the part without photografting (position 0) After ~ 1 min of photografting with MDSA, the BE5 surface became hydrophilic and the static water contact angle decreased to $21.5 \pm 6.5^\circ$ at position 6 on the BE5-MDSA surface. The gradual decrease of the static water contact angle on the BE5-MDSA surface

along the gradient direction (from position 1 to position 6) indicates the formation of a gradient of the functional group density on the surface. It should be noted that the surface wettability depends on both surface morphology and surface chemistry. For BE1-AMPS, BE1-MDSA, BE1-META, BE5-AMPS and BE5-META surfaces, similar changes in the water contact angles along the gradient directions were also observed (see Tab. 3.5).

Table 3.5: Static water contact angles on different positions of BE1-AMPS, BE1-MDSA, BE1-META, BE5-AMPS, BE5-MDSA and BE5-META surfaces.

Surface	Static WCA at Position 0 /°	Static WCA at Position 1 /°	Static WCA at Position 2 /°	Static WCA at Position 3 /°	Static WCA at Position 4 /°	Static WCA at Position 5 /°	Static WCA at Position 6 /°
BE1-AMPS	136.8±3.0	133.6±4.9	128.8±3.7	126.9±5.5	123.8±4.6	111.9±11.8	113.0±4.8
BE1-MDSA	138.0±1.7	121.0±11.8	0	0	0	0	0
BE1-META	136.5±3.8	132.5±6.6	122.1±9.9	0	0	0	0
BE5-AMPS	112.6±4.1	108.2±4.2	61.9±9.4	32.7±7.6	26.3±7.2	26.5±5.2	28.9±2.7
BE5-MDSA	113.8±3.3	73.2±6.4	50.3±6.7	37.6±9.2	33.6±6.5	31.5±9.1	21.5±6.5
BE5-META	111.4±1.0	100.4±15.2	61.7±9.8	45.2±14.2	40.3±18.7	36.7±16.8	39.8±16.4

3.2.4 The impact of surface morphology and surface chemistry on HT-1080 cell morphology To examine the impact of surface morphology on the HT-1080 cells, BMA-EDMA surfaces with different morphologies (BE1 and BE5) were used to study the cell behavior on these surfaces. Hydrophilic HEMA-EDMA surfaces (HM and HN) were also used. Cell staining and culture experiments in this section were performed by Barbara Kwiatkowska (ITG, KIT). On the glass slide, the HT-1080 cells originated from the human fibrocarcinoma exhibit typical fibroblast-like morphology, which is characteristic for the cells of mesenchymal origin (Fig. 5.4). The cells kept bipolar orientation and formed pronounced lamellipodia.¹³⁷ HT-1080 cells grown on the BE1 surfaces exhibited aberrant morphology and only few cells were observed on the surface after 24 hours. In comparison, HT-1080 cells on the BE5 surface maintained normal cell morphology. Neither HM no HN surfaces were able to support cell growth. Cells were rounded with apoptotic-like nuclei and reduced cytoplasm volume on HM and HN surfaces. To sum up, hydrophilic HEMA-EDMA (both HM and HN) surfaces were not suitable for HT-1080 cell growth. Hydrophobic BE5 surface could well support HT-1080 cell growth without changing the morphology of the cells.¹³⁸

Next, the impact of surface chemistry on the HT-1080 cell growth was studied using the surfaces with gradient densities of functional groups. Independent of the grafting time, cells on the BE1-AMPS surfaces had fibroblast-like appearance, similar to the cells on the glass slides. Cells exhibited spindle-shape asymmetric morphology with extended lamellipodia and filopodia, suggesting their high migratory ability. Thus, the phenotype of the HT-1080 cells on the BE1-AMPS surface remained

unchanged (Fig. 5.5(A)). In contrast, HT-1080 cells grown on BE1-MDSA surfaces exhibited a different morphology. The cells had round shape on the whole BE1-MDSA surfaces (Fig. 5.5(B)). It can be observed that the cells built cell-cell contacts and formed compact colonies on the surface. In addition, reduction of cytoplasm volume and stress-fibers was observed. Instead of lamellipodia, cells formed numerous filopodia, distributed around a cell, suggesting reduced migration activity and increased cell-matrix adhesion. It is clear that the presence of the zwitterionic functional groups on the BE1-MDSA surface interfered with the fibroblast-like phenotype, and possibly impairing cell migration. The molecular mechanism of this action should be further analyzed. HT-1080 cells grown on the BE1-META surfaces were examined. Only few cells could be detected on the surfaces 24 hours after seeding, suggesting reduced cell survival on the BE1-META surface. The remaining cells exhibited aberrant morphology. The effect was more pronounced with the increase of grafting time (Fig. 5.5(C)). On the parts corresponding to 3.5 min and 5 min of META grafting, cells possessed low volume of cytoplasm and no stress-fibers could be detected. The cells were rounded and formed filopodia. On the BE5-AMPS surface (Fig. 5.5(D)), HT-1080 cells acquired morphology similar to the cells grown on the glass slides. Increase of AMPS density (increase of grafting time) led to the change of cell phenotype and inhibition of the lamellipodium formation. Instead, the cells formed multiple filopodia, suggesting that AMPS might have an impact on cell migration. By grafting the BE5 surface with AMPS for 5 min, only few cells were detected on the surface. HT-1080 cells on the BE5-MDSA surfaces showed similar behavior to those cultured on the BE5-AMPS surfaces (Fig. 5.5(E)). HT-1080 cells grown on the BE5-META for more than 3.5 min of grafting developed slightly different rounded morphology. Similar to the cells grown on the BE1 surface, cells formed multiple filopodia and colonies.¹³⁸ As shown in Fig. 5.6(A), AMPS grafted hydrophilic macroporous HEMA-EDMA surface (HM-AMPS) did not support cell growth and increased grafting time led to the abrogation of the cell growth. Remaining cells revealed aberrant morphology of the nuclei, suggesting apoptosis induction. The HT-1080 cells grown on the HM-MDSA surfaces formed multiple filopodia and had slightly rounded form as compared to the cells grown on the glass slides (Fig. 5.6(B)). HM-META surfaces led to the abrogation of cell growth (Fig. 5.6(C)). Stained nuclei revealed pro-apoptotic morphology. Single cells could be detected on the positions grafted for 5 minutes. HT-1080 cells grown on the HN-AMPS surface revealed slightly rounded morphology with numerous extensions of filopodia (Fig. 5.6(D)). Cells on HN-MDSA surfaces had slightly rounded form and possessed multiple filopodia (Fig. 5.6(E)). The HN-META surface led to the aberrant morphology and deformed nuclei of the cells cultured (Fig. 5.6(F)).¹³⁸

3.2.5 The impact of surface morphology and surface chemistry on HT-1080 cell adhesion

To examine the impact of surface properties, such as surface morphology and surface chemistry on HT-1080 cell adhesion, the HT-1080-eGFP cells, generated by a stable transfection of HT-1080 human fibrosarcoma cells with eGFP (enhanced green fluorescent protein), were used for the adhesion assay. It was found that the number of adhered HT-1080 cells on the BE1 surface and BE1-AMPS

surface was similar to that on the uncoated control glass surface (Fig. 5.7(A)). In comparison, the cell adhesion on BE1-MDSA surface was reduced. HT-1080 cell adhesion on the BE1-META surface was improved in the part corresponding to shorter photografting time. With the increase of the photografting time, the cell adhesion was reduced on the BE1-META surface. Next, BE5 surfaces grafted with different monomers were tested (Fig. 5.7(B)). Interestingly, 1 min grafting led to an increased cell adhesion for all the grafted BE5 surfaces. On the surfaces grafted for 2.5 min, significant differences were observed among the grafted BE5 surfaces. Three fold higher amounts of cells, as compare to the glass slide, were detected on the surface grafted with META for 2.5 min. HM and HN surfaces grafted with different monomers were also tested. The HT-1080-eGFP cells seeded on the HM surfaces revealed similar adhesion in each monomers group (Fig. 5.7(C)). The strongest cell adhesion was observed on the HM surface. The HM-MDSA surface inhibited cell adhesion. Cell adhesion on the HN surface was similar as on the HM surface. To summarize, the HT-1080 cell adhesion was greatly improved on the BN-META surface. In addition, cell adhesion on the AMPS-grafted surfaces was constant and comparable, independent of the surface morphology.¹³⁸

3.2.6 Summary

The impact of surface morphology and surface chemistry on the HT-1080 fibrosarcoma cells was investigated using photografted porous polymethacrylate surfaces with different morphologies. To facilitate and accelerate this investigation, gradients of functional group density were introduced on the surfaces. Results from the cell experiments show that [2-(methacryloyloxy) ethyl]dimethyl-(3-sulfopropyl)ammonium hydroxide (MDSA)grafted (grafting time 3.5 min) nanoporous BMA-EDMA (BE5) surface supported HT-1080 cell growth and induced severe change in the cell morphology. It was previously shown that a MDSA coating has an apparent biological activity and can affect behavior of different cell types cultured on the coating.^{118, 130} The observed morphology change of HT 1080 cells on MDSA grafted BE5 might be triggered by the interactions with the MDSA groups, More experiments need to be performed to understand the molecular mechanism for this change. The results also suggest that the method developed in this study for creating surface gradients can be useful for the screenings of the effect of surface properties on cell behavior.

3.3. Slippery liquid infused porous surface for antibacterial and marine antifouling applications

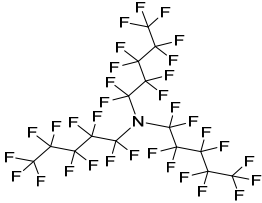
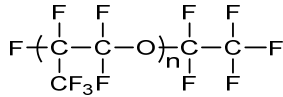
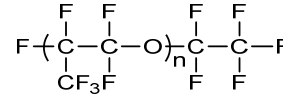
3.3.1 Slippery liquid infused porous surfaces (SLIPS): background

Inspired by the *Nepenthes* pitcher plants, the concept of slippery liquid infused porous surface was introduced by the Aizenberg group.¹³⁹ These surfaces were prepared simply by infusing a hydrophobic and water immiscible liquid into a nanoporous or microporous surface. By carefully matching the surface energy of the porous substrate and that of the liquid, slippery surfaces with high repellency against water, ice, oil and other liquids can be obtained.¹³⁹ Self-healing properties of the surface and its good stability under high pressure were also demonstrated.¹³⁹ Arrays of nanoposts functionalized with perfluoroalkyl silane and commercially available Teflon nanofibers were used as the porous substrate.¹³⁹⁻¹⁴³ As for the lubricant liquid, low surface tension perfluorinated liquid (for example 3M Fluorinert FC-70 and DuPont's Krytox oils) were used.¹³⁹⁻¹⁴³

Owing to the high omniphobicity and slippery properties, SLIPS were expected to be applicable in the fields such as antibacterial and self-cleaning surfaces. Aizenberg et al. investigated the bacterial adhesion on the liquid infused porous surface¹⁴⁴ and they showed that the SLIPS prevented 96.6%, 97.2% and 96% of *Pseudomonas aeruginosa*, *Staphylococcus aureus* and *Escherichia coli* biofilm attachment, respectively. It was also reported that the SLIPS showed much better antibacterial properties than a PEGylated surface.

The liquid infused surface introduced by Aizenberg group was based on rough fluorinated nano-structured silicon or porous Teflon substrates. These substrates are relatively difficult to fabricate and expensive. In the following two subsections (3.3.2 and 3.3.3), preparation, characterization and applications of novel liquid infused surfaces based on hydrophobic porous polymethacrylate surfaces are described. Different slippery liquids are used in this section (Tab. 3.6). The antibacterial properties (Section 3.3.2.) and marine antifouling properties (Section 3.3.3) of the prepared surfaces are investigated.

Table 3.6: Name and properties of the slippery liquids used for the preparation of SLIPS.

Commercial Name	Chemical Name	Kinematic Viscosity (cm ² /s) ¹	Chemical Structure
Fluorinert [®] FC-70	perfluorotri-n-pentylamine	0.12 (at 25°C)	
Krytox [®] GPL 100	poly(hexafluoropropylene oxide)	0.12 (at 20°C)	
Krytox [®] GPL 103	poly(hexafluoropropylene oxide)	0.82 (at 20°C)	

3.3.2 Antibacterial properties of the slippery liquid infused porous surface

A biofilm represents a sessile community of bacteria in which the microorganisms benefit from metabolic exchange, genetic flexibility, and protection.¹⁴⁵ The formation of biofilms of single bacterial species or mixed bacterial populations has been a natural evolutionary development with several selective advantages for the involved organisms.¹⁴⁶⁻¹⁴⁷ One of such advantages is that bacteria are able to form biofilms in a wide variety of natural and anthropogenic environments and on all kinds of technical, medical or biological surfaces being in contact with water.¹⁴⁸⁻¹⁴⁹ Thus, infections associated with biofilm growth on prostheses, catheters, and heart valves are an immense problem in medicine. In addition, biofilm resistance against antibiotics, disinfectants, and biocides is much stronger than that of planktonic bacteria, making biofilm removal more difficult. On technically used surfaces, the same resistance of mature biofilms against antimicrobial substances makes removal of biofilms, efficient disinfection or long-term elimination of mature biofilms either impossible or very difficult.^{147, 149} This makes surface coatings capable of preventing formation of biofilms before their maturation one of the most promising solutions to the biofilm associated problems.

During the last decade, a lot of research on the development of coatings for preventing biofilm formation has been done.¹⁵⁰ Coatings “actively” releasing antibacterial compounds such as antibiotics,¹⁵¹⁻¹⁵⁵ silver nanoparticles or silver ions,¹⁵⁶⁻¹⁵⁹ antibacterial antibodies¹⁶⁰ or nitric oxide¹⁶¹⁻¹⁶² have been reported. The primary advantage of active antibacterial surfaces is that delivering of

antibacterial agents takes place directly from the surface. The disadvantage is that the release rate of agents is usually uncontrolled and decreases with time.¹⁶³ Another strategy for preventing biofilm formation is based on the bacterial resistant properties of either hydrophilic polymers such as poly(ethylene glycol),¹⁶⁴ poly(ethylene oxide) brushes,¹⁶⁵ and hydrophilic polyurethanes¹⁶⁶ or zwitterionic molecules.¹⁶⁷⁻¹⁶⁸ Passive antibacterial surfaces based on toxic materials,¹⁶⁹⁻¹⁷⁵ chitosan,¹⁷⁶ polyethylenimine derivatives¹⁷⁷ or antimicrobial peptides^{129, 178} and some other antimicrobial compounds¹⁷⁹ have been also reported. Surface physical characteristics, such as surface topology or elasticity (or combination of the physical properties with surface chemistry), have also been used to resist the biofilm formation.¹⁸⁰⁻¹⁸¹ The major problem of both passive and active coatings is that adhered “conditioning” layer of proteins and dead bacteria¹⁷⁹ eventually leads to the loss of bacterial resistant properties making such coatings active for only limited period of time. Thus, to achieve long-term biofilm resistance, an easy detachment of the adhered conditioning layer is essential. These serious problems underline the strong demand for more efficient antibacterial coatings that can prevent initial bacterial adhesion and remove already adhered bacteria.

3.3.2.1 Morphology and stability of the slippery porous polymethacrylate surface

The slippery BMA-EDMA surface was prepared by applying the poly(hexafluoropropylene oxide) (PFPE) liquid (Krytox GPL 103) on the porous BMA-EDMA surface. The PFPE liquid spread instantly and formed a fluid layer on top of the porous polymer film (Fig. 3.15A). The BMA-EDMA structure is a highly interconnected network of polymer globules as shown in section 3.1.2. Such micro-textured hydrophobic substrates with large surface area could effectively assist the infusion and stabilization of the liquid lubricants.

It was shown that the property and the stability of the liquid infused porous surface depended partly on the porous properties of the underlying porous substrate.^{143, 182} Therefore, the BE1 surfaces and BE5 surfaces (see Fig. 3.1) were used for the construction stability test of the Krytox 103 infused BE1 and BE5 surfaces. Krytox 103 infused BE1 and BE5 surfaces were denoted as BE103 and BE5-103, respectively. BE103 and BE5-103 were incubated in water under shaking conditions (50 rpm) for 48 hours. The water contact angles of the surfaces were measured before and after incubation. After PFPE infusion, the BE1 surface and BE5 surface showed similar static water contact angles (Fig. 3.14). However, the BE5-103 surface showed large water contact angle hysteresis ($\sim 46^\circ$), suggesting poor slippery properties of the surface. The large water contact angle hysteresis of the surface could be resulted from the inhomogeneous liquid infusion and coating of the surface. In comparison, the BE103 had a low water contact angle hysteresis ($\sim 6^\circ$) and good stability in water under shaking conditions. The BMA-EDMA surface with larger globule size and pore size (BE1) is more suitable and was hence used for construction of the slippery surface in the following experiments.

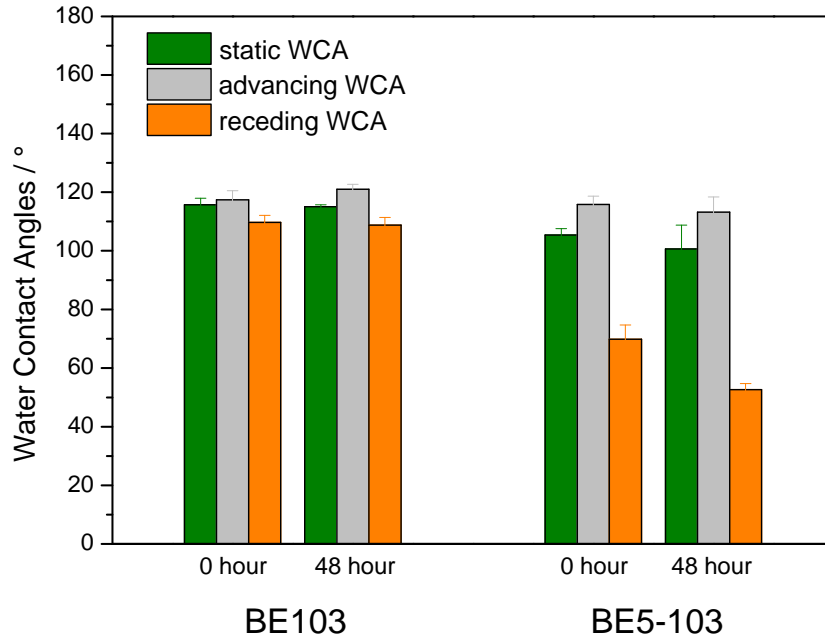


Figure 3.14: Water contact angles on the BE103 and BE5-103 surfaces before and after incubation in water for 48 hours under shaking conditions (50 rpm).

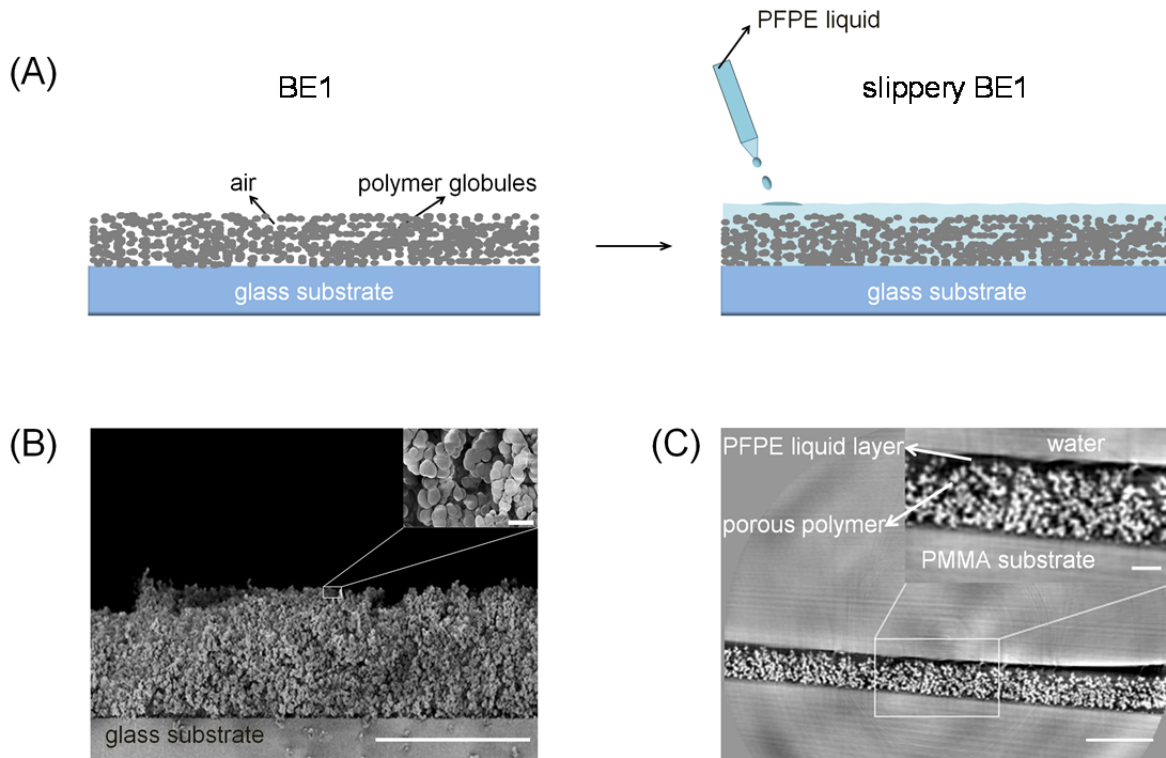


Figure 3.15: (A) Schematic representation of the fabrication of BE103 by infusion of the porous polymer (BE1) with a poly(hexafluoropropylene oxide) fluid. (B) Cross section (scale bar 100 μm) and surface (inset, scale bar 2 μm) SEM micrographs showing the morphology of the porous structure of the BMA-EDMA surface (BE1). (C) Reconstructed X-ray propagation phase contrast tomography of the BMA-EDMA surface (BE1).

image showing the cross section of BE103 surface under water.¹⁸³⁻¹⁸⁴ The liquid PFPE layer is visible on the surface of the porous BE1 (scale bar: 100 μm in the image and 20 μm in the inset).

X-ray phase contrast tomography was for the first time used to investigate the morphology of the BE103 surface under water.¹⁸³⁻¹⁸⁴ The imaging experiments were performed with Yin Cheng (IPS, KIT) and Heikki Suhonen (ESRF). The imaging reconstruction was done by Yin Cheng and Heikki Suhonen. The reconstructed phase-contrast images (Fig. 3.15C) clearly show that the PFPE liquid filled the pores of BE1 and an additional PFPE liquid layer was stabilized on top of the rough BE1. The average thickness of the PFPE liquid layer is $\sim 4\text{-}5\ \mu\text{m}$, as observed from the reconstructed X-ray propagation phase contrast tomography images.¹⁸⁴

Static, advancing, and receding water contact angles (WCA) of the surfaces were measured to characterize the wettability and stability of the surfaces. The WCA hysteresis (the difference between the advancing contact angle and receding contact angle) was also calculated. From the perspective of thermodynamics, the WCA hysteresis originates from the fact that there are multiple local minima points in the Gibbs energy curve for a droplet on a real surface.⁵⁹⁻⁶⁰ Therefore, many metastable apparent WCAs exist on a real surface. The theoretical advancing WCA is defined as the highest angle for which there is a local energy minimum and the receding WCA is defined as the lowest angle with a local energy minimum.⁶⁰ The apparent WCA (the measured advancing WCA) is usually lower than the theoretical advancing WCA because of the existence of an energy input, such as vibration of the system, which helps to overcome the energy barriers to a certain level. Similarly, the apparent receding WCA (the measured WCA) is higher than the theoretical one.⁶⁰ Surface inhomogeneity/defects are believed to be the cause for contact angle hysteresis¹⁸⁵ and the amplitude of the hysteresis is dependent on the number⁵⁷ and the wettability of the defects¹⁸⁶. Thus, contact angle hysteresis changes on the surface can be correlated to the changes in surface chemistry and morphology.¹⁸⁷ The water contact angle measurements showed that static water contact angle decreased from $\sim 133 \pm 3^\circ$ on the BE1 to $\sim 114 \pm 2^\circ$ on the BE103 surface (Fig. 3.16). The WCA hysteresis at the same time dropped from $\sim 58 \pm 4^\circ$ on BE1 to only $\sim 12 \pm 2^\circ$ on the BE103 surface, confirming formation of a PFPE superficial layer on top of the porous BE1 that was visualized by X-ray tomography. The WCAs also agree with the values obtained on other SLIPS surfaces where the same PFPE fluid was used.¹⁸⁸ To test the stability of the surface under the experimental conditions, the static WCA and WCA hysteresis changes were evaluated during the incubation of the surface in both BM2 mineral medium and in high nutrient medium (1:4 BHI broth). The stability of the BE103 surface was compared to the non-infused BE1. The BE103 were incubated in sterile BM2 mineral medium and in sterile high nutrient medium in Petri dishes for 7 days. The sterile incubation medium was replaced every day to avoid bacterial contamination and subsequent growth. The water contact angles of the surfaces were measured before and after the incubation. The surfaces were carefully washed with DI water and then dried in air before the water contact angle measurements. Figure 3.15

shows that WCAs on BE103 remained unchanged after the incubation. However, the static WCAs of the porous BE1 (without PFPE liquid infusion) decreased from $133 \pm 3^\circ$ to $120 \pm 5^\circ$ and the WCA hysteresis increased greatly from $58 \pm 4^\circ$ to $120 \pm 6^\circ$ after 7 days incubation in the BM2 mineral medium. BE1 incubated 7 days in high nutrient medium also showed similar changes. These results indicate that the infusion of the porous BE1 with the PFPE fluid significantly improves its long-term stability in aqueous conditions. Stability experiments performed under flow conditions showed similar results (Fig. 3.17).

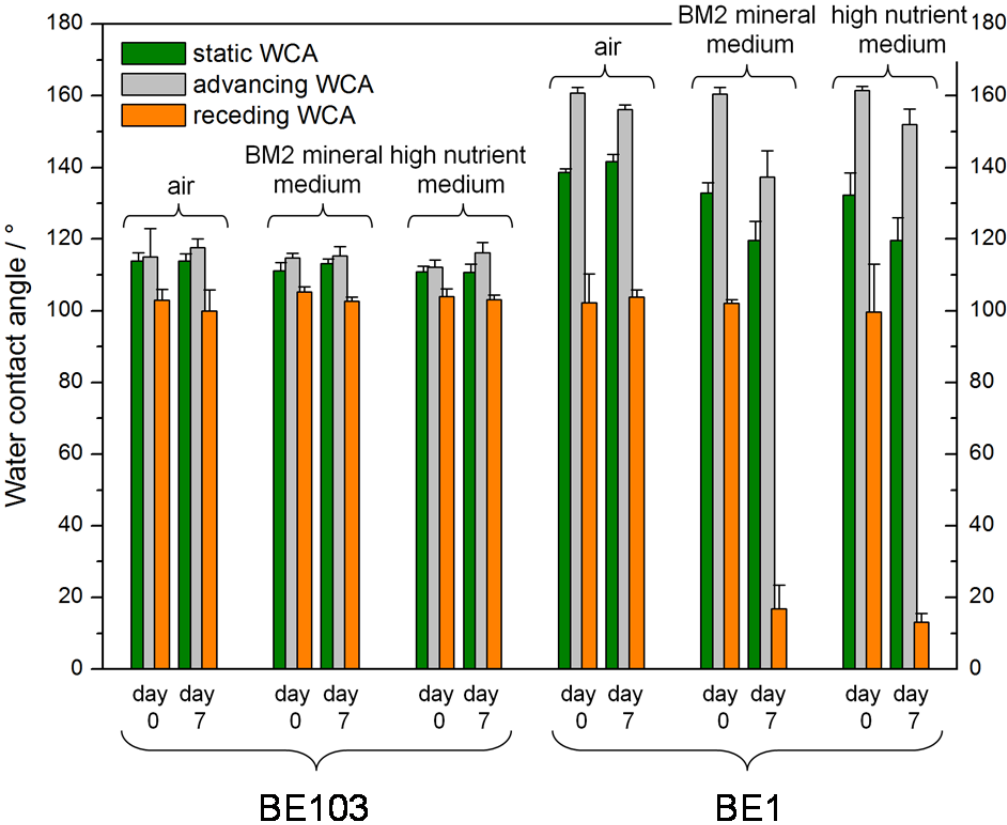


Figure 3.16: Water contact angles on the BE103 and the non-infused porous BE1 before and after a 7 days incubation in BM2 mineral medium and in high nutrient medium.

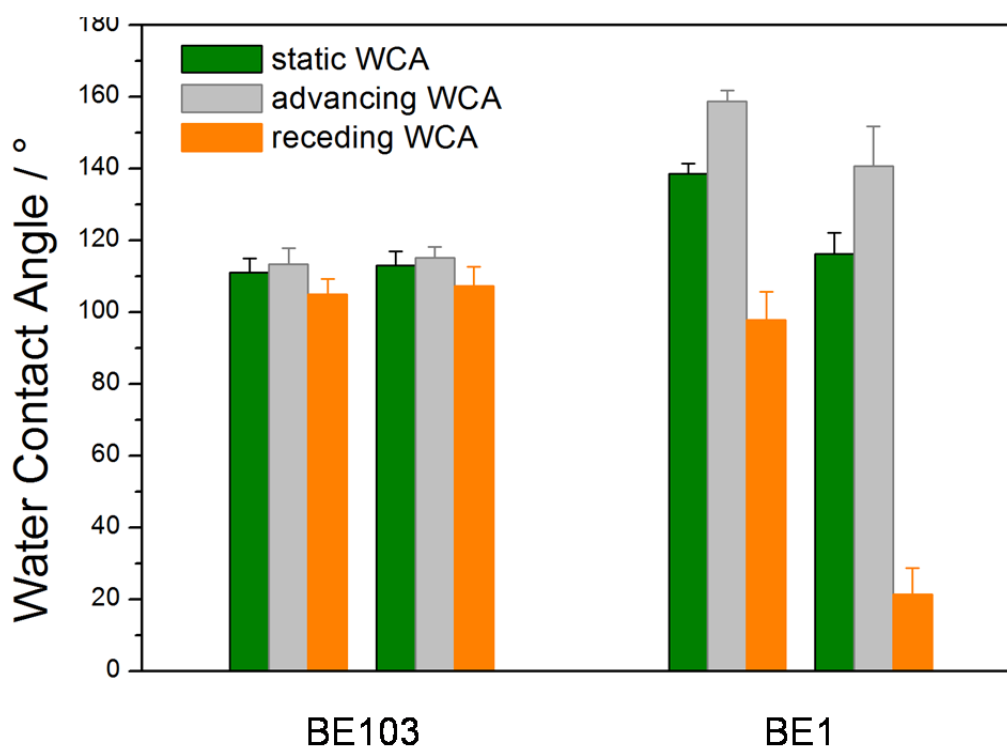


Figure 3.16: Water contact angles on the BE103 and the non-infused porous BE1 before and after 7 days incubation in BM2 mineral medium flow condition. Flow rate: 0.94 ml/min.

The WCA changes of the BE1 may be attributed to the hydrolysis of the ester bonds on the surface and deposition of the components from the medium. To prove this, XPS and Raman measurements were performed. Characteristic peaks from sodium, nitrogen and chloride were observed in the XPS survey spectra of the BE1 surface incubated in high nutrient medium (Fig. 3.18). These peaks were absent in the spectrum of the untreated BE1. The results suggest the deposition of the components (such as salts and proteins) from the high nutrient medium on the BE1 after 7 day incubation of BE1 in rich medium. It was observed that the peak area of the C=O bond increased (Fig. 3.19A) after incubation of the BE1 in high nutrient medium. Besides, the presence of O 1s peak corresponding to the hydroxyl group (HO-C) was also observed from the high resolution O 1s spectrum (Fig. 3.19B). These results indicate either the hydrolysis of the ester bond in the BE1 or deposition of the proteins from the rich nutrient medium. Deposition of the components from the high nutrient medium on the BE1 was also demonstrated using Raman spectroscopy (Fig. 3.20). The Raman peaks at $\sim 1530 \text{ cm}^{-1}$ and $\sim 1160 \text{ cm}^{-1}$ ¹⁸⁹ in the spectra of the surface after incubation in high nutrient medium are from the C=C bond in the lipoproteins. The presence of these peaks indicates the deposition of lipoproteins from the high nutrient medium on the BE1. In contrast, no obvious changes were observed on the XPS spectra of the BE1 incubated in BM2 mineral medium. The reason for this could be that only small portion of ester groups is actually hydrolyzed on this surface. The fact of strong decrease of the water contact angles on this surface is not surprising because even partial hydrolyzation of a highly rough surface can lead to a drastic change in wettability.

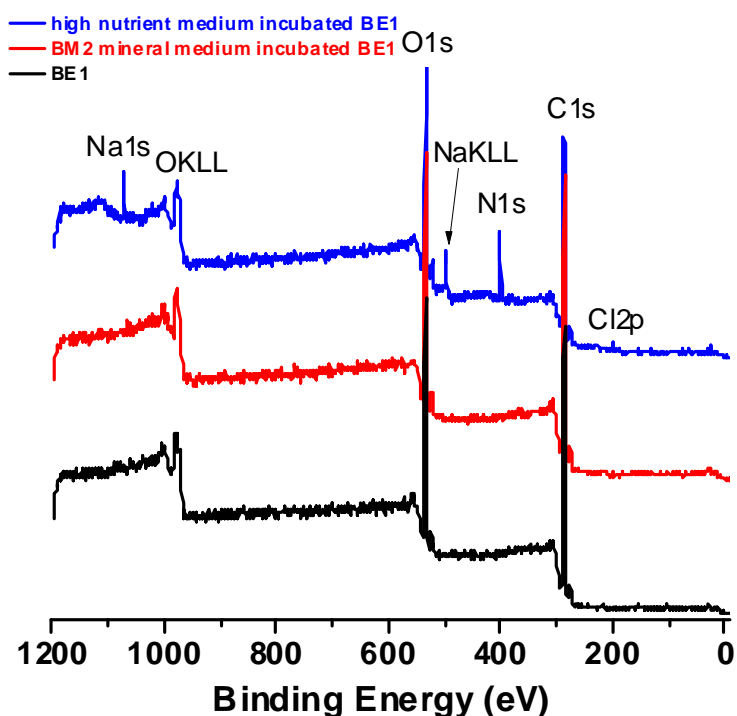


Figure 3.18: XPS survey spectra of the high nutrient medium incubated BE1, BM2 mineral medium incubated BE1 and as-prepared BE1. The XPS spectra were obtained using the VG Scienta R4000 UHV-IR/XPS spectrometer (Bruker, Karlsruhe, Germany).

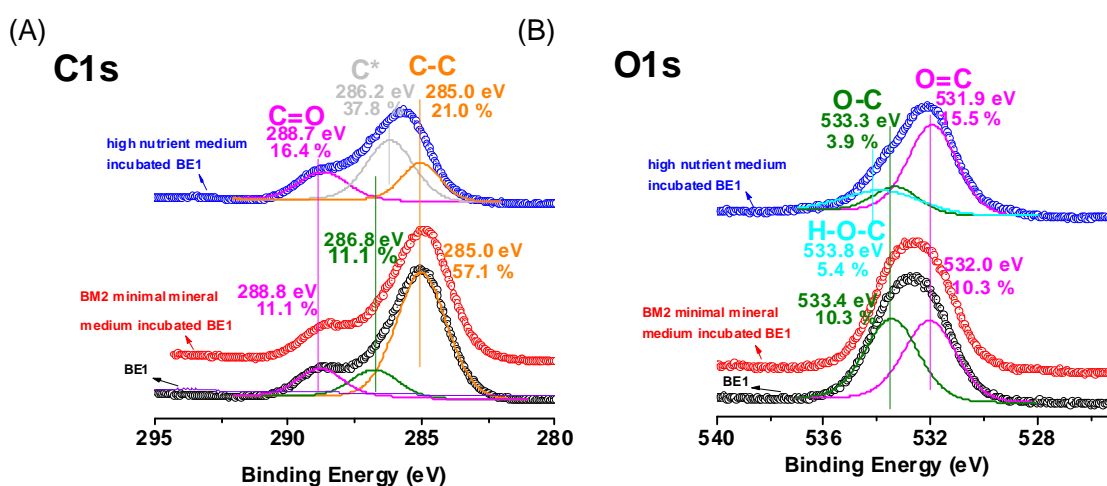


Figure 3.19: XPS high resolution (A) C 1s spectra and (B) O 1s spectra of the BE1 surface incubated with the high nutrient medium (blue line), BE1 surface incubated in BM2 mineral medium (red line) and the untreated BE1 surface (black line).

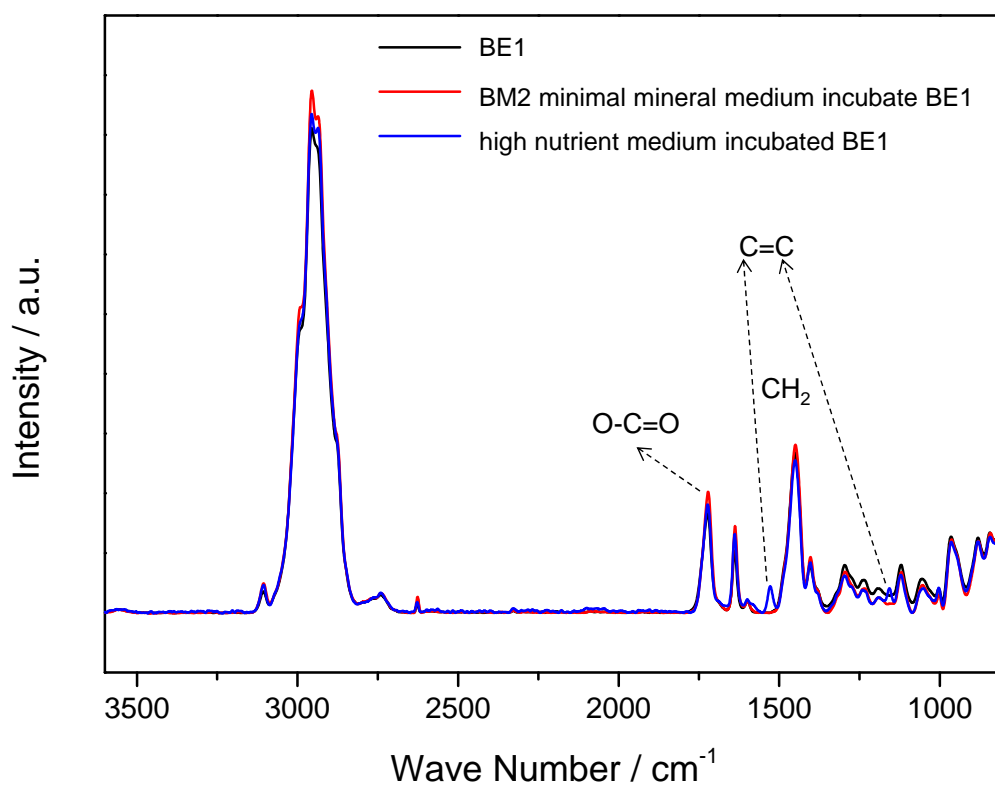


Figure 3.20: Raman spectra of the BE1 before (black line) and after 7 days incubation in BM2 mineral medium (red line) or high nutrient medium (blue line).

3.3.2.2 Biofilm formation of *P. aeruginosa* strain PA49 on the BE103

Bacterial adhesion on the BE103 was studied in a plug flow biofilm reactor, through which the bacterial suspensions were continuously perfused by a peristaltic pump. Two different bacterial culture medium, the BM2 mineral medium and high nutrient medium (1:4 BHI broth), were used for the experiments. The flow rate of the bacterial culture medium in the biofilm reactor was 0.94 mL/min. The BE1 (non-infused) and glass slides were tested as well for comparison. The overnight cultures were diluted with medium to 10^8 CFU/mL and used to start biofilm cultivation. After 7 days or 14 days culture in the biofilm reactor, the surfaces were stained (with CTC and DAPI) and analyzed using fluorescence microscopy with subsequent software mediated data analyses.

The biofilm formation of *P. aeruginosa* strain PA49 on the BE103 was first tested. After 7 days exposure in BM2 mineral medium, DAPI and CTC staining analyses were performed to evaluate the total cell counts and respiratory active cell counts, respectively. Only a few respiring bacteria had adhered on the BE103, while massive biofilm coverage was observed on the glass slides. In both cases, loosely attached bacteria were removed by washing with sterile medium to discriminate between the attached and planktonic bacteria. The fluorescence images are shown in Fig. 3.21. The BE103 prevented up to 97.6 % of *P. aeruginosa* PA49 biofilm formation compared to the glass slides over 7 days period in BM2 mineral medium. The BE103 demonstrated bacterial coverage of 1.8 ± 0.8 % of the area under investigation in three independent experiments. In contrast to these low coverage data,

the glass slides exhibited surface coverage of $32.8 \pm 11.7 \%$ and a maximum value of $98.6 \pm 9.8 \%$ (Table 3.7A-C). Even a 14 days incubation period with an identical setup confirmed the previous results with a bacterial surface coverage of $8.2 \pm 4.8 \%$ on the BE103 and $24.2 \pm 8.3 \%$ on the glass slides (Tab. 3.7D).

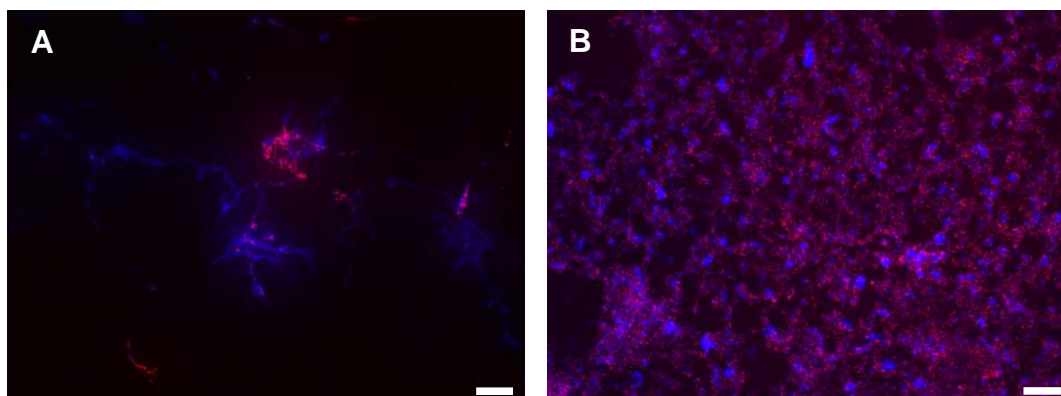


Figure 3.21: Fluorescence micrographs of (A) BE103 and (B) glass slide after 7 days surface exposure in BM2 mineral medium (flow rate: 0.94 mL min^{-1}) of *P. aeruginosa* strain PA49 stained with CTC (red) and DAPI (blue).¹⁸⁴ Scale bar $50 \mu\text{m}$.

Table 3.7: Comparison of the bacterial surface coverage on the BE103 and on glass slides with environmental wastewater *P. aeruginosa* strain PA49 in BM2 mineral medium (flow rate 0.94 mL min^{-1}) for 7 days (A-C) and 14 days (D) incubation period.¹⁸⁴ Data from each independent experiment are listed.

	Surface coverage in %	
	BE103	glass slide (control)
A	0.8 ± 0.5	33.0 ± 10.6
B	0.8 ± 0.3	32.6 ± 12.8
C	3.9 ± 1.6	98.6 ± 9.8
D	8.2 ± 4.8	24.2 ± 8.3

3.3.2.3 Biofilm formation of different strains of *P. aeruginosa* on the BE103 in high nutrient medium

To test the generality of the slippery surfaces, the bacterial adhesion of different *P. aeruginosa* strains was also studied in high nutrient medium (1:4 BHI broth) with identical flow conditions. The bacterial adhesion of the laboratory reference strain *P. aeruginosa* UCBPP-PA14 (PA14) was compared to the environmental strains *P. aeruginosa* PA30, *P. aeruginosa* PA910, and *P. aeruginosa* PA49 (Tab. 3.8), previously isolated from wastewater effluents.¹⁹⁰

In accordance with experiments using BM2 mineral medium, only single cells or micro-colonies of the reference strain *P. aeruginosa* PA14 were observed on BE103 when high nutrient medium (1:4 BHI broth) was used for the 7 days exposure period (Tab. 3.8). These results confirmed the observation from Epstein et al.¹⁴⁴ The *P. aeruginosa* environmental strains PA30 and PA910 showed similar results to the *P. aeruginosa* strain PA14 on the BE103. The multi-resistant environmental *P. aeruginosa* strain PA49 exhibited, however, a significantly increased colonization of the BE103: 11.96 ± 6.27 % (Tab. 3.8), which was about 13 times higher than the coverage values measured for the reference strain *P. aeruginosa* PA14 and almost two times higher than the PA49 occupied the reference glass slide. These results clearly show that the biofilm formation of *P. aeruginosa* on the BE103 was strain dependent. Much higher bacterial coverage was found on BE1 (non-infused) surfaces and glass slides (Tab. 3.8). The bacterial coverage on glass surfaces was much lower in BHI high nutrient medium compared with those in the low nutrient BM2 mineral medium (Tab. 3.8). It could be speculated that these differences in the glass controls might be because that the media dependent surface conditioning changed the adhesion behavior of the *P. aeruginosa* strains under investigations. Therefore, it is more conclusive to compare separately the different *P. aeruginosa* strains and their biofilm formation on each surface to exclude media dependent side effects. The good stability of the BE103 in high nutrient medium indicates that the effect of the culture medium on the PA49 biofilm formation on the BE103 is not due to the instability of the BE103.

Table 3.8: Comparison of the bacterial surface coverage of different *P. aeruginosa* strains on the BE103, on the glass slides and on BE1 after 7 days culture (in 1:4 BHI broth, flow rate: 0.94 mL min⁻¹).¹⁸⁴

Bacterial type	Surface coverage in %		
	BE103	glass slide	BE1
<i>P. aeruginosa</i> PA14	0.92 ± 0.33	2.14 ± 0.5	2.43 ± 0.89
<i>P. aeruginosa</i> PA30	1.95 ± 1.19	2.45 ± 0.16	86.27 ± 4.52
<i>P. aeruginosa</i> PA910	0.87 ± 0.25	2.28 ± 0.37	1.52 ± 0.15
<i>P. aeruginosa</i> PA49	11.96 ± 6.27	6.45 ± 1.87	36.34 ± 14.21

3.3.2.4 Toxicity tests

To demonstrate that the prevention of the biofilm adhesion on the BE103 was not caused by toxicity of the PFPE liquid, the impact of PFPE liquid on the bacterial growth was tested. The toxicity test with PFPE liquid showed that the fluorinate polymer itself did not have an antimicrobial effect. In BM2 mineral medium with up to 12.5% PFPE liquid, the bacteria showed the same growth kinetics as that in pure BM2 mineral medium. Up to 4 hours, no increase in CFU/mL was observed. After 22 hours in all samples bacterial concentrations of $\sim 3.8 \cdot 10^8 \pm 8.3 \cdot 10^7$ CFU/mL were reached (Tab. 5.1).

3.3.2.5 Effect of components in the bacterial culture medium on the biofilm formation of *P. aeruginosa* on the surface

To analyze the effect of the components of the high nutrient medium on the bacteria adhesion, the BE1 was preincubated for 48 hours in high nutrient medium (1:4 BHI broth) and subsequently used for the bacterial adhesion assay of PA 49 strain for 7 days in BM2 mineral medium. The preincubated BE1 was only slightly covered with respiring, CTC active bacteria. Based on these results, no differences of the bacterial surface coverage between the BE1 and the preincubated BE1 were observed. The preincubated BE1 exhibited biofilm coverage of 0.84 ± 0.26 % of the surface, the slippery BE1 without 48 hours of preincubation showed a coverage of 1.3 ± 0.18 %. The surface coverage on glass slides is three fold higher (6.6 ± 1.38 %). These results indicate that the stronger bacterial occupation of the BE1 surface observed in the high nutrient medium was not caused by the modification of the BE1 surface through the interaction with rich medium but was rather the result of a different behavior of the bacteria in the two media: high nutrient and the mineral BM2.

In this section, a novel PFPE liquid infused porous polymer surface based on a porous BE1 with slippery properties and long-term stability in aqueous environments was demonstrated. We have shown that the BE103 prevented biofilm formation of different strains of opportunistic pathogen *P. aeruginosa* up to 7 days in low nutrient medium. In contrast, in high nutrient medium, the biofilm formation on the BE103 was highly strain dependent. The BE103 also exhibited antibacterial properties against laboratory reference clones of *P. aeruginosa* and most of the environmental *P. aeruginosa* strains studied. However, the antibiotic and multi-resistant *P. aeruginosa* isolate PA49 was able to form dense biofilms on the BE103 in the presence of high nutrient milieu. Although the results confirmed the superior antibacterial behavior of BE103, they, at the same time, point to a limit in applications of such surfaces. The difference in biofilm formation between the laboratory reference strains and the environmental *P. aeruginosa* strains was attributed to their specific genotypic background. Finally, our results emphasize the importance of comparing different bacterial strains (both wild type and laboratory strains) as well as different experimental conditions when evaluating antibacterial properties of novel surface coatings.

3.3.3 Marine antifouling properties of the slippery porous polymethacrylate surface

Fouling associated with marine organisms not only causes tremendous economic loss¹⁹¹ but also poses a threat to the ocean environment.¹⁹² Surface coatings capable of preventing marine fouling are greatly desired. Biocides (such as tributyltin oxide) based surfaces were widely used as antifouling surfaces. Although these surfaces have been shown to be efficient in antifouling, the applications of these surfaces are restricted because of their adverse ecological effects.¹⁹³ Novel non-biocidal antifouling surfaces have been developed recently. One of the popular non-biocidal antifouling surfaces is the poly(dimethylsiloxane) (PDMS) elastomer based surface.¹⁹⁴⁻¹⁹⁷ PDMS has very low surface energy, low elastic moduli and thus good fouling release property.¹⁹⁸ It was reported that these surfaces showed good antifouling properties when a “bio-inspired” surface topography was introduced onto the surfaces.¹⁹⁹⁻²⁰² The amphiphilic²⁰³ or zwitterionic²⁰⁴ polymer surfaces have been also used as marine antifouling surfaces recently. Despite of these advancements, the development of a robust antifouling surface is still challenging. To achieve an efficient non-biocidal marine antifouling surface, different aspects of the surface property such as morphology, chemistry, elasticity and lubricity should be carefully designed.²⁰⁵ In this section, the interactions between slippery BMA-EDMA surfaces and marine fouling organisms are investigated to gain a better understanding of the antifouling properties of the newly developed surfaces. The motile spores (zoospores) of the marine macroalga (seaweed) *Ulva linza* and cypris larvae of the barnacle *Balanus amphitrite* are used for the study.

BMA-EDMA SLIPS surfaces are prepared in the same way as described in Section 3.3.2. The BE1 surfaces (abbreviated as BE in this section) are used for preparation of slippery surfaces. Different liquids: poly(hexafluoropropylene oxide) (Krytox GPL 103 and Krytox GPL 100) and perfluorotripropylamine (Fluorinert FC-70) are used. The surfaces infused with Krytox GPL 103, Krytox GPL 100 and Fluorinert FC-70 are called BE103, BE100 and BE70, respectively.

3.3.3.1. Stability of the slippery BMA-EDMA surface in artificial seawater

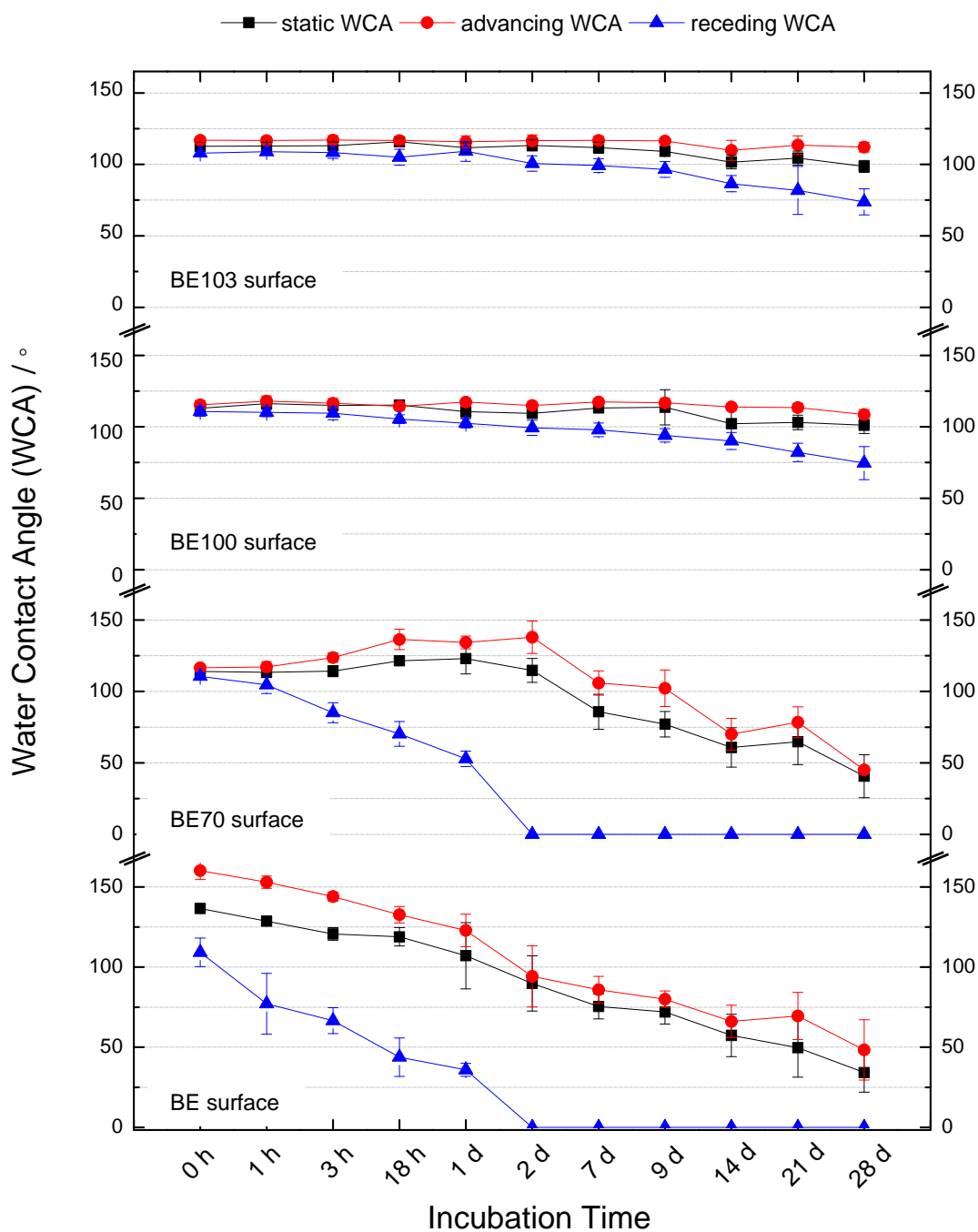


Figure 3.22: Water contact angles of different slippery BMA-EDMA surfaces and non-infused BMA-EDMA surfaces as a function of the incubation time in artificial seawater (ASW) under shaking condition (50 rpm). The reported values are the means of nine measurements, with the error bars representing the standard deviations.

The surface stability is important for practical applications of such coatings in marine environment. The stability of the surfaces was tested by incubating the substrates in ASW for up to 28 days under shaking condition. The surfaces were taken out from the ASW at certain time points and water contact

angles (static, advancing and receding water contact angles) were measured. As shown in Fig. 3.22, the water contact angles obtained on pristine BE surfaces decreased gradually with time. These changes in water contact angles of BE surfaces could be caused either by adsorption of components from the solution or by the slow hydrolysis of the ester bonds on the surface. In comparison, the water contact angles measured on the BE103 and BE100 surfaces remained unchanged for at least up to 7 days of incubation in ASW (Fig 3.21). After 7 days, the receding water contact angle of the BE100 and BE103 surfaces slightly decreased. The initial BE70 surface had a WCA of $\sim 114^\circ$ and very low water contact angle hysteresis ($\sim 6^\circ$) (Fig. 3.22). After 2 days of incubation, the static WCA of the BE 70 surface increased slightly while the WCA hysteresis increased significantly. Considering the slight increase in static WCA of BE70 within 2 days of immersion, the possible explanation for this change is that the lubricant layer has been partially removed from the surface, making the surface rougher and, therefore, leading to the increase of the static WCA and larger WCA hysteresis. The further decrease of the static and advancing WCAs can be explained by the change of the surface chemistry of the BMA-EDMA porous surface caused by hydrolysis of the ester bonds in slightly alkaline environment (pH ~ 8.2 , Instant Ocean). This behavior is obvious from the decrease of WCAs on the non-infused BE polymer surface exposed to ASW.

Marine antifouling properties of the surfaces were tested and reported elsewhere.²⁰⁶

3.3.4 Summary

By infusing perfluorinated liquids into the BE1 surface, water-repellent slippery surfaces were obtained. It was proved that the poly(hexafluoropropylene oxide) (Krytox 103) infused BE1 surface (BE103) showed good stability in bacterial culture medium and artificial seawater. The superior antibacterial properties of BE103 surfaces were demonstrated. However, it was also shown that the antibacterial properties of BE103 surface are bacterial strain dependent. The antibiotic multi-resistant *P. aeruginosa* isolate PA49 was able to form dense biofilms on BE103 surface in presence of high nutrient milieu. The results also emphasized the importance of comparing different bacterial strains as well as different experimental conditions when evaluating antibacterial properties of novel antibacterial surface coatings.

It was observed that the poly(hexafluoropropylene oxide) liquid layer was not homogeneously distributed and minor defects were identified on BE103 by X-ray tomography.¹⁸³ The presence of these surface defects (polymer globules not covered by the PFPE liquid) may lead to the formation of the conditioning film and subsequent bacterial/marine fouling organism attachment on the surface. For the future studies of the antibacterial/antifouling properties of slippery BMA-EDMA surfaces, slippery surface with less defect sites, which might be achieved by reducing the roughness and increasing hydrophobicity of the surface matrix, should be tested.

3.4. Printable superhydrophobic-superhydrophilic micropatterns based on supported lipid layers.

3.4.1 Background

The ability to create superhydrophilic-superhydrophobic micropatterns and arrays is essential for a variety of applications ranging from microfluidics to cell microarrays and high-throughput screenings. Despite a lot of research done on the development of new superhydrophobic²⁰⁷⁻²¹² and superhydrophilic surfaces,²¹³ creating precise and stable micropatterns of superhydrophilic and superhydrophobic areas has proven to be challenging. Plasma treatments have been commonly used to create hydrophobic-hydrophilic micropatterns on a hydrophobic surface.²¹⁴⁻²¹⁷ For example, Zimmermann et al.²¹⁴ prepared superhydrophobic-superhydrophilic (SH-SL) micropatterns by spatially confined oxygen plasma treatment of the superhydrophobic silicone coating by using of a glass mask. This method is simple and straightforward. However, SH-SL micropatterns with sharp boundaries were difficult to achieve because effective shielding of the surface from the reactive plasma atmosphere is difficult. Construction of the SH-SL micropatterns using a soft-lithography technique was also reported.²¹⁸⁻²¹⁹ To achieve the SH-SL micropattern, Kang et al.²¹⁹ selectively deposited of poly(dopamine) on the superhydrophobic anodic aluminum oxide surface through a soft-lithography technique. Another method for the creation of the SH-SL polymer surface is the photoinitiated surface modification. The primary advantage of the photo-initiated surface modification is that they enable the precise spatial control of the modification simply by using a photo mask. Notsu et al. prepared SH-SL micropattern on a superhydrophobic surface using the UV triggered oxidation of the surface.²²⁰ Photoinitiated polymer surface grafting was also used recently in our group to create SH-SL micropatterns on the polymethacrylate surfaces.^{38, 40} Despite of these advances, facial and versatile methods for creating the SH-SL micropatterns on different substrates are still rare. In this section, a new and facile method for the modification of the superhydrophobic BMA-EDMA surface using phospholipid is described. SH-SL micropatterns are also prepared using the method.

3.4.2 Modification of porous polymethacrylate surfaces with phospholipids

In order to investigate the influence of the morphology of the porous structure on hydrophobicity, BMA-EDMA surfaces with different morphologies were prepared by varying the composition of the porogens present in the polymerization mixtures. The average size of polymer globules of all prepared BMA-EDMA surfaces (BE1, BE3 and BE5, respectively) determined from SEM images were 1143 ± 169 nm, 205 ± 58 nm and 112 ± 39 nm (Figure 3.23). Non porous BMA-EDMA surfaces (BE6) were also prepared by polymerization of a polymerization mixture without porogens.

It is known that deposition of an amphiphilic lipid onto a hydrophobic surface can lead to formation of lipid mono- or multilayers depending on the conditions. Stable lipid layers have been formed on polystyrene,²²¹ polyvinylchloride,²²² alkanethiol modified gold,²²³⁻²²⁴ and silicon substrate.²²⁵ However, in most cases flat substrates have been used for lipid studies. In this section, I will show that simple

wetting of the porous BMA-EDMA surface with a 10 mg/mL ethanol solution of 1,2-Dioleoyl-*sn*-glycero-3-phosphoethanolamine (DOPE) or 2-oleoyl-1-palmitoyl-*sn*-glycero-3-phospho-*rac*-(1-glycerol) ammonium salt (POPG) transformed the surface into a highly hydrophilic surface only at the positions where the solution is applied. The water contact angles of the modified surfaces were measured after rinsing the surface with water and drying. The changes of static water contact angles after the POPG lipid modification of surfaces with different morphologies are shown in Figure 3.23E. The effect of surface morphology and porosity on the ability of lipid modification to make surfaces superhydrophilic is clearly seen from the figure. The water contact angle on porous surfaces drops significantly after the modification, while only a slight change is visible after modification of a nonporous surface. For further experiments on the superhydrophilic surfaces and preparation of superhydrophobic-superhydrophilic patterns we used surface with globule sizes of 205 nm (BE3), which showed the largest decrease of hydrophobicity after modification.

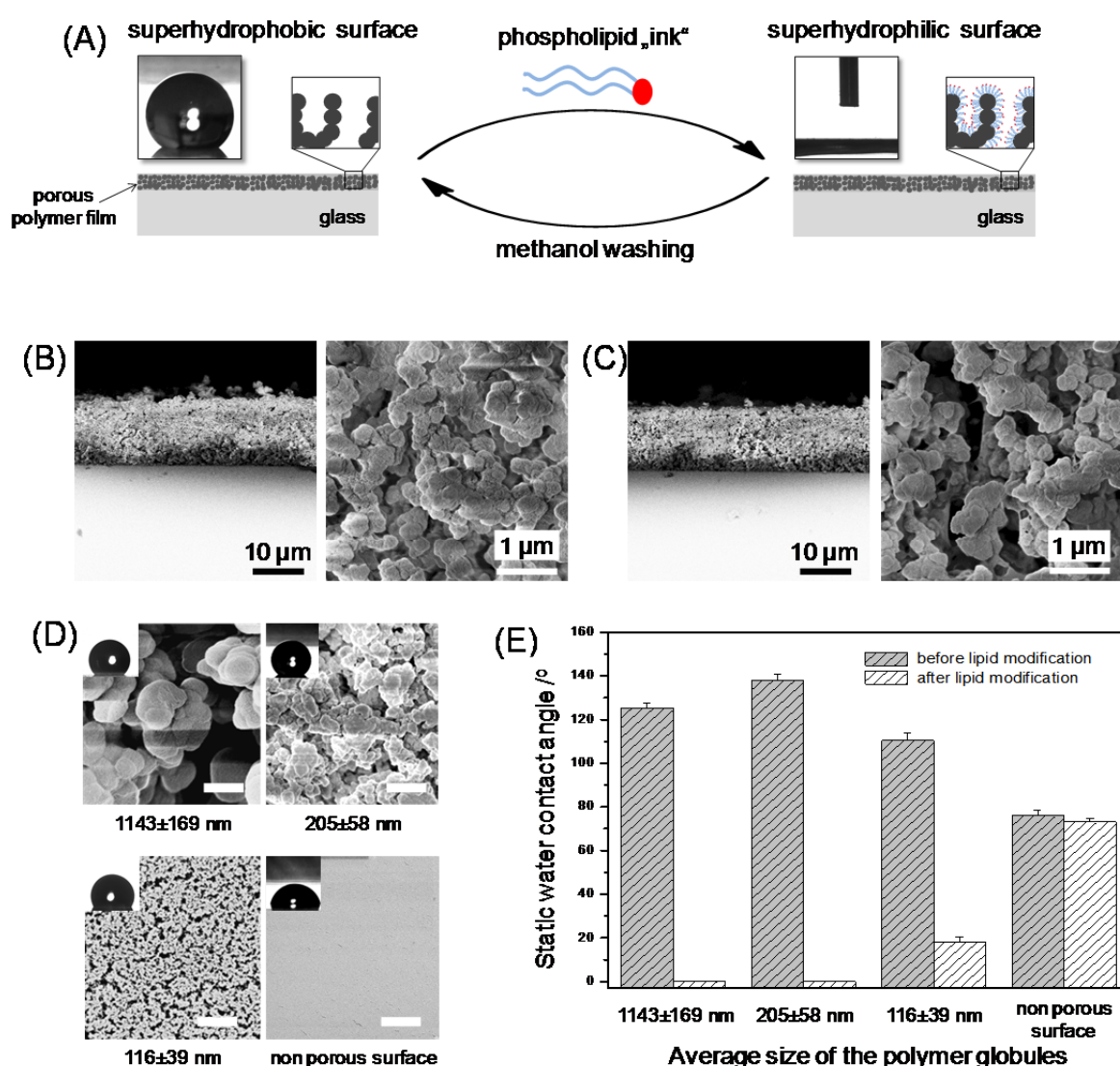


Figure 3.23: (A) Schematic representation of switching from superhydrophobicity to superhydrophilicity by applying an “ink” containing a phospholipid on porous BMA-EDMA surfaces.

SEM images of the microporous structure of (B) superhydrophobic and (C) superhydrophilic porous BE3. (D) SEM images and images of water droplets on the BMA-EDMA surfaces with different morphologies (scale bars 1 μm ; average sizes of polymer globules are indicated under SEM images). (E) Static water contact angles on BMA-EDMA surfaces with different morphologies before and after modification with the POPG lipid. Average sizes of polymer globules are indicated.

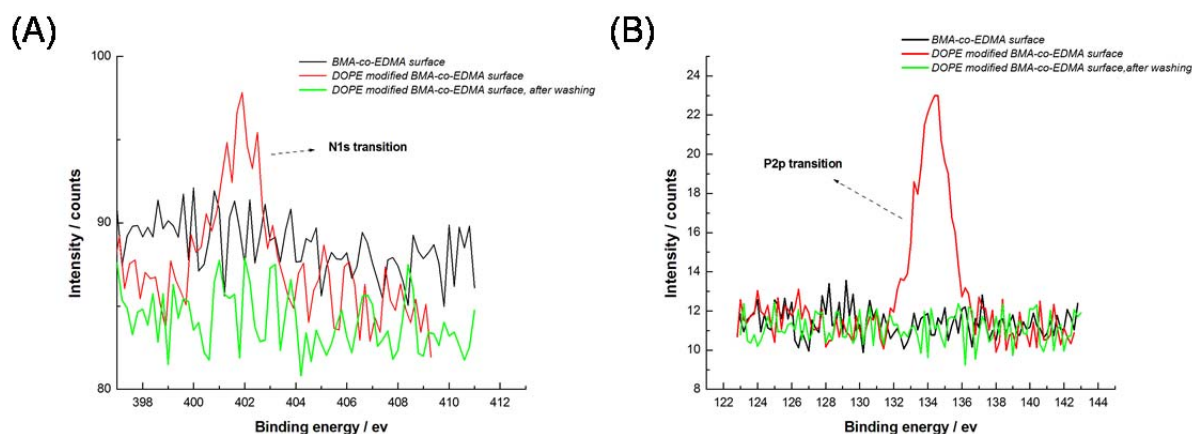


Figure 3.24: X-ray photoelectron spectroscopy (XPS) spectra of BE3 before (black) and after modification with DOPE (red) as well as after washing with methanol (green). (A) N 1s signal; (B) P 2p signal.

The hydrophobicity switch is a result of the formation of a stable lipid layer on the hydrophobic surface of the polymer globules (Figure 3.23A), which was confirmed by XPS measurements (see Fig. 3.24). The N 1s and P 2p peaks correspond to the amine group and phosphate group of the DOPE, respectively. Both the N 1s and P 2p peaks are clearly visible on the XPS spectrum of DOPE modified BE3. On the contrary, the BE3 surface without modification has no P 2p or N 1s peaks. These characteristic peaks were also not present in the spectrum of the DOPE modified BE3 which was washed after modification, suggesting that a simple washing process could remove most of the lipid molecules on the modified BE3.

To verify the successful lipid modification on the surface, Time of Flight Secondary Ion Mass Spectrometry (ToF-SIMS) was used. ToF-SIMS is a highly sensitive characterization method for surface analysis and can be used for many types of materials and different sample forms.²²⁶ During the ToF-SIMS measurement, a pulsed ion beam is generated from the primary ion source (Bi cluster liquid metal in the current experiment) and used to bombard the surface.²²⁷ Upon ion bombardment, electrons, photon and secondary ions are emitted from the surface and the produced secondary ions are used for surface characterization. Only secondary ions produced at the very outermost surface (\sim 2-3 monolayers) of the sample could overcome the surface binding energy and leave the sample.²²⁷

Therefore, ToF-SIMS is highly surface specific. The primary ion dose has to be well controlled to avoid damaging the sample.²²⁸ A Time of Flight (ToF) analyzer is used in ToF-SIMS because it allows for high resolution and parallel detection of ions of all masses. Secondary ion mass spectra are obtained by analyzing the mass to charge ratios (m/z) of the charged species from the fragments. ToF-SIMS can be also used for high resolution (with lateral resolution down to 50nm) chemical mapping.²²⁸⁻²³⁰ For the ToF-SIMS test, a reference sample, BE3, a DOPE modified BE3 and a modified BE3 which was washed with methanol after modification were used. The reference sample was prepared by deposition of DOPE solution (in ethanol, 10mg/mL) on the gold coated silica wafer. The obtained spectra are shown in Fig. 3.25. After DOPE modification, characteristic peaks (e.g.: $C_{41}H_{77}O_8PN^-$ at 742.5 and $C_{18}H_{33}O_2^-$ at 281.2) from DOPE could be clearly identified in the spectrum of modified BE3 while these peaks were absent in the spectrum of BE3. In addition, these characteristic peaks were also found in the spectrum of the modified BE3 after washing (magenta line in Fig. 3.25). This could be a result from the residual DOPE left on the surface after washing. However, the WCA measurements showed that the residual DOPE on the surface did not change the WCA of the surface (Fig. 3.28). The isotope ratios of these characteristic peaks were analyzed to further confirm the assignment of the peaks. Experimental isotope ratios of the characteristic fragments were calculated with the areas of the isotope peaks and compared to the theoretical value. As shown in Fig. 3.26, the theoretical isotope ratio of $C_{41}H_{77}O_8PN^-$ and $C_{18}H_{33}O_2^-$ are close to their corresponding experimental values. These results clearly demonstrate that DOPE was immobilized on the BE3 surface.

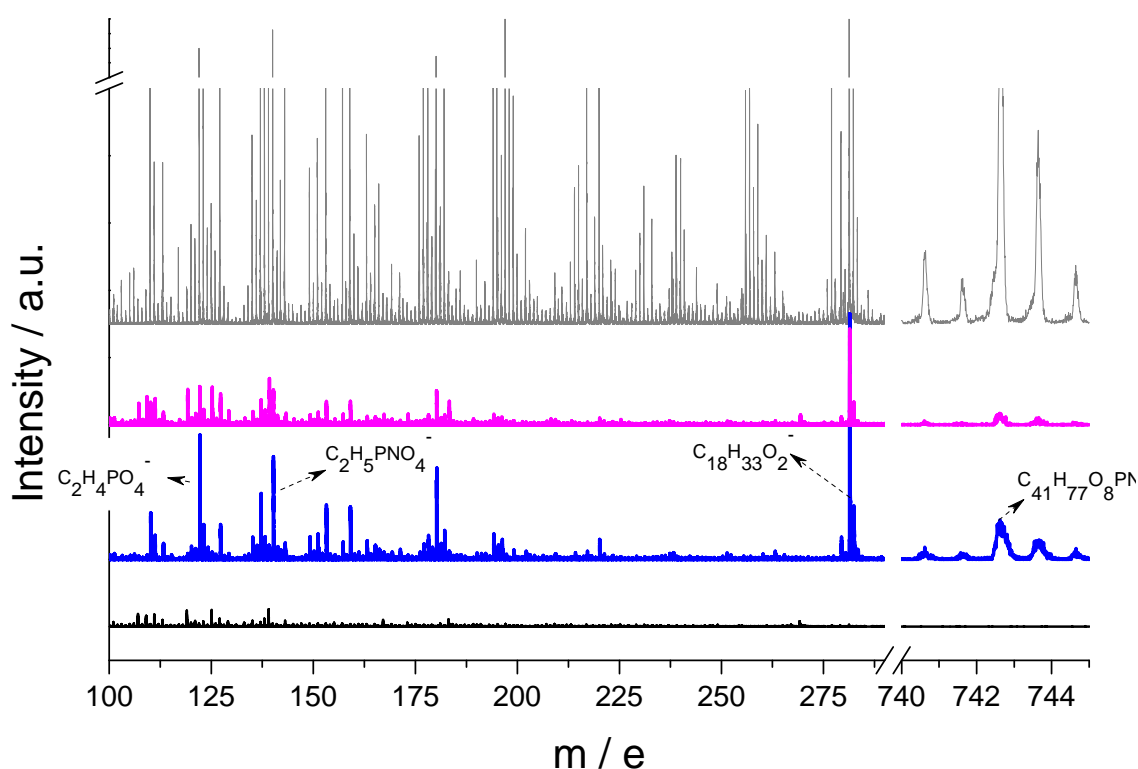


Figure 3.25: ToF-SIMS mass spectra of the BE3 (black line), DOPE coated gold surface (gray line), DOPE modified BE3 (blue line) and DOPE modified BE3 after methanol washing (magenta line).

Negative mode; the DOPE modified surface was washed with water before the measurements.

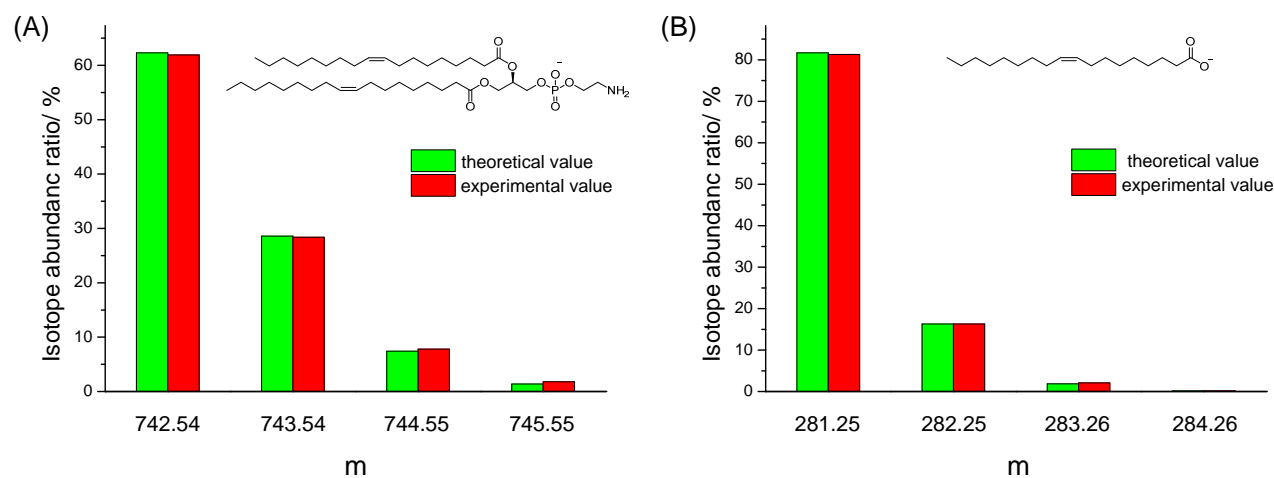


Figure 3.26. Theoretical and experimental isotope abundance ratios of (A) $C_{41}H_{77}O_8PN^-$ and (B) $C_{18}H_{33}O_2^-$.

The long-term preservation of the superhydrophobicity/superhydrophilicity contrast is critical for the real application of superhydrophobic/superhydrophilic micropatterns. The long term stability of the surface's hydrophobicity was tested by measuring the water contact angle on one surface after six months (the surface was kept in a Petri dish in air). The static water contact angle for the surface with average globule size of 205 nm decreased only by 2° (from $140 \pm 3^\circ$ to $138 \pm 2^\circ$), confirming the good stability of the surface. The superhydrophobic surface is constituted of a porous structure that encompassed the entire thickness as wiping their surface only removes the most superficial layer of the structure. When the top layer becomes damaged, the underlying structure becomes exposed and the superhydrophobicity remains unaffected.²⁴ The superhydrophilicity of the lipid coated BE3 also appears to be stable under aqueous conditions. Even 30 consecutive steps of washing with water and drying did not deteriorate the superhydrophilicity of the surface resulting from the modification (Figure 3.27 A and Figure 3.28 A). Apparently, this surprising stability is endowed by the porosity of BE3, which protects the lipid layer from the action of the applied water flow. On the contrary, a nonporous BMA-EDMA surface made hydrophilic by coating with a lipid layer transformed back to a hydrophobic surface after a single washing with water.

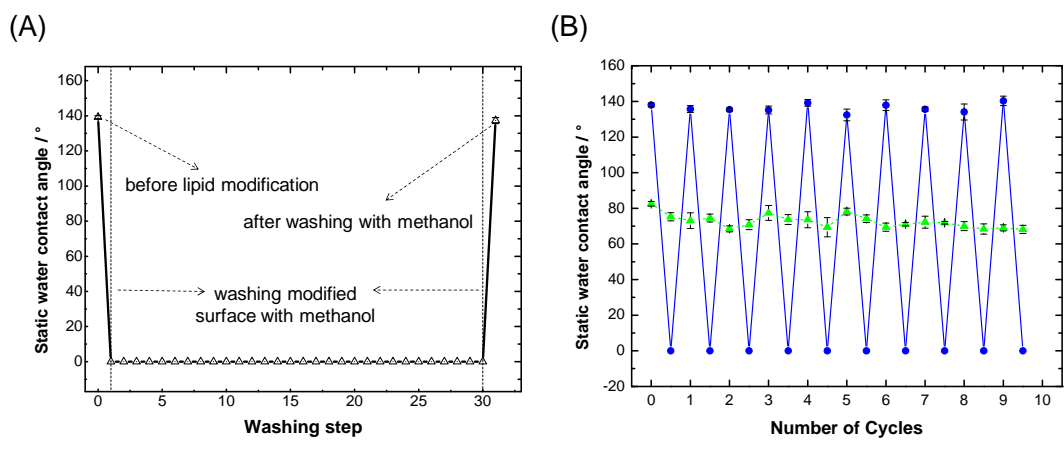


Figure 3.27: (A) Static water contact angle on a superhydrophilic POPG lipid modified BE3 during 30 consecutive steps of washing with water. Superhydrophobicity is restored after a single washing with methanol. (B) Repetitive switching between superhydrophobicity and superhydrophilicity by modifying a BE3 with a phospholipid and erasing the superhydrophilicity by washing with methanol (blue); corresponding changes of the static water contact angle on a nonporous BMA-EDMA surface (green).

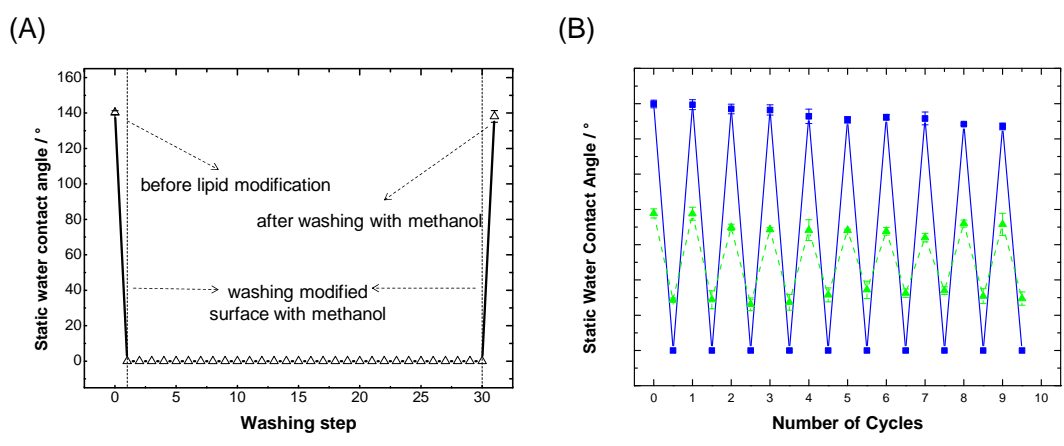


Figure 3.28: Static water contact angle on a superhydrophilic DOPE lipid modified BE3 during 30 consecutive steps of washing with water. Superhydrophobicity is restored after a single washing with methanol. (B) Repetitive switching between superhydrophobicity and superhydrophilicity by modifying BE3 with DOPE phospholipid and erasing the superhydrophilicity by washing with methanol (solid line); corresponding changes of the water contact angle on a nonporous BMA-EDMA surface (dashed line).

The ability to erase a surface property such as superhydrophilicity and rapidly transform it back to superhydrophobic is useful for different applications such as lab-on-chip systems²³¹ or for creating biofunctional stimuli-responsive materials. We found that a single washing of the lipid-coated superhydrophilic BE3 with organic solvents makes it again superhydrophobic (Figure 3.27A). Figure

3.27B shows 10 repetitions of switching between superhydrophobicity and superhydrophilicity by modifying BE3 with a phospholipid and erasing the superhydrophilicity by washing with methanol. Corresponding changes of the static water contact angle on a nonporous surface are significantly smaller (Fig. 3.27B).

3.4.3 Fabrication of the superhydrophobic-superhydrophilic micropatterns

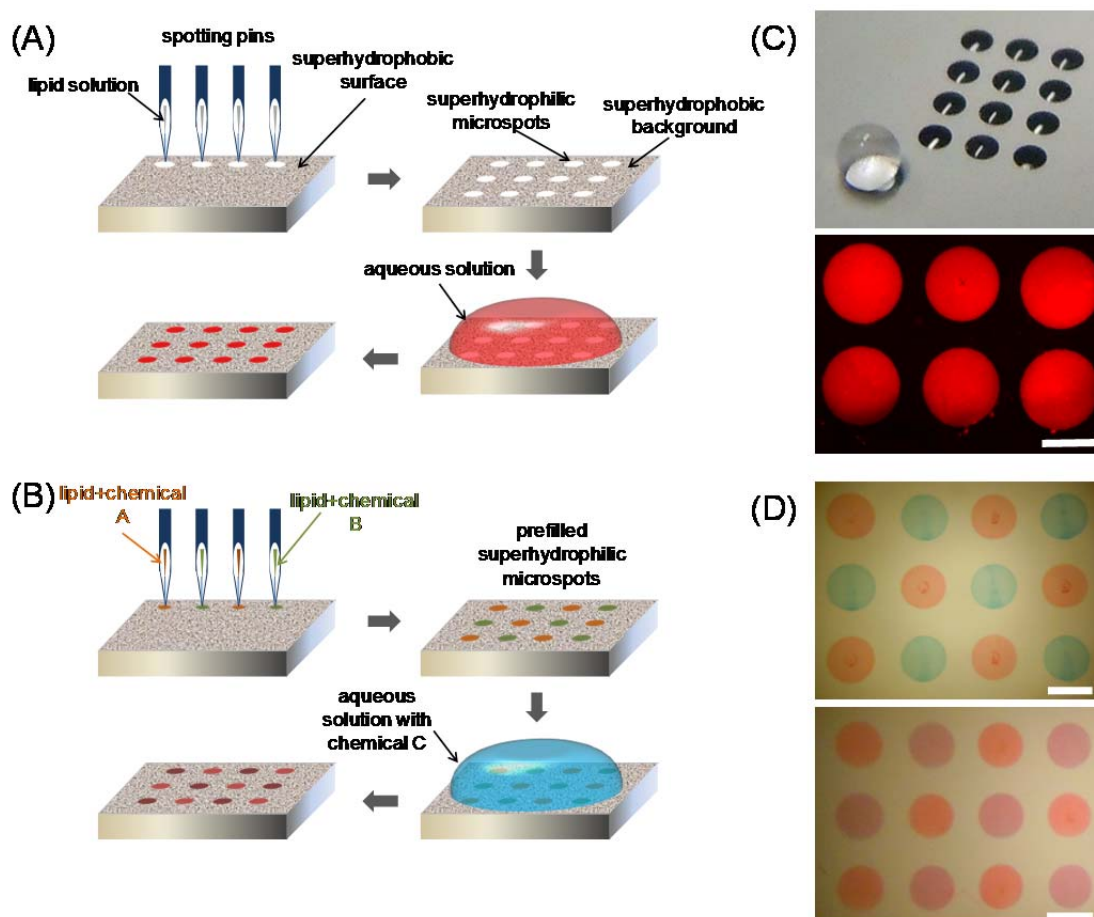


Figure 3.29: (A, B) An example of the application of a μ -contact printer to create an array of superhydrophilic microspots on a superhydrophobic BE3 using a lipid/ethanol solution as an ink. (C) Image of an array of superhydrophilic spots filled with water and a water droplet on the superhydrophobic BE3 (top). A fluorescent image of an array of superhydrophilic spots filled with Rhodamine 6G (bottom). (D, top) An array of superhydrophilic spots pre-filled with methylene blue and neutral red dyes in an alternating array pattern. The array was formed by printing ethanol solutions containing the dyes as well as POPG lipid “ink”. (D, bottom) Image of the pattern subsequently wetted with a 0.1 mg/ml Rhodamine 6G solution. Scale bars are 500 μ m.

The advantage of such a mild single-step method for transforming superhydrophobicity into superhydrophilicity is its compatibility with well-established techniques for printing, including microcontact printing, dip-pen nanolithography (DPN), or ink-jet printers. To create the SH-SL

micropattern, we used a contract printer to print the phospholipid on the BE3. It was found that the type of phospholipid, concentration of the phospholipid, thickness of the BE3 influence the formation of the SH-SL micropattern. These influences are summarized in Table 3.9.

The size of the printed lipid spot depends on the lipid concentration and solvent (Tab. 3.9). More uniform spots were obtained with 2-oleoyl-1-palmitoyl-*sn*-glycero-3-phospho-*rac*-(1-glycerol) ammonium salt (POPG) than with 1,2-Dioleoyl-*sn*-glycero-3-phosphoethanolamine (DOPE) (both lipid concentrations were 10 mg/ml in ethanol). The diffusion of DOPE solutions (ethanol) on BE3 was slow and inhomogeneous. An array pattern could not be obtained for 10 mg/ml POPG solutions in chloroform, although it turned the lipid-modified surface hydrophilic. Alcoholic solvents were more reliable than non-alcoholic solvents to print the lipid arrays. Ethanol and 2-propanol gave similar results. The higher viscosity of 2-propanol in comparison to ethanol did not have much effect on the printed lipid spot diameter. However, for larger array patterns, reproducible lipid spots were produced with a 10 mg/ml POPG solution in ethanol rather than in 2-propanol. The standard deviation of the spot diameters was higher when POPG solutions in tetrahydrofuran were used. An array pattern printed with a 10 mg/ml POPG solution in DMF was observed only once when the polymer surface was wetted with water as soon as the array was printed. The concentration of the lipid solution has a considerable effect on the spot size. Higher concentration lipid solutions produced lipid spots with smaller diameters. Dilute lipid solutions of 1 mg/ml POPG solution (ethanol) and 5 mg/ml POPG solution (ethanol and tetrahydrofuran) were not able to produce the desired transition of the superhydrophobic polymer surface to superhydrophilic. The thickness of the polymer film also influenced the lipid array pattern. The polymer thickness affected the lipid spot diameter and reproducibility of the lipid array pattern. With increasing thickness of the polymer film, although the lipid spot diameter was reduced, the spots were not well-wetted and the reproducibility of the pattern decreased. This may be because the depth to which the lipid solution penetrates a thicker polymer film will not be the same in all cases, which was reflected in the differing transparency of the spots. For thinner polymer films, the depth of penetration would be similar in all cases and this can be seen from the uniform transparency of the spots and reproducibility of the lipid array pattern.

Figure 3.29A shows an example of the application of a μ -contact printer to create an array of superhydrophilic microspots on a superhydrophobic background using a lipid/ethanol solution as an ink. The lipid solution was printed in an array pattern onto a $\sim 10 \mu\text{m}$ -thin superhydrophobic BE3 using metal spotting pins. After the lipid array was printed, the polymer substrate was wetted with water to observe the array of superhydrophilic circular spots of $\sim 500 \mu\text{m}$ in diameter on the superhydrophobic background (Figure 3.29C).

Due to the difference in wettability of the spots and the background, the superhydrophilic spots can be filled with an aqueous solution. Figure 3.29 shows an array of superhydrophilic spots filled with a solution of Rhodamine 6G by briefly wetting a lipid array with this solution and allowing the spots to

dry. The Rhodamine 6G solution was only present in the lipid spots and did not adhere to the superhydrophobic background. In addition to first printing the lipid array and then filling the superhydrophilic lipid spots with a solution, a substance can be added directly to the lipid printing solution and printed directly onto the BE3 to create patterns prefilled with the desired substance (Figure 3.29B, D). This allows the flexibility to pattern more than one compound in a specific pattern on the same surface. The prefilled spots are still superhydrophilic, so they can be filled with another solution if desired (Figure 3.29B, D).

Table 3.9: Average spot diameter and observation of lipid array patterns printed with various lipid solutions on BE3 of different thickness.

Lipid solution	Thickness of BE3[μm]	Contact print time [ms]	Spot diameter [μm]	Observation
10mg/ml DOPE sol.(ethanol)	50.0	0	441.0 \pm 9.42	Less transparent, non-uniform spot size
10mg/ml DOPE sol.(ethanol)	12.5	0, 20, 50, 100	--	Non-uniform spot size
10mg/ml POPG sol.(ethanol)	500.	0	454.0 \pm 2.45	Less transparent, not reproducible
10mg/ml POPG sol.(ethanol)	25.0	0	573.0 \pm 3.42	Less transparent, not reproducible
10mg/ml POPG sol.(ethanol)	12.5	0	550.0 \pm 2.60	Reproducible with uniform spot size
1mg/ml POPG sol.(ethanol)	12.5	0	-	No hydrophilic spots
5mg/ml POPG sol.(ethanol)	12.5	0	567.6 \pm 10.3	Less transparent
100mg/ml POPG sol.(ethanol)	50.0	0	163.9 \pm 46.4	Non-uniform spot size
10mg/ml POPG sol.(THF)	25.0	0	638.0 \pm 11.68	Non-uniform spot size for larger array patterns, less transparent
10mg/ml POPG sol.(THF)	12.5	0	559.0 \pm 10.49	Non-uniform spot size for larger array patterns
10mg/ml POPG sol.(ethanol)	50.0	10	479 \pm 8.79	Less transparent
10mg/ml POPG sol.(ethanol)	50.0	20	472 \pm 7.98	Less transparent

3.4.4 Summary

In summary, a new and simple method for creating superhydrophilic micropatterns on a superhydrophobic surface was demonstrated. The method is based on printing an “ink” – an ethanol solution of a lipid – onto a porous superhydrophobic surface and is compatible with different printing techniques, for example, microcontact or ink-jet printing. It was shown that the hydrophilic lipid-coated microspots could be easily filled with an aqueous solution by dipping or wetting the surface. In

addition, the lipid spots can be prefilled with a substance by adding it to the “ink” and printing it onto the superhydrophobic surface. Since the lipid layer can also incorporate different bioactive molecules, transmembrane proteins, or other functional lipids, we envision that this facile procedure for creating superhydrophilic patterns combined with contemporary printing technology will lead to numerous applications.

4. Conclusion and outlook

This PhD work described the preparation, characterization and application of functional polymethacrylate surfaces with well-defined chemical and physical surface properties. The aims of my work were: (1) development of methods for the preparation of polymethacrylate surfaces with a gradient surface morphology, as well as a gradient density of surface functional groups and explore the possibility of using these gradient surfaces for cell-surface interaction studies; (2) develop surfaces with special wettability and slippery properties for antibacterial and marine antifouling applications; (3) development of new methods for making superhydrophobic-superhydrophilic micropatterns on macroporous poly(butyl methacrylate-*co*-ethylene dimethacrylate) surfaces.

Since the porous properties of the poly(butyl methacrylate-*co*-ethylene dimethacrylate) (BMA-EDMA) surfaces could be controlled by changing the amount and the type of porogens in the polymerization mixture, a BMA-EDMA surface with gradual porous properties could be readily prepared by polymerization of a pre-polymer mixture with a gradient composition of porogens. To generate the gradient, a PDMS microfluidic chip with a cascade micromixer and a subsequent reaction chamber was fabricated and used. A 450 μm thick BMA-EDMA polymer surface possessing a gradient of pore size was obtained after polymerization in the micro-fluidic chip. The gradient formation in the microfluidic reaction chamber was studied using microscopic laser induced fluorescence (μLIF). Formation of linear gradients via both diffusive and convective mixing was visualized. By using fluid with different densities, formation of a two dimensional wedge-like gradient controlled by the density difference and orientation of the microfluidic chip was observed. The generation of BMA-EDMA polymer surface possessing a gradient of globule sizes from $\sim 0.5 \mu\text{m}$ to $\sim 0.2 \mu\text{m}$ defined by the composition of two polymerization mixtures injected into a microfluidic chip was demonstrated.

The chemical properties of the polymethacrylate surfaces can be controlled by UV initiated photografting with acrylate monomers on the surface. Since the extent of the modification is dependent on the UV dosage during photografting, this method was used to form polymethacrylate surfaces with gradients of functional group density by using a moveable UV mask to gradually vary the UV dosage along the polymer surface. The formation of the gradient on the BMA-EDMA surface was confirmed by XPS measurements. To prove that the surface with a chemistry gradient could be used as a screening platform to study cell-surface interaction, the behavior of HT-1080 cells on the gradient surfaces was investigated. The results showed that the chemistry of the surface played a decisive role in HT-1080 cell adhesion and growth on the surface. It is anticipated that the developed method could be employed for the screening of cell-surface interactions.

Following the pioneering work of Joanna Aizenberg et al., new slippery surfaces based on the porous BMA-EDMA surface were developed. The results showed that the slippery BMA-EDMA surfaces infused with poly(hexafluoropropylene oxide) (Krytox 100 and Krytox 103) have excellent long term stability under aqueous conditions. It was also found that the slippery BMA-EDMA surface was able

to prevent biofilm formation of different strains of the opportunistic pathogen *Pseudomonas aeruginosa* for at least up to 14 days in low nutrient medium. Only 1.8% of the slippery surface was covered by the environmental *P. aeruginosa* PA49 strain under investigation. For uncoated glass controls the coverage of surfaces reached 55% under the same conditions. However, in high nutrient medium, which is more relevant to physiological conditions, the biofilm formation on the slippery surface turned out to be highly dependent on the bacterial strain. Although the slippery surface could prevent biofilm formation of most of the *P. aeruginosa* strains tested (1% surface coverage), the multi-resistant *P. aeruginosa* strain isolated from wastewater was able to cover up to 12% of the surface during 7 days of incubation. RAPD-PCR analysis of the used *P. aeruginosa* strains demonstrated their high genome variability, which might be responsible for their difference in biofilm formation on the slippery BMA-EDMA surface. The results show that although the slippery BMA-EDMA surface has great potential to prevent biofilm formation, the generality of its bacteria resistant properties still needs to be improved. The investigation of the marine antifouling properties of the slippery BMA-EDMA demonstrated that the Krytox 100 infused macroporous BMA-EDMA surface (BE100) and Krytox 103 infused macroporous BMA-EDMA surface (BE103) surfaces could dramatically inhibit settlement of both spores and cyprids. However, the fouling release performance of the slippery BMA-EDMA surfaces was shown to be limited.

Superhydrophobic-superhydrophilic (SH-SL) micropatterns are of great interest for not only fundamental research but also for practical applications. To create a SH-SL micropattern on a BMA-EDMA surface, a facile surface modification method to transform the superhydrophobic BMA-EDMA surface to a superhydrophilic one was developed. Such modification was done simply by applying a solution of phospholipid on the porous BMA-EDMA surface. It was shown that this method of surface modification can be used for creating a SH-SL micropattern using a contact printer. The formation of superhydrophilic areas is based on printing an ethanol solution containing a phospholipid onto a superhydrophobic BMA-EDMA surface. This creates a supported lipid layer on the polymer surface, thereby switching from superhydrophobicity to superhydrophilicity. Therefore, the amphiphilic lipid functions as an ink that can be printed to create superhydrophilic patterns on the superhydrophobic surface.

In conclusion, different functional porous polymethacrylate surfaces were successfully developed. These functional porous polymethacrylate surfaces can find many applications in different fields. Polymethacrylate surfaces with a gradient in pore size or the density of functional groups can be used as a platform for efficient cell-surface screenings. The methods developed for the preparation of gradient surfaces in this work can be used for the future development of surfaces with a two-dimensional gradient (gradient in pore size and gradient in density of functional groups). Slippery surfaces based on porous BMA-EDMA surfaces show promising antibacterial and marine antifouling properties. Due to the fact that porous BMA-EDMA coatings can be fabricated on different materials,

it is expected that slippery surfaces with antibacterial and marine antifouling properties can be created on different substrates. Superhydrophobic-superhydrophilic micropatterns hold great promise in a number of applications. Since the method developed for creating a superhydrophobic-superhydrophilic micropattern in this thesis is based on a phospholipid and is compatible with contact printing techniques, it is anticipated that different bioactive molecules such as proteins or other functional lipids could be easily patterned and used for biological applications. The developed method can be also useful for creating of high density (up to ~ 400 spots per cm^2 theoretically (spot size: $440 \mu\text{m}$, distance between spots: $40 \mu\text{m}$)) droplet and cell array.

5. Appendix

5.1 Hydrodynamic characterization of the microfluidic chip

These experiments were designed with Kristina Kreppenhofer (IMT, KIT) and Massimiliano Rossi (Institute of Fluid Mechanics and Aerodynamics, Universität der Bundeswehr München). The experiments were performed at Universität der Bundeswehr München by Massimiliano Rossi.

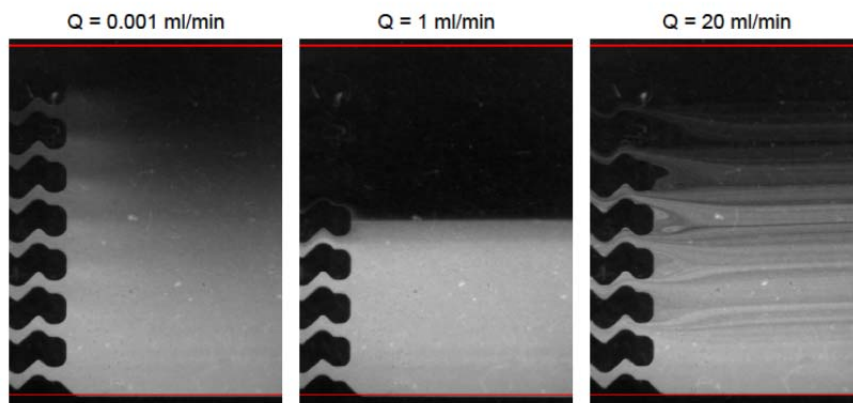


Figure 5.1: Isopropanol (upper inlet) and Rhodamine B diluted in isopropanol (lower inlet) injected in the micromixer (flow direction left to right) and observed by fluorescence microscopy.¹⁰² The red lines mark the boundaries of the chamber.

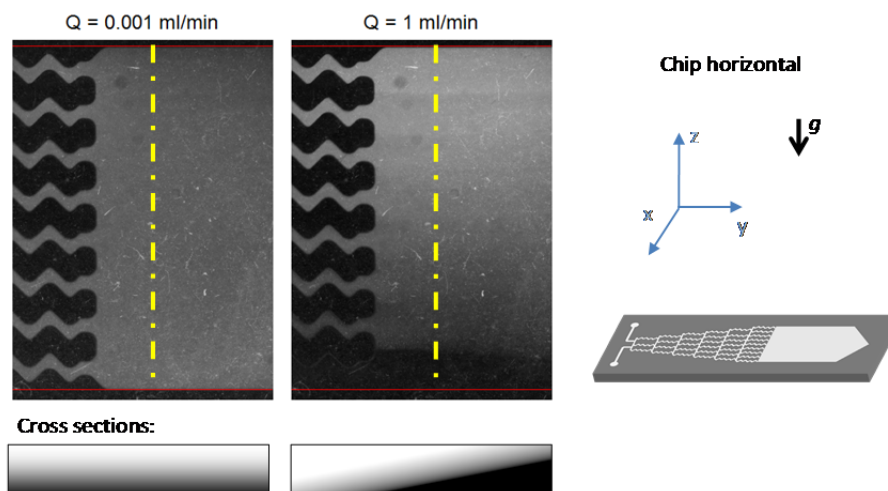


Figure 5.2: Images from μ LIF measurements (left) using isopropanol marked with Rhodamine B (upper inlet) and water (lower inlet) for the injection in the micro-mixer (flow direction left to right).¹⁰² Schemes below the microscope images show the arrangement of the two fluids in a cross section of the reaction chamber. The chip was used in a horizontal position (right). At 0.001 ml/min, water and isopropanol are stacked horizontally one on top of the other. At 1 ml/min the isopropanol slips over the water resulting in a two-dimensional wedge-like gradient (see schemes at the bottom).

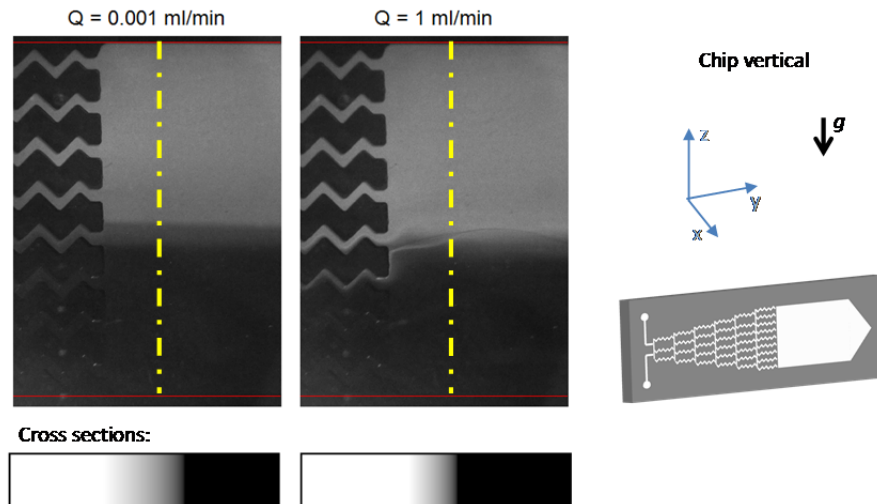


Figure 5.3: Images from μ LIF measurements (left) using isopropanol dyed with Rhodamine B (upper inlet) and water (lower inlet) for the injection in the micromixer (flow direction left to right).¹⁰² Below the microscope images schemes show the arrangement of the two fluids in a cross section of the reaction chamber. The chip was used in a vertical position (right). At 0.001 ml/min, water and isopropanol are again stacked one on top of the other, leading to a vertical stacking in the cross section (microscope image and scheme). Diffusive mixing of the two fluids can be observed in-between the two phases. At 1 ml/min the isopropanol slips again over the water.

5.2 The impact of surface morphology and surface chemistry on HT-1080 cell behavior

These experiments were designed with Barbara Kwiatkowska (ITG, KIT) and Dr. Irina Nazarenko (ITG, KIT). The cell experiments were performed by Barbara Kwiatkowska at ITG.

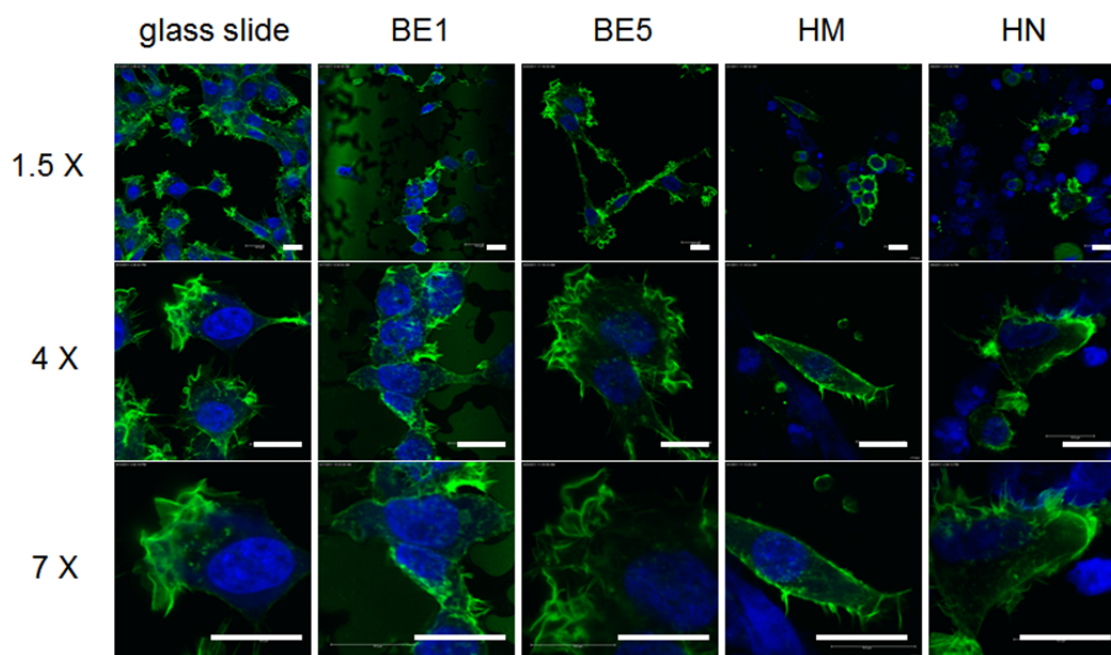


Figure 5.4: Microscope images of HT-1080 cells on glass slide, BE1, BE5, HM and HN surfaces. The images were taken 24 hours after seeding. 1.5, 4 and 7 X digital zoom were used with the water objective 63 X. Nuclei are stained with DAPI and F-actin is stained with Phalloidin (scale bar 15 μm).¹³⁸

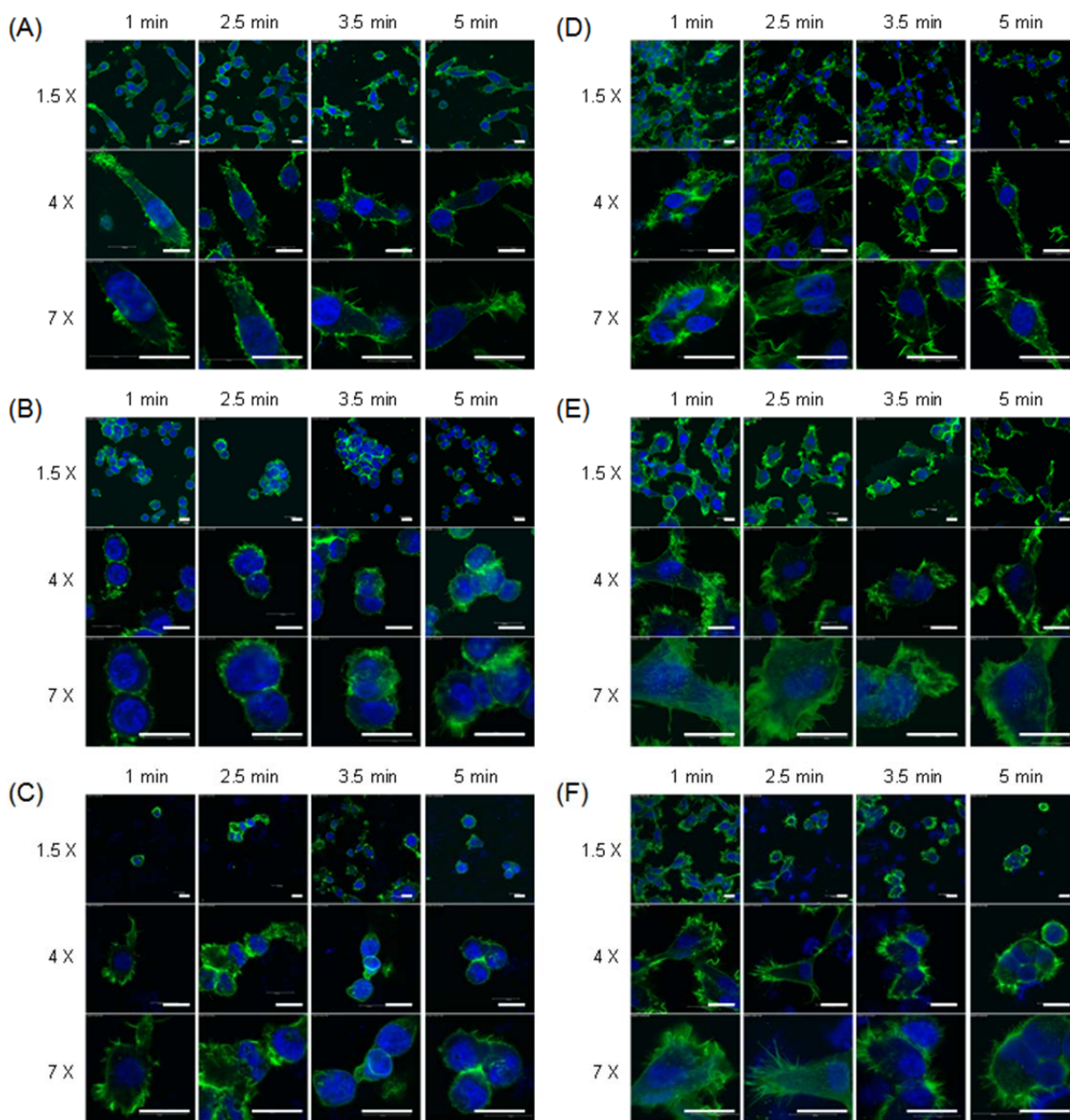


Figure 5.5: Microscope images of HT-1080 cells on the following surfaces possessing gradients of functional group density (time of photografting): (A) BE1-AMPS, (B) BE1-MDSA, (C) BE1-META, (D) BE5-AMPS, (E) BE5-MDSA and (F) BE5-META. The images were taken 24 hours after seeding. 1.5, 4 and 7 X digital zoom were used with the water objective 63 X. Nuclei are stained with DAPI and F-actin is stained with phalloidin (scale bar 15 μm).¹³⁸

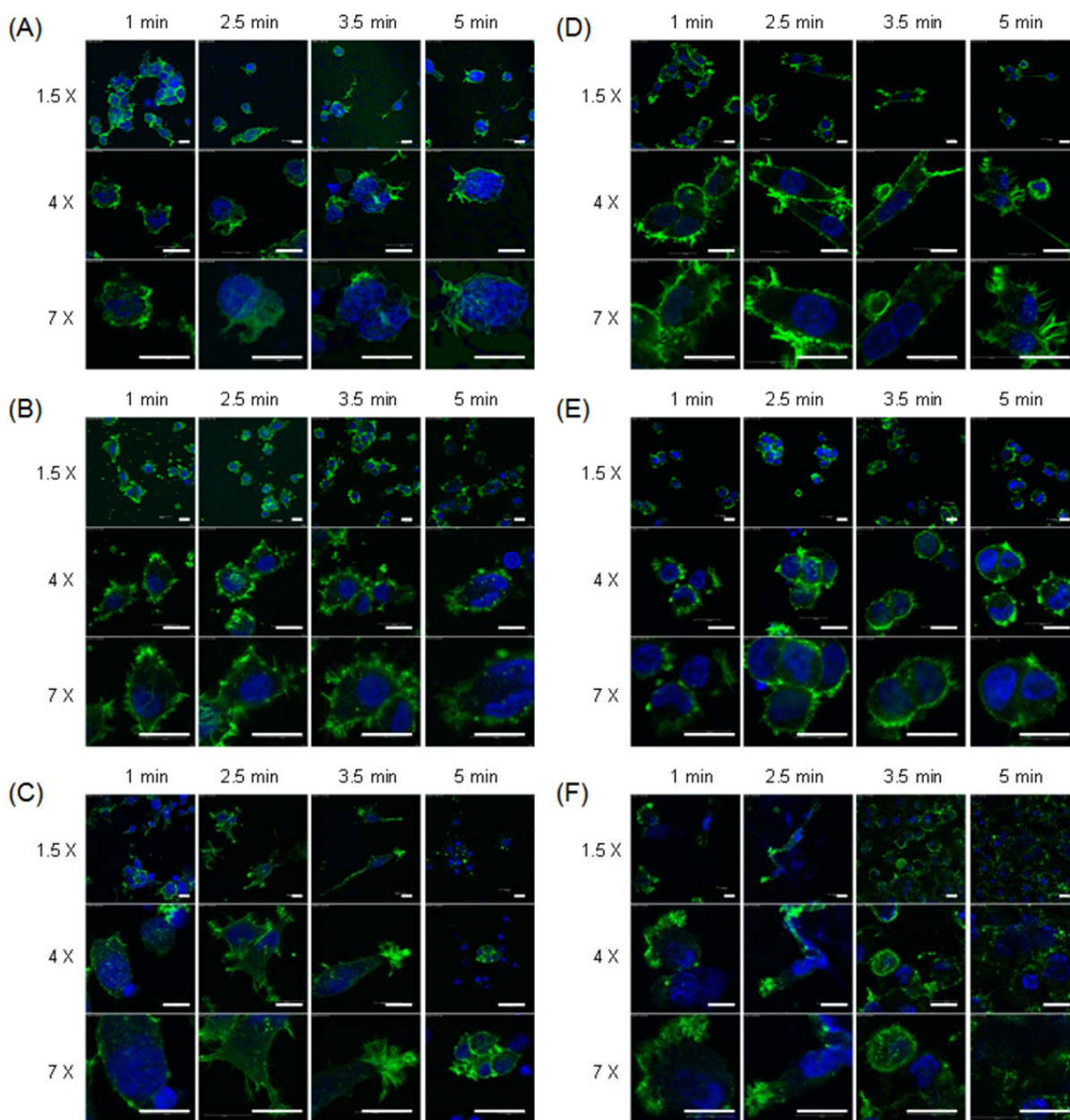


Figure 5.6: Microscope images of HT-1080 cells on the following surfaces possessing gradients of functional group density (time of photografting): (A) HM-AMPS, (B) HM-MDSA, (C) HM-META, (D) HN-AMPS, (E) HN-MDSA and (F) HN-META. The images were taken 24 hours after seeding. 1.5, 4 and 7 X digital zoom were used with the water objective 63 X. Nuclei are stained with DAPI and F-actin is stained with phalloidin (scale bar 15 μm).¹³⁸

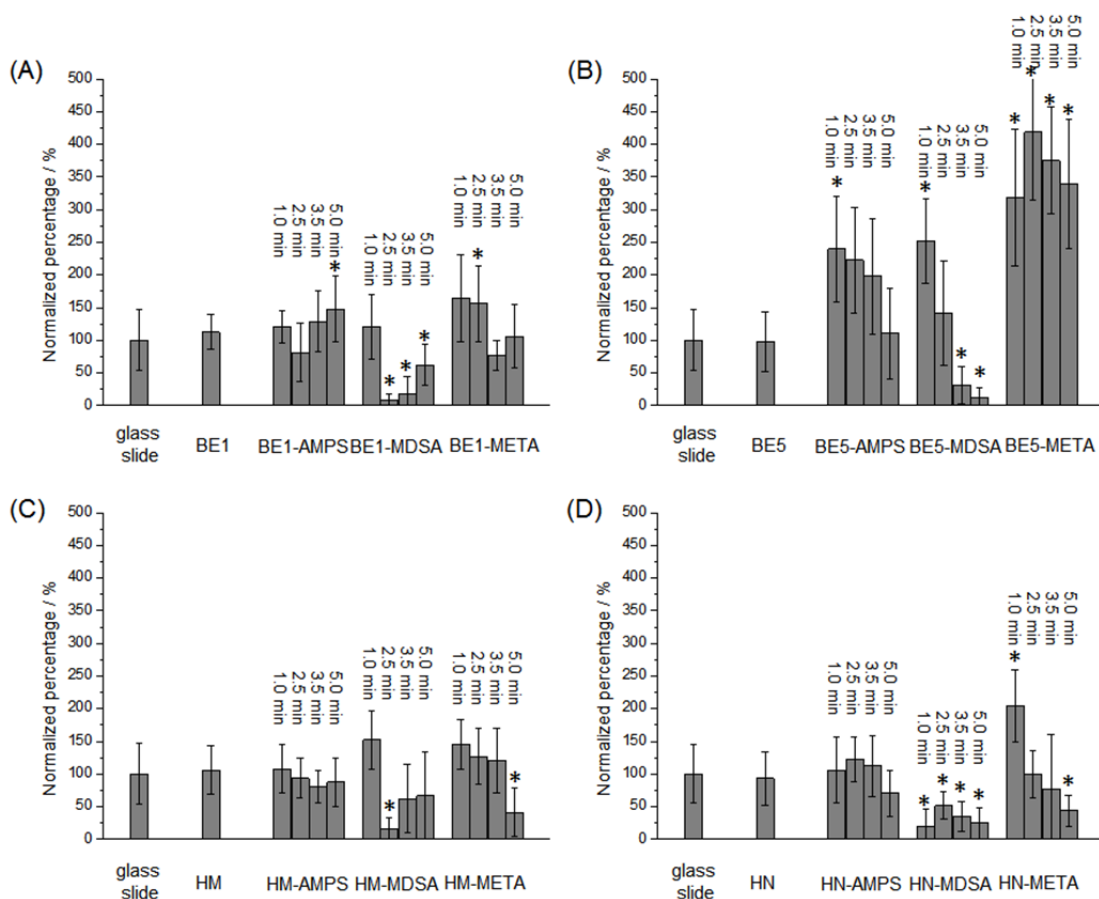


Figure 5.7: Quantitative analysis of the number of adhered HT-1080-eGFP cells on (A) BE1 surface and photografted BE1 surface, (B) BE5 surface and photografted BE5 surfaces, (C) HM surfaces and photografted surfaces and (D) HN surfaces and photografted HN surfaces. Cell adhesion was examined 1 hour after seeding. The number of the adhered cells on the polymer surface was normalized to that on the glass slide.¹³⁸

5.3 Toxicity test of PFPE liquid

This experiment was designed with Tanja Kleintschek (IFG, KIT) and Dr. Thomas Schwartz (IFG, KIT) and was performed by Tanja Kleintschek at IFG.

Table 5.1: Growth of *P. aeruginosa* strains of PA14, PA30, PA910 and PA 49 was monitored in BM2 medium with up to 12.5% PFPE liquid.¹⁸⁴

Concentration of PFPE liquid	Average CFU/mL (PA14, PA30, PA910 and PA 49)	
	8 h incubation	22 h incubation
0.0 %	$6.4 \cdot 10^5 \pm 5.9 \cdot 10^5$	$3.2 \cdot 10^8 \pm 5.4 \cdot 10^7$
0.4 %	$5.7 \cdot 10^5 \pm 4.6 \cdot 10^5$	$2.7 \cdot 10^8 \pm 1.4 \cdot 10^8$
0.8 %	$3.8 \cdot 10^5 \pm 1.3 \cdot 10^5$	$5.2 \cdot 10^8 \pm 2.8 \cdot 10^7$
1.6 %	$7.1 \cdot 10^5 \pm 2.6 \cdot 10^5$	$4.6 \cdot 10^8 \pm 2.3 \cdot 10^8$
3.1 %	$5.9 \cdot 10^5 \pm 3.2 \cdot 10^5$	$3.8 \cdot 10^8 \pm 2.1 \cdot 10^8$
6.3 %	$6.8 \cdot 10^5 \pm 4.3 \cdot 10^5$	$3.0 \cdot 10^8 \pm 1.4 \cdot 10^8$
12.5 %	$5.5 \cdot 10^5 \pm 4.7 \cdot 10^5$	$3.9 \cdot 10^8 \pm 2.2 \cdot 10^7$

5.4 Acknowledgement

This work was performed in the group of Dr. Pavel A. Levkin (Group of Chemical Engineering of Biofunctional Materials, Institute of Toxicology and Genetics, Karlsruhe Institute of Technology) and at the department of Applied Physical Chemistry (APC) at the University of Heidelberg. It was funded by the Helmholtz Association's Initiative and Networking Fund (Grant VH-NG-621) and CSC scholarship (2010695023).

First of all, I would like to thank Prof. Dr. Michael Grunze for supervising and reviewing my Ph.D. work. His insightful advices on my thesis and continuous support during my Ph.D. period helped me a lot in performing the Ph.D. thesis. I would also like to thank Prof. Dr. Hans-Robert Volpp for kindly accepting to be my second reviewer.

I would like to give my special thanks to Dr. Pavel A Levkin who offered the opportunity to perform the Ph.D. thesis in his research group. Without his supervision and kind help this thesis would not have been possible. His guidance always helped me to solve the problems I encountered and his great enthusiasm for the research work motivates me to continue and finish my Ph.D. thesis all the time.

I especially thank Erica Boles, Dr. Alexander Welle, Girish Shankara, Victoria Nedashkivska, Florian Geyer, David Zahner and Longjia Wu for their work on the correction and proof-reading of my thesis.

I would like to thank all my friendly colleagues: Linxian Li, Xin Du, Wenqian Feng, Alexander Efremov, Erica Boles, Victoria Nedashkivska, Girish Shankara, Fengjian Wang, David Zahner, Florian Geyer, Zewei Bai, Asritha Nallapaneni and all other colleagues at APC. It was great to work with these young and brilliant people. I would like to thank Prof. Dr. Jonathan Sleeman, Dr. Alexander Welle and Prof. Dr. Axel Rosenhahn for being my TAC members and their valuable scientific suggestions. I thank Hao Lu and Hikmet Sezen for their help with the XPS measurements and analysis. I thank Dr. Alexander Welle for his help with the ToF-SIMS measurements and analysis. I thank Dr. Stefan Heissler for his assistance with Raman measurements. I thank Zhengbang Wang and Wei Guo for their help with O₂ plasma devices. I thank Guo Peng for his help with the FTIR measurements. I thank the European Synchrotron Radiation Facility for providing the beamtime (SI-2552) for the X-ray tomography imaging.

I would like to thank Prof. Dr. Haolin Tang, who has been helping me in all aspects of scientific researches since the time I became a master student. My thanks also go to Dr. Thomas Swartz, Dr. Irina Nazarenko, Dr. Kristina Kreppenhofner, Ludmilla Popp, Linlin Xiao, Kleintschek Tanja, Yin Cheng, Dr. Heikki Suhonen, Dr. Lukas Helfen, Prof. Dr. Tilo Baumbach and Barbara Kwiatkowska for the scientific discussions and collaborations.

I would like to express my sincere gratitude to my family members who have been supporting me all the time. For most I thank my parents, who did their best to help me with everything. I thank my wife,

without her support I would never have come this far.

I would like to thank the China Scholarship Council for a Ph.D. scholarship. I would like to thank Tingting Liu and Xiangwen Zhou for their help during my scholarship application process.

5.5 List of publications

Publications related to the Ph.D. thesis:

Li J.[‡], Kleintschek T.[‡], Rieder A., Cheng, Y., Baumbach T., Obst U., Schwartz T., Levkin P., Hydrophobic Liquid-Infused Porous Polymer Surfaces for Antibacterial Applications. *ACS Applied Materials & Interfaces* **2013**, 5, 6704-6711.

Kreppenhofer K.[‡], **Li J.**[‡], Segura R., Popp L., Rossi M., Tzvetkova P., Luy B., Kähler C. J., Guber A. E., Levkin P., Formation of a Polymer Surface with a Gradient of Pore Size Using a Microfluidic Chip. *Langmuir* **2013**, 29, 3797-3804.

Li J., Ueda E., Nallapaneni A., Li L., Levkin P., Printable Superhydrophilic-Superhydrophobic Micropatterns Based on Supported Lipid Layers. *Langmuir* **2012**, 28, 8286-8291.

Xiao L.[‡], **Li J.**[‡], Mieszkin S., Fino A. D., Clare A. S., Callow M. E., Callow J. A., Grunze M., Rosenhahn A., Levkin P., Liquid-infused Slippery Surfaces Showing Marine Antibiofouling Properties. *ACS applied materials & Interfaces*, **2013**, 5, 10074-10080.

Du X., **Li J.**, Li L., Levkin, P., Porous Poly(2-octyl cyanoacrylate): A Facile One-step Preparation of Superhydrophobic Coatings on Different Substrates. *Journal of Materials Chemistry A* **2013**, 1, 1026-1029.

Kreppenhofer K., **Li J.**, Popp L., Segura R., Rossi M., Kahler C., Levkin P., Guber A, Microfluidic Chip for Generating Gradient Polymer Films for Biological Applications. *Procedia Engineering*, **2012**, 47, 458-461.

Li L.[‡], **Li J.**[‡], Du X., Welle A., Grunze M., Levkin P., Light-driven Surface Modification by Thiol-ol Chemistry. (submitted to *Angewandte Chemie International Edition*)

Li J., Kwiatkowska B., Lv H., Bundschuh S., Grunze M., Sleeman J., Nazarenko I., Levkin P. Gradient Surfaces for the Study of Synergistic Effects of Surface Morphology and Surface Chemistry on the Behaviors of HT-1080 Fibroblast Cells. (in preparation)

Cheng Y., Suhonen H., Helfen L., **Li J.**, Xu F., Grunze M., Levkin P., Baumbach T., Direct Three-dimensional Imaging of Surface-water Interface on Polymer Substrates with Special Wettability by Nanoscale Hard X-ray Phase Tomography. (submitted to *Soft Matter*)

Feng W., Li L., Ueda E., **Li J.**, Heißler S., Welle A., Trapp O., Levkin P., Surface Patterning via Thiol-Yne Click Chemistry: an Extremely Fast and Versatile Approach to Superhydrophobic-Superhydrophilic Micropatterns. (submitted to *Advanced Materials Interfaces*)

[‡] **These authors contribute equally to this work.**

Other publications:

Xiao P.[‡], **Li J.**[‡], Tang H., Wang Z., Pan, M., Physically Stable and High Performance Aquivion/ePTFE Composite Membrane for High Temperature Fuel Cell Application. *Journal of Membrane Science* **2013**, 442, 65-71.

Liang C.[‡], **Li J.**[‡], Tang H., Zhang H., Zhang HN., Pan M., Approach high temperature performance for proton exchange membrane fuel cell with 3D ordered silica/Cs_{2.5}H_{0.5}PW electrolytes. *Journal of Materials Chemistry A*, **2014**, 2, 753-760.

Li J., Yang X., Tang H., Pan M., Durable and High Performance Nafion Membrane Prepared Through High-Temperature Annealing Methodology. *Journal of Membrane Science* **2010**, 361, 38-42.

Li J.[‡], Wang Z.[‡], Li J.R., Pan M., Tang H., Nanostructure-Based Proton Exchange Membrane for Fuel Cell Applications at High Temperature. *Journal of Nanoscience and Nanotechnology* **2014**, in press.

Wang Z., Tang H., **Li J.**, Pan M., Morphology Change of Biaxially Oriented Polytetrafluoroethylene Membranes Caused by Solvent Soakage. *Journal of Applied Polymer Science* **2011**, 121, 1464-1468.

[‡]**These authors contribute equally to this work.**

Conference abstracts:

Li J., Li L., Du X., Welle A., Levkin P., UV Triggered Surface Modification Through Thiol-ol Chemistry, *3rd International Symposium - Frontiers in Polymer Science*, 2013, Barcelona, Spain.

Li J., Kreppenhofer K, Popp L., Segura R., Rossi, M., Kahler C, Levkin P., Guber A., Microfluidic Chip for Generating Gradient Polymer Films for Biological Applications. *Euroensors Conferences* 2012, Krakow, Poland.

5.6 List of abbreviations

HEMA: 2-hydroxyethyl methacrylate

EDMA: ethylene glycol dimethacrylate

AIBN: azobisisobutyronitrile

GMA: glycidyl methacrylate

BET: Brunauer-Emmett-Teller

TRIM: trimethylolpropane trimethacrylate

BMA: butyl methacrylate

DMPAP: 2,2-dimethoxy-2-phenylacetophenone

AMPS: 2-acrylamido-2-methyl-1-propanesulfonic acid

BE1: BMA-EDMA surface prepared from a mixture of 0.5 wt% DMPAP, 20 wt% of BMA, 30 wt% EDMA and 50 wt% 1-decanol.

BE2: BMA-EDMA surface prepared from a mixture of 0.5 wt% DMPAP, 20 wt% of BMA, 30 wt% EDMA, 40 wt% 1-decanol and 10 wt% cyclohexanol.

BE3: BMA-EDMA surface prepared from a mixture of 0.5 wt% DMPAP, 20 wt% of BMA, 30 wt% EDMA, 30 wt% 1-decanol and 20 wt% cyclohexanol.

BE4: BMA-EDMA surface prepared from a mixture of 0.5 wt% DMPAP, 20 wt% of BMA, 30 wt% EDMA, 20 wt% 1-decanol and 30 wt% cyclohexanol.

BE5: BMA-EDMA surface prepared from a mixture of 0.5 wt% DMPAP, 20 wt% of BMA, 30 wt% EDMA and 50 wt% cyclohexanol.

BE6: BMA-EDMA surface prepared from a mixture of 1 wt% DMPAP, 40 wt% of BMA, 60 wt% EDMA and 50 wt% cyclohexanol.

BE100: Krytox 100 infused BE1 surface.

BE103: Krytox 103 infused BE1 surface.

BE70: Fluorinert FC 70 infused BE1 surface.

HM: HEMA-EDMA surface prepared from a mixture of 0.5 wt% DMPAP, 20 wt% of HEMA, 30 wt% EDMA and 50 wt% 1-decanol.

HN: HEMA-EDMA surface prepared from a mixture of 0.5 wt% DMPAP, 20 wt% of HEMA, 30 wt% EDMA, 20 wt% 1-decanol and 30 wt% cyclohexanol.

MDSA: [2-(Methacryloyloxy) ethyl]dimethyl-(3-sulfopropyl)ammonium hydroxide

META: [2-(methacryloyloxy) ethyl] trimethylammonium chloride

PFPE liquid: poly(hexafluoropropylene oxide)

DOPE: 1,2-Dioleoyl-*sn*-glycero-3-phosphoethanolamine

POPG: 2-oleoyl-1-palmitoyl-*sn*-glycero-3-phospho-*rac*-(1-glycerol) ammonium salt

PDMS: poly(dimethylsiloxane)

SEM: Scanning Electron Microscope

XPS: X-ray photoelectron Microscopy

ToF-SIMS: Time of Flight Secondary Ion Mass Spectroscopy

PBI: propagation-based imaging

ABI: analyzer-based imaging

GI: grating interferometric

5.7 Bibliography

1. Rouquerol, J.; Avnir, D.; Fairbridge, C. W.; Everett, D. H.; Haynes, J. H.; Pernicone, N.; Ramsay, J. D. F.; Sing, K. S. W.; Unger, K. K., Recommendations for the characterization of porous solids. *Pure Appl. Chem.* **1994**, *66* (8), 1739-1758.
2. Burwell, R. L., Manul of symbols and terminology for physicochemical quantities and units - Appendix 2 - Definitions, terminology and symbols in colloid and surface chemistry. 2. Heterogeneous catalysis. *Pure Appl. Chem.* **1976**, *46* (1), 71-&.
3. Wu, D. C.; Xu, F.; Sun, B.; Fu, R. W.; He, H. K.; Matyjaszewski, K., Design and Preparation of Porous Polymers. *Chem. Rev.* **2012**, *112* (7), 3959-4015.
4. Ma, S. Q.; Zhou, H. C., Gas storage in porous metal-organic frameworks for clean energy applications. *Chem. Commun.* **2010**, *46* (1), 44-53.
5. Makal, T. A.; Li, J. R.; Lu, W. G.; Zhou, H. C., Methane storage in advanced porous materials. *Chem. Soc. Rev.* **2012**, *41* (23), 7761-7779.
6. Peters, E. C.; Svec, F.; Frechet, J. M. J., Rigid macroporous polymer monoliths. *Adv. Mater.* **1999**, *11* (14), 1169-1181.
7. Pandey, P.; Chauhan, R. S., Membranes for gas separation. *Progress in Polymer Science* **2001**, *26* (6), 853-893.
8. Dell'Anna, M. M.; Romanazzi, G.; Mastroilli, P., Polymer Supported Catalysts Obtained from Metal-Containing Monomers. *Curr. Org. Chem.* **2013**, *17* (12), 1236-1273.
9. Nair, L. S.; Laurencin, C. T., Biodegradable polymers as biomaterials. *Progress in Polymer Science* **2007**, *32* (8-9), 762-798.
10. Wang, Y.; Angelatos, A. S.; Caruso, F., Template synthesis of nanostructured materials via layer-by-layer assembly. *Chem. Mater.* **2008**, *20* (3), 848-858.
11. Sokolsky-Papkov, M.; Agashi, K.; Olaye, A.; Shakesheff, K.; Domb, A. J., Polymer carriers for drug delivery in tissue engineering. *Adv. Drug Delivery Rev.* **2007**, *59* (4-5), 187-206.
12. Vlach, E. G.; Tennikova, T. B., Preparation of methacrylate monoliths. *Journal of Separation Science* **2007**, *30* (17), 2801-2813.
13. Svec, F., Porous polymer monoliths: Amazingly wide variety of techniques enabling their preparation. *Journal of Chromatography A* **2010**, *1217* (6), 902-924.
14. Namera, A.; Nakamoto, A.; Saito, T.; Miyazaki, S., Monolith as a new sample preparation material: Recent devices and applications. *Journal of Separation Science* **2011**, *34* (8), 901-924.
15. Nischang, I., Porous polymer monoliths: Morphology, porous properties, polymer nanoscale gel structure and their impact on chromatographic performance. *Journal of Chromatography A* **2013**, *1287*, 39-58.
16. Svec, F.; Frechet, J. M. J., Temperature, a Simple and Efficient Tool for the Control of Pore Size Distribution in Macroporous Polymers. *Macromolecules* **1995**, *28* (22), 7580-7582.
17. Svec, F.; Frechet, J. M. J., New designs of macroporous polymers and supports: From

separation to biocatalysis. *Science* **1996**, 273 (5272), 205-211.

18. Svec, F.; Fréchet, J. M. J., Pore-size-specific modification of porous materials. *Adv. Mater.* **1994**, 6 (3), 242-244.
19. Čoupek, J.; Křiváková, M.; Pokorný, S., New hydrophilic materials for chromatography: Glycol methacrylates. *Journal of Polymer Science: Polymer Symposia* **1973**, 42 (1), 185-190.
20. Švec, F.; Hradil, J.; Čoupek, J.; Kálal, J., Reactive polymers I. Macroporous methacrylate copolymers containing epoxy groups. *Die Angewandte Makromolekulare Chemie* **1975**, 48 (1), 135-143.
21. Tennikova, T. B.; Svec, F.; Belenkii, B. G., High-Performance Membrane Chromatography. A Novel Method of Protein Separation. *Journal of Liquid Chromatography* **1990**, 13 (1), 63-70.
22. Svec, F.; Frechet, J. M. J., Continuous rods of macroporous polymer as high-performance liquid chromatography separation media. *Analytical Chemistry* **1992**, 64 (7), 820-822.
23. Viklund, C.; Pontén, E.; Glad, B.; Irgum, K.; Hörstedt, P.; Svec, F., "Molded" Macroporous Poly(glycidyl methacrylate-co-trimethylolpropane trimethacrylate) Materials with Fine Controlled Porous Properties: Preparation of Monoliths Using Photoinitiated Polymerization. *Chem. Mater.* **1997**, 9 (2), 463-471.
24. Levkin, P. A.; Svec, F.; Frechet, J. M. J., Porous Polymer Coatings: a Versatile Approach to Superhydrophobic Surfaces. *Advanced Functional Materials* **2009**, 19 (12), 1993-1998.
25. Yu, C.; Davey, M. H.; Svec, F.; Frechet, J. M. J., Monolithic porous polymer for on-chip solid-phase extraction and preconcentration prepared by photoinitiated in situ polymerization within a microfluidic device. *Analytical Chemistry* **2001**, 73 (21), 5088-5096.
26. Viklund, C.; Svec, F.; Frechet, J. M. J.; Irgum, K., Monolithic, "molded", porous materials with high flow characteristics for separations, catalysis, or solid-phase chemistry: Control of porous properties during polymerization. *Chem. Mater.* **1996**, 8 (3), 744-750.
27. Svec, F.; Peters, E. C.; Sykora, D.; Frechet, J. M. J., Design of the monolithic polymers used in capillary electrochromatography columns. *Journal of Chromatography A* **2000**, 887 (1-2), 3-29.
28. Moravcová, D.; Jandera, P.; Urban, J.; Planeta, J., Characterization of polymer monolithic stationary phases for capillary HPLC. *Journal of Separation Science* **2003**, 26 (11), 1005-1016.
29. Svec, F., Preparation and HPLC applications of rigid macroporous organic polymer monoliths. *Journal of Separation Science* **2004**, 27 (10-11), 747-766.
30. Peters, E. C.; Svec, F.; Fréchet, J. M. J., Preparation of Large-Diameter "Molded" Porous Polymer Monoliths and the Control of Pore Structure Homogeneity. *Chem. Mater.* **1997**, 9 (8), 1898-1902.
31. Pan, Z.; Zou, H.; Mo, W.; Huang, X.; Wu, R., Protein A immobilized monolithic capillary column for affinity chromatography. *Analytica Chimica Acta* **2002**, 466 (1), 141-150.
32. Yang, W. T.; Ranby, B., Bulk surface photografting process and its applications .1. Reactions and kinetics. *J. Appl. Polym. Sci.* **1996**, 62 (3), 533-543.

33. Yang, W. T.; Ranby, B., Bulk surface photografting process and its applications .2. Principal factors affecting surface photografting. *J. Appl. Polym. Sci.* **1996**, *62* (3), 545-555.
34. Ranby, B.; Yang, W. T.; Tretinnikov, O., Surface photografting of polymer fibers, films and sheets. *Nuclear Instruments & Methods in Physics Research Section B-Beam Interactions with Materials and Atoms* **1999**, *151* (1-4), 301-305.
35. Bhattacharya, A.; Misra, B. N., Grafting: a versatile means to modify polymers - Techniques, factors and applications. *Progress in Polymer Science* **2004**, *29* (8), 767-814.
36. Rohr, T.; Hilder, E. F.; Donovan, J. J.; Svec, F.; Frechet, J. M. J., Photografting and the control of surface chemistry in three-dimensional porous polymer monoliths. *Macromolecules* **2003**, *36* (5), 1677-1684.
37. Rohr, T.; Ogletree, D. F.; Svec, F.; Frechet, J. M. J., Surface functionalization of thermoplastic polymers for the fabrication of microfluidic devices by photoinitiated grafting. *Advanced Functional Materials* **2003**, *13* (4), 264-270.
38. Geyer, F. L.; Ueda, E.; Liebel, U.; Grau, N.; Levkin, P. A., Superhydrophobic-Superhydrophilic Micropatterning: Towards Genome-on-a-Chip Cell Microarrays. *Angewandte Chemie-International Edition* **2011**, *50* (36), 8424-8427.
39. Han, Y. H.; Levkin, P.; Abarientos, I.; Liu, H. W.; Svec, F.; Frechet, J. M. J., Monolithic Superhydrophobic Polymer Layer with Photopatterned Virtual Channel for the Separation of Peptides Using Two-Dimensional Thin Layer Chromatography-Desorption Electrospray Ionization Mass Spectrometry. *Analytical Chemistry* **2010**, *82* (6), 2520-2528.
40. Zahner, D.; Abagat, J.; Svec, F.; Fréchet, J. M. J.; Levkin, P. A., A Facile Approach to Superhydrophilic-Superhydrophobic Patterns in Porous Polymer Films. *Adv. Mater.* **2011**, *23* (27), 3030-3034.
41. Guiochon, G., Monolithic columns in high-performance liquid chromatography. *Journal of Chromatography A* **2007**, *1168* (1-2), 101-168.
42. Nischang, I.; Teasdale, I.; Bruggemann, O., Porous polymer monoliths for small molecule separations: advancements and limitations. *Analytical and Bioanalytical Chemistry* **2011**, *400* (8), 2289-2304.
43. Cassie, A. B. D.; Baxter, S., Wettability of porous surfaces. *Transactions of the Faraday Society* **1944**, *40* (0), 546-551.
44. Ueda, E.; Geyer, F. L.; Nedashkivska, V.; Levkin, P. A., Droplet Microarray: facile formation of arrays of microdroplets and hydrogel micropads for cell screening applications. *Lab on a Chip* **2012**, *12* (24), 5218-5224.
45. Efremov, A. N.; Stanganello, E.; Welle, A.; Scholpp, S.; Levkin, P. A., Micropatterned superhydrophobic structures for the simultaneous culture of multiple cell types and the study of cell-cell communication. *Biomaterials* **2013**, *34* (7), 1757-1763.
46. Buchmeiser, M. R., Polymeric monolithic materials: Syntheses, properties, functionalization

and applications. *Polymer* **2007**, *48* (8), 2187-2198.

47. Bandari, R.; Hoche, T.; Prager, A.; Dirnberger, K.; Buchmeiser, M. R., Ring-Opening Metathesis Polymerization Based Pore-Size-Selective Functionalization of Glycidyl Methacrylate Based Monolithic Media: Access to Size-Stable Nanoparticles for Ligand-Free Metal Catalysis. *Chemistry-a European Journal* **2010**, *16* (15), 4650-4658.

48. Young, T., An Essay on the Cohesion of Fluids. *Philosophical Transactions of the Royal Society of London* **1805**, *95* (ArticleType: research-article / Full publication date: 1805 /), 65-87.

49. Wenzel, R. N., Resistance of Solid Surfaces to Wetting by Water *Industrial & Engineering Chemistry* **1936**, *28* (8), 988-994.

50. Koishi, T.; Yasuoka, K.; Fujikawa, S.; Ebisuzaki, T.; Zeng, X. C., Coexistence and transition between Cassie and Wenzel state on pillared hydrophobic surface. *Proceedings of the National Academy of Sciences of the United States of America* **2009**, *106* (21), 8435-8440.

51. Lafuma, A.; Quere, D., Superhydrophobic states. *Nat Mater* **2003**, *2* (7), 457-460.

52. Rykaczewski, K.; Landin, T.; Walker, M. L.; Scott, J. H. J.; Varanasi, K. K., Direct Imaging of Complex Nano- to Microscale Interfaces Involving Solid, Liquid, and Gas Phases. *Acs Nano* **2012**, *6* (10), 9326-9334.

53. Ensikat, H. J.; Schulte, A. J.; Koch, K.; Barthlott, W., Droplets on Superhydrophobic Surfaces: Visualization of the Contact Area by Cryo-Scanning Electron Microscopy. *Langmuir* **2009**, *25* (22), 13077-13083.

54. Luo, C.; Zheng, H.; Wang, L.; Fang, H.; Hu, J.; Fan, C.; Cao, Y.; Wang, J., Direct Three-Dimensional Imaging of the Buried Interfaces between Water and Superhydrophobic Surfaces. *Angew. Chem. Int. Ed.* **2010**, *49* (48), 9145-9148.

55. Good, R. J., Contact-angle, wetting and adhesion - A critical review. *Journal of Adhesion Science and Technology* **1992**, *6* (12), 1269-1302.

56. Drelich, J., The effect of drop (bubble) size on contact angle at solid surfaces. *Journal of Adhesion* **1997**, *63* (1-3), 31-51.

57. Hong, S. J.; Chang, F. M.; Chou, T. H.; Chan, S. H.; Sheng, Y. J.; Tsao, H. K., Anomalous Contact Angle Hysteresis of a Captive Bubble: Advancing Contact Line Pinning. *Langmuir* **2011**, *27* (11), 6890-6896.

58. Drelich, J.; Miller, J. D.; Good, R. J., The effect of drop (bubble) size on advancing and receding contact angles for heterogeneous and rough solid surfaces as observed with sessile-drop and captive-bubble techniques. *Journal of Colloid and Interface Science* **1996**, *179* (1), 37-50.

59. Marmur, A., Contact-angle hysteresis on heterogeneous smooth surfaces: theoretical comparison of the captive bubble and drop methods. *Colloid Surf. A-Physicochem. Eng. Asp.* **1998**, *136* (1-2), 209-215.

60. Marmur, A., Soft contact: measurement and interpretation of contact angles. *Soft Matter* **2006**, *2* (1), 12-17.

61. Ruiz-Cabello, F. J. M.; Rodriguez-Valverde, M. A.; Marmur, A.; Cabrerizo-Vilchez, M. A., Comparison of Sessile Drop and Captive Bubble Methods on Rough Homogeneous Surfaces: A Numerical Study. *Langmuir* **2011**, *27* (15), 9638-9643.
62. Smith, K. C. A.; Oatley, C. W., THE SCANNING ELECTRON MICROSCOPE AND ITS FIELDS OF APPLICATION. *British Journal of Applied Physics* **1955**, *6* (11), 391-399.
63. P. J. Goodhew, J. H., R. Beanland., *Electron Microscopy and Analysis*. Taylor & Francis: London, 2001.
64. Nixon, W. C., General Principles of Scanning Electron Microscopy. *Philos. Trans. R. Soc. Lond. Ser. B-Biol. Sci.* **1971**, *261* (837), 45-&.
65. Heide, P. V. d., *X-Ray Photoelectron Spectroscopy: An Introduction to Principles and Practices*. 1 ed.; John Wiley & Sons, Inc.: 2012.
66. Oster, G.; Yang, N.-L., Photopolymerization of vinyl monomers. *Chem. Rev.* **1968**, *68* (2), 125-151.
67. Odian, G., *Principles of polymerization, fourth edition*. John Wiley & Sons, Inc.: Staten Island, Newyork 2004.
68. Aydin, M.; Arsu, N.; Yagci, Y.; Jockusch, S.; Turro, N. J., Mechanistic study of photoinitiated free radical polymerization using thioxanthone thioacetic acid as one-component type II photoinitiator. *Macromolecules* **2005**, *38* (10), 4133-4138.
69. Oster, G.; Shibata, O., Graft Copolymer of Polyacrylamide and Natural Rubber Produced by Means of Ultraviolet Light. *J Polym Sci* **1957**, *26* (113), 233-234.
70. Ranby, B., Surface Modification of Polymers by Photoinitiated Graft-Polymerization. *Makromol Chem-M Symp* **1992**, *63*, 55-67.
71. Stachowiak, T. B.; Svec, F.; Frechet, J. M. J., Patternable protein resistant surfaces for multifunctional microfluidic devices via surface hydrophilization of porous polymer monoliths using photografting. *Chem. Mater.* **2006**, *18* (25), 5950-5957.
72. Peterson, D. S.; Rohr, T.; Svec, F.; Frechet, J. M. J., Dual-function microanalytical device by in situ photolithographic grafting of porous polymer monolith: Integrating solid-phase extraction and enzymatic digestion for peptide mass mapping. *Analytical Chemistry* **2003**, *75* (20), 5328-5335.
73. Krenkova, J.; Lacher, N. A.; Svec, F., Highly Efficient Enzyme Reactors Containing Trypsin and Endoproteinase LysC Immobilized on Porous Polymer Monolith Coupled to MS Suitable for Analysis of Antibodies. *Analytical Chemistry* **2009**, *81* (5), 2004-2012.
74. Eeltink, S.; Hilder, E. F.; Geiser, L.; Svec, F.; Frechet, J. M. J.; Rozing, G. P.; Schoenmakers, P. J.; Kok, W. T., Controlling the surface chemistry and chromatography properties of methacrylate-ester-based monolithic capillary columns via photografting. *Journal of Separation Science* **2007**, *30* (3), 407-413.
75. Sakdinawat, A.; Attwood, D., Nanoscale X-ray imaging. *Nat. Photonics* **2010**, *4* (12), 840-848.
76. Robinson, I.; Harder, R., Coherent X-ray diffraction imaging of strain at the nanoscale. *Nat.*

Mater. **2009**, 8 (4), 291-298.

77. Momose, A., Recent advances in X-ray phase imaging. *Japanese Journal of Applied Physics Part 1-Regular Papers Brief Communications & Review Papers* **2005**, 44 (9A), 6355-6367.

78. Bravin, A.; Coan, P.; Suortti, P., X-ray phase-contrast imaging: from pre-clinical applications towards clinics. *Phys. Med. Biol.* **2013**, 58 (1), R1-R35.

79. Davis, T. J.; Gao, D.; Gureyev, T. E.; Stevenson, A. W.; Wilkins, S. W., PHASE-CONTRAST IMAGING OF WEAKLY ABSORBING MATERIALS USING HARD X-RAYS. *Nature* **1995**, 373 (6515), 595-598.

80. Nugent, K. A.; Gureyev, T. E.; Cookson, D. F.; Paganin, D.; Barnea, Z., Quantitative phase imaging using hard x rays. *Physical Review Letters* **1996**, 77 (14), 2961-2964.

81. Wilkins, S. W.; Gureyev, T. E.; Gao, D.; Pogany, A.; Stevenson, A. W., Phase-contrast imaging using polychromatic hard X-rays. *Nature* **1996**, 384 (6607), 335-338.

82. Cloetens, P.; Ludwig, W.; Baruchel, J.; Van Dyck, D.; Van Landuyt, J.; Guigay, J. P.; Schlenker, M., Holotomography: Quantitative phase tomography with micrometer resolution using hard synchrotron radiation x rays. *Applied Physics Letters* **1999**, 75 (19), 2912-2914.

83. Cloetens, P.; Ludwig, W.; Baruchel, J.; Guigay, J. P.; Pernot-Rejmankova, P.; Salome-Pateyron, M.; Schlenker, M.; Buffiere, J. Y.; Maire, E.; Peix, G., Hard x-ray phase imaging using simple propagation of a coherent synchrotron radiation beam. *Journal of Physics D-Applied Physics* **1999**, 32 (10A), A145-A151.

84. Momose, A.; Takeda, T.; Itai, Y.; Hirano, K., Phase-contrast X-ray computed tomography for observing biological soft tissues. *Nat. Med.* **1996**, 2 (4), 473-475.

85. Gittens, R. A.; McLachlan, T.; Olivares-Navarrete, R.; Cai, Y.; Berner, S.; Tannenbaum, R.; Schwartz, Z.; Sandhage, K. H.; Boyan, B. D., The effects of combined micron-/submicron-scale surface roughness and nanoscale features on cell proliferation and differentiation. *Biomaterials* **2011**, 32 (13), 3395-3403.

86. Ross, A. M.; Jiang, Z.; Bastmeyer, M.; Lahann, J., Physical Aspects of Cell Culture Substrates: Topography, Roughness, and Elasticity. *Small* **2012**, 8 (3), 336-355.

87. Collins, B. E.; Dancil, K. P. S.; Abbi, G.; Sailor, M. J., Determining protein size using an electrochemically machined pore gradient in silicon. *Advanced Functional Materials* **2002**, 12 (3), 187-191.

88. Khung, Y. L.; Barritt, G.; Voelcker, N. H., Using continuous porous silicon gradients to study the influence of surface topography on the behaviour of neuroblastoma cells. *Experimental Cell Research* **2008**, 314 (4), 789-800.

89. Wang, P.-Y.; Clements, L. R.; Thissen, H.; Jane, A.; Tsai, W.-B.; Voelcker, N. H., Screening Mesenchymal Stem Cell Attachment and Differentiation on Porous Silicon Gradients. *Advanced Functional Materials* **2012**, n/a-n/a.

90. Woodfield, T. B. F.; Van Blitterswijk, C. A.; De Wijn, J.; Sims, T. J.; Hollander, A. P.; Riesle,

- J., Polymer scaffolds fabricated with pore-size gradients as a model for studying the zonal organization within tissue-engineered cartilage constructs. *Tissue Engineering* **2005**, *11* (9-10), 1297-1311.
91. Oh, S. H.; Park, I. K.; Kim, J. M.; Lee, J. H., In vitro and in vivo characteristics of PCL scaffolds with pore size gradient fabricated by a centrifugation method. *Biomaterials* **2007**, *28* (9), 1664-1671.
92. Toepke, M. W.; Beebe, D. J., PDMS absorption of small molecules and consequences in microfluidic applications. *Lab on a Chip* **2006**, *6* (12), 1484-1486.
93. Lee, J. N.; Park, C.; Whitesides, G. M., Solvent compatibility of poly(dimethylsiloxane)-based microfluidic devices. *Analytical Chemistry* **2003**, *75* (23), 6544-6554.
94. Belmares, M.; Blanco, M.; Goddard, W. A.; Ross, R. B.; Caldwell, G.; Chou, S. H.; Pham, J.; Olofson, P. M.; Thomas, C., Hildebrand and Hansen solubility parameters from molecular dynamics with applications to electronic nose polymer sensors. *J Comput Chem* **2004**, *25* (15), 1814-1826.
95. Coufal, P.; Čihák, M.; Suchánková, J.; Tesařová, E.; Bosáková, Z.; Štulík, K., Methacrylate monolithic columns of 320 μm I.D. for capillary liquid chromatography. *Journal of Chromatography A* **2002**, *946* (1-2), 99-106.
96. Whitesides, G. M., The origins and the future of microfluidics. *Nature* **2006**, *442* (7101), 368-373.
97. Jeon, N. L.; Dertinger, S. K. W.; Chiu, D. T.; Choi, I. S.; Stroock, A. D.; Whitesides, G. M., Generation of Solution and Surface Gradients Using Microfluidic Systems. *Langmuir* **2000**, *16* (22), 8311-8316.
98. Dertinger, S. K. W.; Chiu, D. T.; Jeon, N. L.; Whitesides, G. M., Generation of Gradients Having Complex Shapes Using Microfluidic Networks. *Analytical Chemistry* **2001**, *73* (6), 1240-1246.
99. Howell, P. B.; Mott, D. R.; Golden, J. P.; Ligler, F. S., Design and evaluation of a Dean vortex-based micromixer. *Lab on a Chip* **2004**, *4* (6), 663-669.
100. Mengeaud, V.; Jossierand, J.; Girault, H. H., Mixing processes in a zigzag microchannel: Finite element simulations and optical study. *Analytical Chemistry* **2002**, *74* (16), 4279-4286.
101. Pennella, F.; Rossi, M.; Ripandelli, S.; Rasponi, M.; Mastrangelo, F.; Deriu, M. A.; Ridolfi, L.; Kahler, C. J.; Morbiducci, U., Numerical and experimental characterization of a novel modular passive micromixer. *Biomedical Microdevices* **2012**, *14* (5), 849-862.
102. Kreppenhofer, K.; Li, J.; Segura, R.; Popp, L.; Rossi, M.; Tzvetkova, P.; Luy, B.; Kähler, C. J.; Guber, A. E.; Levkin, P. A., Formation of a Polymer Surface with a Gradient of Pore Size Using a Microfluidic Chip. *Langmuir* **2013**, *29* (11), 3797-3804.
103. Sia, S. K.; Whitesides, G. M., Microfluidic devices fabricated in poly(dimethylsiloxane) for biological studies. *Electrophoresis* **2003**, *24* (21), 3563-3576.
104. Mei, Y.; Saha, K.; Bogatyrev, S. R.; Yang, J.; Hook, A. L.; Kalcioğlu, Z. I.; Cho, S. W.; Mitalipova, M.; Pyzocha, N.; Rojas, F.; Van Vliet, K. J.; Davies, M. C.; Alexander, M. R.; Langer, R.;

- Jaenisch, R.; Anderson, D. G., Combinatorial development of biomaterials for clonal growth of human pluripotent stem cells. *Nat. Mater.* **2010**, *9* (9), 768-778.
105. Thapa, A.; Miller, D. C.; Webster, T. J.; Haberstroh, K. M., Nano-structured polymers enhance bladder smooth muscle cell function. *Biomaterials* **2003**, *24* (17), 2915-2926.
106. Villa-Diaz, L. G.; Nandivada, H.; Ding, J.; Nogueira-de-Souza, N. C.; Krebsbach, P. H.; O'Shea, K. S.; Lahann, J.; Smith, G. D., Synthetic polymer coatings for long-term growth of human embryonic stem cells. *Nat Biotech* **2010**, *28* (6), 581-583.
107. Oliveira, S. M.; Song, W. L.; Alves, N. M.; Mano, J. F., Chemical modification of bioinspired superhydrophobic polystyrene surfaces to control cell attachment/proliferation. *Soft Matter* **2011**, *7* (19), 8932-8941.
108. Miller, D. C.; Thapa, A.; Haberstroh, K. M.; Webster, T. J., Endothelial and vascular smooth muscle cell function on poly(lactic-co-glycolic acid) with nano-structured surface features. *Biomaterials* **2004**, *25* (1), 53-61.
109. Lalani, R.; Liu, L., Electrospun Zwitterionic Poly(Sulfobetaine Methacrylate) for Nonadherent, Superabsorbent, and Antimicrobial Wound Dressing Applications. *Biomacromolecules* **2012**, *13* (6), 1853-1863.
110. Dong, R.; Molloy, R. P.; Lindau, M.; Ober, C. K., Direct Synthesis of Quaternized Polymer Brushes and Their Application for Guiding Neuronal Growth. *Biomacromolecules* **2010**, *11* (8), 2027-2032.
111. Lee, J. H.; Lee, J. W.; Khang, G.; Lee, H. B., Interaction of cells on chargeable functional group gradient surfaces. *Biomaterials* **1997**, *18* (4), 351-358.
112. Murata, H.; Koepsel, R. R.; Matyjaszewski, K.; Russell, A. J., Permanent, non-leaching antibacterial surfaces - 2: How high density cationic surfaces kill bacterial cells. *Biomaterials* **2007**, *28* (32), 4870-4879.
113. Cai, T.; Wang, R.; Neoh, K. G.; Kang, E. T., Functional poly(vinylidene fluoride) copolymer membranes via surface-initiated thiol-ene click reactions. *Polym. Chem.* **2011**, *2* (Copyright (C) 2012 American Chemical Society (ACS). All Rights Reserved.), 1849-1858.
114. Chang, Y.; Chang, Y.; Higuchi, A.; Shih, Y.-J.; Li, P.-T.; Chen, W.-Y.; Tsai, E.-M.; Hsiue, G.-H., Bioadhesive control of plasma proteins and blood cells from umbilical cord blood onto the interface grafted with zwitterionic polymer brushes. *Langmuir* **2012**, *28* (Copyright (C) 2012 American Chemical Society (ACS). All Rights Reserved.), 4309-4317.
115. Gam-Derouich, S.; Gosecka, M.; Lepinay, S.; Turmine, M.; Carbonnier, B.; Basinska, T.; Slomkowski, S.; Millot, M. C.; Othmane, A.; Ben Hassen-Chehimi, D.; Chehimi, M. M., Highly Hydrophilic Surfaces from Polyglycidol Grafts with Dual Antifouling and Specific Protein Recognition Properties. *Langmuir* **2011**, *27* (15), 9285-9294.
116. Zhou, M.-Y.; Liu, H.-W.; Venkiteshwaran, A.; Kilduff, J.; Anderson, D. G.; Langer, R.; Belfort, G., High throughput discovery of new fouling-resistant surfaces. *J. Mater. Chem.* **2011**, *21*

(Copyright (C) 2012 American Chemical Society (ACS). All Rights Reserved.), 693-704.

117. Zhao, C.; Li, L.; Zheng, J., Achieving Highly Effective Nonfouling Performance for Surface-Grafted Poly(HPMA) via Atom-Transfer Radical Polymerization. *Langmuir* **2010**, *26* (Copyright (C) 2012 American Chemical Society (ACS). All Rights Reserved.), 17375-17382.

118. Zhang, Z.; Chao, T.; Chen, S. F.; Jiang, S. Y., Superlow fouling sulfobetaine and carboxybetaine polymers on glass slides. *Langmuir* **2006**, *22* (24), 10072-10077.

119. Lalani, R.; Liu, L., Electrospun Zwitterionic Poly(Sulfobetaine Methacrylate) for Nonadherent, Superabsorbent, and Antimicrobial Wound Dressing Applications. *Biomacromolecules* **2012**, *13* (Copyright (C) 2012 American Chemical Society (ACS). All Rights Reserved.), 1853-1863.

120. Tesema, Y.; Raghavan, D.; Stubbs, J., Bone cell viability on methacrylic acid grafted and collagen immobilized porous poly(3-hydroxybutyrate-co-3-hydroxyvalerate). *J. Appl. Polym. Sci.* **2005**, *98* (5), 1916-1921.

121. Steele, J. G.; Johnson, G.; McLean, K. M.; Beumer, G. J.; Griesser, H. J., Effect of porosity and surface hydrophilicity on migration of epithelial tissue over synthetic polymer. *Journal of Biomedical Materials Research* **2000**, *50* (4), 475-482.

122. Phong, H. Q.; Wang, S. L.; Wang, M. J., Cell behaviors on micro-patterned porous thin films. *Materials Science and Engineering B-Advanced Functional Solid-State Materials* **2010**, *169* (1-3), 94-100.

123. Lin, D. T.; Young, T. H.; Fang, Y., Studies on the effect of surface properties on the biocompatibility of polyurethane membranes. *Biomaterials* **2001**, *22* (12), 1521-1529.

124. Hajicharalambous, C. S.; Lichter, J.; Hix, W. T.; Swierczewska, M.; Rubner, M. F.; Rajagopalan, P., Nano- and sub-micron porous polyelectrolyte multilayer assemblies: Biomimetic surfaces for human corneal epithelial cells. *Biomaterials* **2009**, *30* (23-24), 4029-4036.

125. Fukano, Y.; Usui, M. L.; Underwood, R. A.; Isenath, S.; Marshall, A. J.; Hauch, K. D.; Ratner, B. D.; Olerud, J. E.; Fleckman, P., Epidermal and dermal integration into sphere-templated porous poly(2-hydroxyethyl methacrylate) implants in mice. *Journal of Biomedical Materials Research Part A* **2010**, *94A* (4), 1172-1186.

126. Lanniel, M.; Huq, E.; Allen, S.; Buttery, L.; Williams, P. M.; Alexander, M. R., Substrate induced differentiation of human mesenchymal stem cells on hydrogels with modified surface chemistry and controlled modulus. *Soft Matter* **2011**, *7* (14), 6501-6514.

127. Romeo, S.; Bovee, J.; Kroon, H. M.; Tirabosco, R.; Natali, C.; Zanatta, L.; Sciot, R.; Mertens, F.; Athanasou, N.; Alberghini, M.; Szuhai, K.; Hogendoorn, P. C. W.; Tos, A. P. D., Malignant fibrous histiocytoma and fibrosarcoma of bone: a re-assessment in the light of currently employed morphological, immunohistochemical and molecular approaches. *Virchows Archiv* **2012**, *461* (5), 561-570.

128. Wolf, K.; Friedl, P., Molecular mechanisms of cancer cell invasion and plasticity. *British Journal of Dermatology* **2006**, *154*, 11-15.

129. Costa, F.; Carvalho, I. F.; Montelaro, R. C.; Gomes, P.; Martins, M. C. L., Covalent immobilization of antimicrobial peptides (AMPs) onto biomaterial surfaces. *Acta Biomaterialia* **2011**, *7* (4), 1431-1440.
130. Villa-Diaz, L. G.; Nandivada, H.; Ding, J.; Nogueira-De-Souza, N. C.; Krebsbach, P. H.; O'Shea, K. S.; Lahann, J.; Smith, G. D., Synthetic polymer coatings for long-term growth of human embryonic stem cells. *Nat Biotechnol* **2010**, *28* (6), 581-583.
131. Pucci, V.; Raggi, M. A.; Svec, F.; Frechet, J. M. J., Monolithic columns with a gradient of functionalities prepared via photoinitiated grafting for separations using capillary electrochromatography. *Journal of Separation Science* **2004**, *27* (10-11), 779-788.
132. Enright, T. P.; Hagaman, D.; Kokoroz, M.; Coleman, N.; Sidorenko, A., Gradient and Patterned Polymer Brushes by Photoinitiated "Grafting Through" Approach. *J Polym Sci Pol Phys* **2010**, *48* (14), 1616-1622.
133. Blondiaux, N.; Zurcher, S.; Liley, M.; Spencer, N. D., Fabrication of multiscale surface-chemical gradients by means of photocatalytic lithography. *Langmuir* **2007**, *23* (7), 3489-3494.
134. Coen, M. C.; Keller, B.; Groening, P.; Schlapbach, L., Functionalization of graphite, glassy carbon, and polymer surfaces with highly oxidized sulfur species by plasma treatments. *Journal of Applied Physics* **2002**, *92* (9), 5077-5083.
135. Moulder, J. F.; Chastain, J., *Handbook of X-Ray Photoelectron Spectroscopy: A Reference Book of Standard Spectra for Identification and Interpretation of XPS Data*. Perkin-Elmer Corporation, Physical Electronics Division: 1992.
136. Scofield, J. H., Hartree-Slater Subshell Photoionization Cross-Sections at 1254 and 1487ev. *Journal of Electron Spectroscopy and Related Phenomena* **1976**, *8* (2), 129-137.
137. Rasheed, S.; Nelsonre.Wa; Toth, E. M.; Arnstein, P.; Gardner, M. B., Characterization of a Newly Derived Human Sarcoma Cell Line (Ht-1080). *Cancer* **1974**, *33* (6), 1027-1033.
138. Kwiatkowska, B. The influence of chemical and physical properties of surfaces on cell behavior. Hochschule Offenburg, Offenburg, 2011.
139. Wong, T. S.; Kang, S. H.; Tang, S. K. Y.; Smythe, E. J.; Hatton, B. D.; Grinthal, A.; Aizenberg, J., Bioinspired self-repairing slippery surfaces with pressure-stable omniphobicity. *Nature* **2011**, *477* (7365), 443-447.
140. Pokroy, B.; Epstein, A. K.; Persson-Gulda, M. C. M.; Aizenberg, J., Fabrication of Bioinspired Actuated Nanostructures with Arbitrary Geometry and Stiffness. *Adv. Mater.* **2009**, *21* (4), 463-+.
141. Xu, W.; Choi, C. H., From Sticky to Slippery Droplets: Dynamics of Contact Line Depinning on Superhydrophobic Surfaces. *Physical Review Letters* **2012**, *109* (2).
142. Wilson, P. W.; Lu, W. Z.; Xu, H. J.; Kim, P.; Kreder, M. J.; Alvarenga, J.; Aizenberg, J., Inhibition of ice nucleation by slippery liquid-infused porous surfaces (SLIPS). *Physical Chemistry Chemical Physics* **2013**, *15* (2), 581-585.

143. Smith, J. D.; Dhiman, R.; Anand, S.; Reza-Garduno, E.; Cohen, R. E.; McKinley, G. H.; Varanasi, K. K., Droplet mobility on lubricant-impregnated surfaces. *Soft Matter* **2013**, *9*, 1772-1780.
144. Epstein, A. K.; Wong, T. S.; Belisle, R. A.; Boggs, E. M.; Aizenberg, J., Liquid-infused structured surfaces with exceptional anti-biofouling performance. *Proceedings of the National Academy of Sciences of the United States of America* **2012**, *109* (33), 13182-13187.
145. Flemming, H. C.; Wingender, J., The biofilm matrix. *Nature Reviews Microbiology* **2010**, *8* (9), 623-633.
146. McDougald, D.; Rice, S. A.; Barraud, N.; Steinberg, P. D.; Kjelleberg, S., Should we stay or should we go: mechanisms and ecological consequences for biofilm dispersal. *Nature Reviews Microbiology* **2012**, *10* (1), 39-50.
147. Epstein, A. K.; Pokroy, B.; Seminara, A.; Aizenberg, J., Bacterial biofilm shows persistent resistance to liquid wetting and gas penetration. *Proceedings of the National Academy of Sciences of the United States of America* **2011**, *108* (3), 995-1000.
148. Boe-Hansen, R.; Martiny, A. C.; Arvin, E.; Albrechtsen, H. J., Monitoring biofilm formation and activity in drinking water distribution networks under oligotrophic conditions. *Water Science and Technology* **2003**, *47* (5), 91-97.
149. Donlan, R. M.; Costerton, J. W., Biofilms: Survival mechanisms of clinically relevant microorganisms. *Clinical Microbiology Reviews* **2002**, *15* (2), 167-+.
150. Timofeeva, L.; Kleshcheva, N., Antimicrobial polymers: mechanism of action, factors of activity, and applications. *Applied Microbiology and Biotechnology* **2011**, *89* (3), 475-492.
151. Chuang, H. F.; Smith, R. C.; Hammond, P. T., Polyelectrolyte multilayers for tunable release of antibiotics. *Biomacromolecules* **2008**, *9* (6), 1660-1668.
152. Wu, P.; Grainger, D. W., Drug/device combinations for local drug therapies and infection prophylaxis. *Biomaterials* **2006**, *27* (11), 2450-2467.
153. Price, J. S.; Tencer, A. F.; Arm, D. M.; Bohach, G. A., Controlled release of antibiotics from coated orthopedic implants. *Journal of Biomedical Materials Research* **1996**, *30* (3), 281-286.
154. Stigter, M.; Bezemer, J.; de Groot, K.; Layrolle, P., Incorporation of different antibiotics into carbonated hydroxyapatite coatings on titanium implants, release and antibiotic efficacy. *Journal of Controlled Release* **2004**, *99* (1), 127-137.
155. Zodrow, K. R.; Schiffman, J. D.; Elimelech, M., Biodegradable Polymer (PLGA) Coatings Featuring Cinnamaldehyde and Carvacrol Mitigate Biofilm Formation. *Langmuir* **2012**, *28* (39), 13993-13999.
156. Kumar, R.; Munstedt, H., Silver ion release from antimicrobial polyamide/silver composites. *Biomaterials* **2005**, *26* (14), 2081-2088.
157. Monteiro, D. R.; Gorup, L. F.; Takamiya, A. S.; Ruvollo, A. C.; Camargo, E. R.; Barbosa, D. B., The growing importance of materials that prevent microbial adhesion: antimicrobial effect of medical devices containing silver. *International Journal of Antimicrobial Agents* **2009**, *34* (2), 103-

110.

158. Mulligan, A. M.; Wilson, M.; Knowles, J. C., Effect of increasing silver content in phosphate-based glasses on biofilms of *Streptococcus sanguis*. *Journal of Biomedical Materials Research Part A* **2003**, *67A* (2), 401-412.

159. Balan, L.; Schneider, R.; Lougnot, D. J., A new and convenient route to polyacrylate/silver nanocomposites by light-induced cross-linking polymerization. *Prog. Org. Coat.* **2008**, *62* (3), 351-357.

160. Hetrick, E. M.; Schoenfisch, M. H., Reducing implant-related infections: active release strategies. *Chem. Soc. Rev.* **2006**, *35* (9), 780-789.

161. Schoenfisch, M. H.; Mowery, K. A.; Rader, M. V.; Baliga, N.; Wahr, J. A.; Meyerhoff, M. E., Improving the thromboresistivity of chemical sensors via nitric oxide release: Fabrication and in vivo evaluation of NO-releasing oxygen-sensing catheters. *Analytical Chemistry* **2000**, *72* (6), 1119-1126.

162. Zhang, H. P.; Annich, G. M.; Miskulin, J.; Osterholzer, K.; Merz, S. I.; Bartlett, R. H.; Meyerhoff, M. E., Nitric oxide releasing silicone rubbers with improved blood compatibility: preparation, characterization, and in vivo evaluation. *Biomaterials* **2002**, *23* (6), 1485-1494.

163. Anderson, J. M., Biological responses to materials. *Annual Review of Materials Research* **2001**, *31*, 81-110.

164. Kingshott, P.; Wei, J.; Bagge-Ravn, D.; Gadegaard, N.; Gram, L., Covalent attachment of poly(ethylene glycol) to surfaces, critical for reducing bacterial adhesion. *Langmuir* **2003**, *19* (17), 6912-6921.

165. Kaper, H. J.; Busscher, H. J.; Norde, W., Characterization of poly(ethylene oxide) brushes on glass surfaces and adhesion of *Staphylococcus epidermidis*. *J. Biomater. Sci.-Polym. Ed.* **2003**, *14* (4), 313-324.

166. Nagel, J. A.; Dickinson, R. B.; Cooper, S. L., Bacterial adhesion to polyurethane surfaces in the presence of pre-adsorbed high molecular weight kininogen. *J. Biomater. Sci.-Polym. Ed.* **1996**, *7* (9), 769-780.

167. Cheng, G.; Zhang, Z.; Chen, S. F.; Bryers, J. D.; Jiang, S. Y., Inhibition of bacterial adhesion and biofilm formation on zwitterionic surfaces. *Biomaterials* **2007**, *28* (29), 4192-4199.

168. Jiang, S. Y.; Cao, Z. Q., Ultralow-Fouling, Functionalizable, and Hydrolyzable Zwitterionic Materials and Their Derivatives for Biological Applications. *Adv. Mater.* **2010**, *22* (9), 920-932.

169. Stiriba, S. E.; Frey, H.; Haag, R., Dendritic polymers in biomedical applications: From potential to clinical use in diagnostics and therapy. *Angewandte Chemie-International Edition* **2002**, *41* (8), 1329-1334.

170. Lee, S. B.; Koepsel, R. R.; Morley, S. W.; Matyjaszewski, K.; Sun, Y. J.; Russell, A. J., Permanent, nonleaching antibacterial surfaces. 1. Synthesis by atom transfer radical polymerization. *Biomacromolecules* **2004**, *5* (3), 877-882.

171. Thorsteinsson, T.; Loftsson, T.; Masson, M., Soft antibacterial agents. *Current Medicinal*

Chemistry **2003**, *10* (13), 1129-1136.

172. Kenawy, E. R.; Mahmoud, Y. A. G., Biologically active polymers, 6 - Synthesis and antimicrobial activity of some linear copolymers with quaternary ammonium and phosphonium groups.

Macromolecular Bioscience **2003**, *3* (2), 107-116.

173. Tashiro, T., Antibacterial and bacterium adsorbing macromolecules. *Macromolecular Materials and Engineering* **2001**, *286* (2), 63-87.

174. Xu, F. J.; Neoh, K. G.; Kang, E. T., Bioactive surfaces and biomaterials via atom transfer radical polymerization. *Progress in Polymer Science* **2009**, *34* (8), 719-761.

175. Worley, S. D.; Sun, G., Biocidal polymers. *Trends in Polymer Science* **1996**, *4* (11), 364-370.

176. Carlson, R. P.; Taffs, R.; Davison, W. M.; Stewart, P. S., Anti-biofilm properties of chitosan-coated surfaces. *J. Biomater. Sci.-Polym. Ed.* **2008**, *19* (8), 1035-1046.

177. Schaer, T. P.; Stewart, S.; Hsu, B. B.; Klibanov, A. M., Hydrophobic polycationic coatings that inhibit biofilms and support bone healing during infection. *Biomaterials* **2012**, *33* (5), 1245-1254.

178. Hequet, A.; Humblot, V.; Berjeaud, J. M.; Pradier, C. M., Optimized grafting of antimicrobial peptides on stainless steel surface and biofilm resistance tests. *Colloids and Surfaces B-Biointerfaces* **2011**, *84* (2), 301-309.

179. Kugel, A.; Stafslin, S.; Chisholm, B. J., Antimicrobial coatings produced by "tethering" biocides to the coating matrix: A comprehensive review. *Prog. Org. Coat.* **2011**, *72* (3), 222-252.

180. Epstein, A. K.; Hochbaum, A. I.; Kim, P.; Aizenberg, J., Control of bacterial biofilm growth on surfaces by nanostructural mechanics and geometry. *Nanotechnology* **2011**, *22* (49).

181. Wang, Y.; Subbiahdoss, G.; Swartjes, J.; van der Mei, H. C.; Busscher, H. J.; Libera, M., Length-Scale Mediated Differential Adhesion of Mammalian Cells and Microbes. *Advanced Functional Materials* **2011**, *21* (20), 3916-3923.

182. Kim, P.; Kreder, M. J.; Alvarenga, J.; Aizenberg, J., Hierarchical or Not? Effect of the Length Scale and Hierarchy of the Surface Roughness on Omniphobicity of Lubricant-Infused Substrates. *Nano Lett* **2013**, *13* (4), 1793-1799.

183. Cheng, Y.; Suhonen, H.; Helfen, L.; Li, J.; Xu, F.; Grunze, M.; Levkin, P. A.; Baumbach, T., Direct three-dimensional imaging of surface-water interface on polymer substrates with special wettability by nanoscale hard X-ray phase tomography (in preparation). **2013**.

184. Li, J.; Kleintschek, T.; Rieder, A.; Cheng, Y.; Baumbach, T.; Obst, U.; Schwartz, T.; Levkin, P. A., Hydrophobic Liquid-Infused Porous Polymer Surfaces for Antibacterial Applications. *Acs Applied Materials & Interfaces* **2013**.

185. Joanny, J. F.; Degennes, P. G., A Model for Contact-Angle Hysteresis. *Journal of Chemical Physics* **1984**, *81* (1), 552-562.

186. Chang, F. M.; Hong, S. J.; Sheng, Y. J.; Tsao, H. K., High contact angle hysteresis of superhydrophobic surfaces: Hydrophobic defects. *Applied Physics Letters* **2009**, *95* (6).

187. Pogorzelski, S. J.; Berezowski, Z.; Rochowski, P.; Szurkowski, J., A novel methodology based

on contact angle hysteresis approach for surface changes monitoring in model PMMA-Corega Tabs system. *Applied Surface Science* **2012**, 258 (8), 3652-3658.

188. Wong, T.-S.; Kang, S. H.; Tang, S. K. Y.; Smythe, E. J.; Hatton, B. D.; Grinthal, A.; Aizenberg, J., Bioinspired self-repairing slippery surfaces with pressure-stable omniphobicity. *Nature* **2011**, 477 (7365), 443-447.

189. Verma, S. P.; Philippot, J. R.; Bonnet, B.; Saintemarie, J.; Moschetto, Y.; Wallach, D. F. H., RAMAN STUDIES OF STRUCTURAL REARRANGEMENTS INDUCED IN HUMAN-PLASMA LIPOPROTEIN CAROTENOIDS BY MALONDIALDEHYDE. *Lipids* **1985**, 20 (12), 890-896.

190. Bruchmann, S.; Dotsch, A.; Nouri, B.; Chaberny, I. F.; Haussler, S., Quantitative Contributions of Target Alteration and Decreased Drug Accumulation to Pseudomonas aeruginosa Fluoroquinolone Resistance. *Antimicrobial Agents and Chemotherapy* **2013**, 57 (3), 1361-1368.

191. Schultz, M. P.; Bendick, J. A.; Holm, E. R.; Hertel, W. M., Economic impact of biofouling on a naval surface ship. *Biofouling* **2011**, 27 (1), 87-98.

192. Piola, R. F.; Johnston, E. L., The potential for translocation of marine species via small-scale disruptions to antifouling surfaces. *Biofouling* **2008**, 24 (3), 145-155.

193. Dafforn, K. A.; Lewis, J. A.; Johnston, E. L., Antifouling strategies: History and regulation, ecological impacts and mitigation. *Marine Pollution Bulletin* **2011**, 62 (3), 453-465.

194. Hoipkemeier-Wilson, L.; Schumacher, J.; Carman, M.; Gibson, A.; Feinberg, A.; Callow, M.; Finlay, J.; Callow, J.; Brennan, A., Antifouling potential of lubricious, micro-engineered, PDMS elastomers against zoospores of the green fouling alga *Ulva* (Enteromorpha). *Biofouling* **2004**, 20 (1), 53-63.

195. Holland, R.; Dugdale, T. M.; Wetherbee, R.; Brennan, A. B.; Finlay, J. A.; Callow, J. A.; Callow, M. E., Adhesion and motility of fouling diatoms on a silicone elastomer. *Biofouling* **2004**, 20 (6), 323-329.

196. Sommer, S.; Ekin, A.; Webster, D. C.; Stafslie, S. J.; Daniels, J.; VanderWal, L. J.; Thompson, S. E. M.; Callow, M. E.; Callow, J. A., A preliminary study on the properties and fouling-release performance of siloxane-polyurethane coatings prepared from poly(dimethylsiloxane) (PDMS) macromers. *Biofouling* **2010**, 26 (8), 961-972.

197. Berglin, M.; Larsson, A.; Jonsson, P. R.; Gatenholm, P., The adhesion of the barnacle, *Balanus improvisus*, to poly(dimethylsiloxane) fouling-release coatings and poly(methyl methacrylate) panels: The effect of barnacle size on strength and failure mode. *Journal of Adhesion Science and Technology* **2001**, 15 (12), 1485-1502.

198. Brady, R. F.; Singer, I. L., Mechanical factors favoring release from fouling release coatings. *Biofouling* **2000**, 15 (1-3), 73-81.

199. Carman, M. L.; Estes, T. G.; Feinberg, A. W.; Schumacher, J. F.; Wilkerson, W.; Wilson, L. H.; Callow, M. E.; Callow, J. A.; Brennan, A. B., Engineered antifouling microtopographies - correlating wettability with cell attachment. *Biofouling* **2006**, 22 (1), 11-21.

200. Schumacher, J. F.; Aldred, N.; Callow, M. E.; Finlay, J. A.; Callow, J. A.; Clare, A. S.; Brennan, A. B., Species-specific engineered antifouling topographies: correlations between the settlement of algal zoospores and barnacle cyprids. *Biofouling* **2007**, *23* (5), 307-317.
201. Schumacher, J. F.; Carman, M. L.; Estes, T. G.; Feinberg, A. W.; Wilson, L. H.; Callow, M. E.; Callow, J. A.; Finlay, J. A.; Brennan, A. B., Engineered antifouling microtopographies - effect of feature size, geometry, and roughness on settlement of zoospores of the green alga *Ulva*. *Biofouling* **2007**, *23* (1), 55-62.
202. Scardino, A. J.; Zhang, H.; Cookson, D. J.; Lamb, R. N.; de Nys, R., The role of nano-roughness in antifouling. *Biofouling* **2009**, *25* (8), 757-767.
203. Martinelli, E.; Agostini, S.; Galli, G.; Chiellini, E.; Glisenti, A.; Pettitt, M. E.; Callow, M. E.; Callow, J. A.; Graf, K.; Bartels, F. W., Nanostructured Films of Amphiphilic Fluorinated Block Copolymers for Fouling Release Application. *Langmuir* **2008**, *24* (22), 13138-13147.
204. Zhang, Z.; Finlay, J. A.; Wang, L. F.; Gao, Y.; Callow, J. A.; Callow, M. E.; Jiang, S. Y., Polysulfobetaine-Grafted Surfaces as Environmentally Benign Ultralow Fouling Marine Coatings. *Langmuir* **2009**, *25* (23), 13516-13521.
205. Rosenhahn, A.; Ederth, T.; Pettitt, M. E., Advanced nanostructures for the control of biofouling: The FP6 EU Integrated Project AMBIO. *Biointerphases* **2008**, *3* (1), IR1-IR5.
206. Xiao, L. L.; Li, J. S.; Mieszkin, S.; Di Fino, A.; Clare, A. S.; Callow, M. E.; Callow, J. A.; Grunze, M.; Rosenhahn, A.; Levkin, P. A., Slippery Liquid-Infused Porous Surfaces Showing Marine Antibiofouling Properties. *Acs Applied Materials & Interfaces* **2013**, *5* (20), 10074-10080.
207. Budunoglu, H.; Yildirim, A.; Guler, M. O.; Bayindir, M., Highly Transparent, Flexible, and Thermally Stable Superhydrophobic ORMOSIL Aerogel Thin Films. *Acs Applied Materials & Interfaces* **2011**, *3* (2), 539-545.
208. Xu, Q. F.; Wang, J. N.; Sanderson, K. D., Organic-Inorganic Composite Nanocoatings with Superhydrophobicity, Good Transparency, and Thermal Stability. *Acs Nano* **2010**, *4* (4), 2201-2209.
209. Zimmermann, J.; Reifler, F. A.; Fortunato, G.; Gerhardt, L. C.; Seeger, S., A Simple, One-Step Approach to Durable and Robust Superhydrophobic Textiles. *Advanced Functional Materials* **2008**, *18* (22), 3662-3669.
210. Zhang, J. P.; Seeger, S., Superoleophobic Coatings with Ultralow Sliding Angles Based on Silicone Nanofilaments. *Angewandte Chemie-International Edition* **2011**, *50* (29), 6652-6656.
211. Cao, L. L.; Gao, D., Transparent superhydrophobic and highly oleophobic coatings. *Faraday Discussions* **2010**, *146*, 57-65.
212. Cebeci, F. Ç.; Wu, Z.; Zhai, L.; Cohen, R. E.; Rubner, M. F., Nanoporosity-Driven Superhydrophilicity: A Means to Create Multifunctional Antifogging Coatings. *Langmuir* **2006**, *22* (6), 2856-2862.
213. Cebeci, F. C.; Wu, Z. Z.; Zhai, L.; Cohen, R. E.; Rubner, M. F., Nanoporosity-driven superhydrophilicity: A means to create multifunctional antifogging coatings. *Langmuir* **2006**, *22* (6),

2856-2862.

214. Zimmermann, J.; Rabe, M.; Artus, G. R. J.; Seeger, S., Patterned superfunctional surfaces based on a silicone nanofilament coating. *Soft Matter* **2008**, *4* (3), 450-452.
215. Li, X.; Tian, J. F.; Shen, W., Progress in patterned paper sizing for fabrication of paper-based microfluidic sensors. *Cellulose* **2010**, *17* (3), 649-659.
216. Guckenberger, D. J.; Berthier, E.; Young, E. W. K.; Beebe, D. J., Induced hydrophobic recovery of oxygen plasma-treated surfaces. *Lab on a Chip* **2012**, *12* (13), 2317-2321.
217. Zhang, X. T.; Jin, M.; Liu, Z. Y.; Tryk, D. A.; Nishimoto, S.; Murakami, T.; Fujishima, A., Superhydrophobic TiO₂ surfaces: Preparation, photocatalytic wettability conversion, and superhydrophobic-superhydrophilic patterning. *J. Phys. Chem. C* **2007**, *111* (39), 14521-14529.
218. Manna, U.; Broderick, A. H.; Lynn, D. M., Chemical Patterning and Physical Refinement of Reactive Superhydrophobic Surfaces. *Adv. Mater.* **2012**, *24* (31), 4291-+.
219. Kang, S. M.; You, I.; Cho, W. K.; Shon, H. K.; Lee, T. G.; Choi, I. S.; Karp, J. M.; Lee, H., One-Step Modification of Superhydrophobic Surfaces by a Mussel-Inspired Polymer Coating. *Angewandte Chemie-International Edition* **2010**, *49* (49), 9401-9404.
220. Notsu, H.; Kubo, W.; Shitanda, I.; Tatsuma, T., Super-hydrophobic/super-hydrophilic patterning of gold surfaces by photocatalytic lithography. *J. Mater. Chem.* **2005**, *15* (15), 1523-1527.
221. Elliott, J. T.; Burden, D. L.; Woodward, J. T.; Sehgal, A.; Douglas, J. F., Phospholipid Monolayers Supported on Spun Cast Polystyrene Films. *Langmuir* **2003**, *19* (6), 2275-2283.
222. Yamazaki, M.; Kobayashi, K.; Nakai, T.; Mikami, M.; Yoshioka, H.; Mori, Y.; Satoh, T.; Kubota, S., A novel method to immobilize bioactive substances on hydrophobic surfaces using a polymerizable cationic lipid. *Artificial Organs* **1998**, *22* (10), 873-878.
223. Plant, A. L., Self-assembled phospholipid alkanethiol biomimetic bilayers on gold *Langmuir* **1993**, *9* (11), 2764-2767.
224. Lingler, S.; Rubinstein, I.; Knoll, W.; Offenhausser, A., Fusion of small unilamellar lipid vesicles to alkanethiol and thiolipid self-assembled monolayers on gold. *Langmuir* **1997**, *13* (26), 7085-7091.
225. Diguët, A.; Le Berre, M.; Chen, Y.; Baigl, D., Preparation of Phospholipid Multilayer Patterns of Controlled Size and Thickness by Capillary Assembly on a Microstructured Substrate. *Small* **2009**, *5* (14), 1661-1666.
226. Benninghoven, A., Chemical-analysis of inorganic and organic-surfaces and thin-films by static time-of-flight secondary-ion mass-spectrometry (TOF-SIMS). *Angewandte Chemie-International Edition in English* **1994**, *33* (10), 1023-1043.
227. Belu, A. M.; Graham, D. J.; Castner, D. G., Time-of-flight secondary ion mass spectrometry: techniques and applications for the characterization of biomaterial surfaces. *Biomaterials* **2003**, *24* (21), 3635-3653.
228. McDonnell, L. A.; Heeren, R. M. A., Imaging mass spectrometry. *Mass Spectrom. Rev.* **2007**,

26 (4), 606-643.

229. Adriaens, A.; Van Vaeck, L.; Adams, F., Static secondary ion mass spectrometry (S-SIMS) Part 2: Material science applications. *Mass Spectrom. Rev.* **1999**, *18* (1), 48-81.

230. Pacholski, M. L.; Winograd, N., Imaging with mass spectrometry. *Chem. Rev.* **1999**, *99* (10), 2977-+.

231. Xin, B. W.; Hao, J. C., Reversibly switchable wettability. *Chem. Soc. Rev.* **2010**, *39* (2), 769-782.

**Eidesstattliche Versicherung gemäß § 8 der Promotionsordnung
der Naturwissenschaftlich-Mathematischen Gesamtfakultät
der Universität Heidelberg**

1. Bei der eingereichten Dissertation zu dem Thema

Preparation, characterization and application of functional surfaces based on porous polymethacrylates

handelt es sich um meine eigenständig erbrachte Leistung.

2. Ich habe nur die angegebenen Quellen und Hilfsmittel benutzt und mich keiner unzulässigen Hilfe Dritter bedient. Insbesondere habe ich wörtlich oder sinngemäß aus anderen Werken übernommene Inhalte als solche kenntlich gemacht.

3. Die Arbeit oder Teile davon habe ich wie folgt/bislang nicht¹⁾ an einer Hochschule des In- oder Auslands als Bestandteil einer Prüfungs- oder Qualifikationsleistung vorgelegt.

Titel _____ der _____ Arbeit:

Hochschule und Jahr: _____

Art der Prüfungs- oder Qualifikationsleistung: _____

4. Die Richtigkeit der vorstehenden Erklärungen bestätige ich.

5. Die Bedeutung der eidesstattlichen Versicherung und die strafrechtlichen Folgen einer unrichtigen oder unvollständigen eidesstattlichen Versicherung sind mir bekannt.

Ich versichere an Eides statt, dass ich nach bestem Wissen die reine Wahrheit erklärt und nichts verschwiegen habe.

Ort und datum

Unterschrift

¹⁾Nicht Zutreffendes streichen. Bei Bejahung sind anzugeben: der Titel der andernorts vorgelegten Arbeit, die Hochschule, das Jahr der Vorlage und die Art der Prüfungs- oder Qualifikationsleistung.